CHALMERS
UNIVERSITY OF TECHNOLOGY

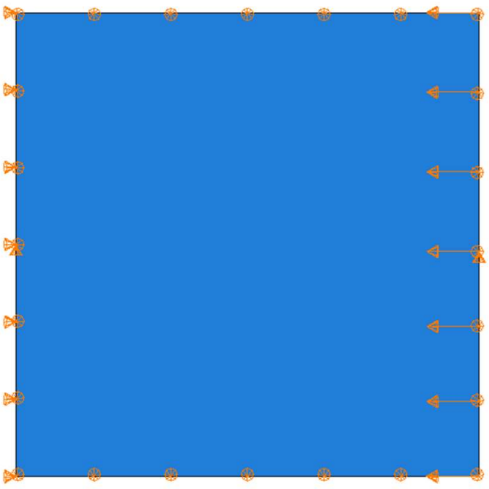

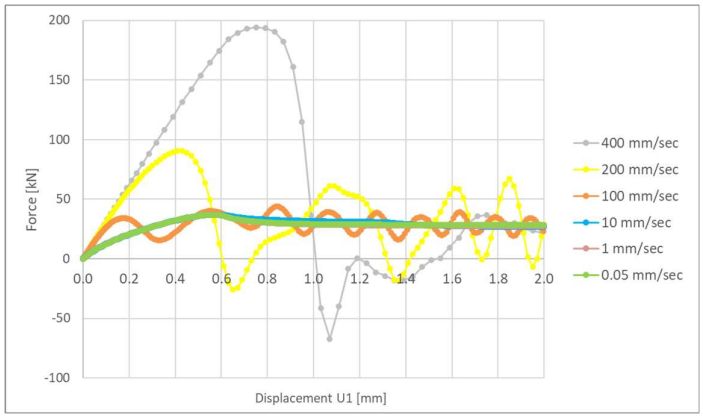

Buckling of a steel plate subjected to axial compression loading of various load rates

Master's thesis in the Master´s Programme Structural Engineering and Building Technology

RAIZA BERNADETTE FRANCIS GERARD
NATALIE LARSSON

DEPARTMENT OF ARCHITECTURE AND CIVIL ENGINEERING
DIVISION OF STRUCTURAL ENGINEERING

CHALMERS UNIVERSITY OF TECHNOLOGY
Gothenburg, Sweden 2023
www.chalmers.se

MASTER'S THESIS ACEX30

Buckling of a steel plate subjected to axial compression loading of various load rates

Master's Thesis in the Master's Programme Structural Engineering and Building Technology

RAIZA BERNADETTE FRANCIS GERARD
NATALIE LARSSON

Department of Architecture and Civil Engineering
Division of Structural Engineering
Lightweight Structures
CHALMERS UNIVERSITY OF TECHNOLOGY
Göteborg, Sweden 2023

Buckling of a steel plate subjected to axial compression loading of various load rates

Master's Thesis in the Master's Programme Structural Engineering and Building Technology

RAIZA BERNADETTE FRANCIS GERARD

NATALIE LARSSON

Examensarbete ACEX30
Institutionen för arkitektur och samhällsbyggnadsteknik
Chalmers tekniska högskola, 2023

Department of Architecture and Civil Engineering
Division of Structural Engineering
Lightweight Structures
Chalmers University of Technology
SE-412 96 Göteborg
Sweden
Telephone: + 46 (0)31-772 1000

Cover:
The studied plain steel plate where the boundary conditions are shown and a force vs. in-plane displacement curve for various load velocities.
Department of Architecture and Civil Engineering
Göteborg, Sweden, 2023

Buckling of a steel plate subjected to axial compression loading of various load rates

Master's thesis in the Master's Programme Structural Engineering and Building Technology

RAIZA BERNADETTE FRANCIS GERARD

NATALIE LARSSON

Department of Architecture and Civil Engineering
Division of Structural Engineering
Lightweight Structures
Chalmers University of Technology

ABSTRACT

To be able to meet the desire of densifying the existing urban environment there is a need to handle increased requirements against exceptional accidents such as explosions. As a step towards this, a study on the dynamic buckling resistance of a flat thin and thick steel plate is conducted. This is done by studying a steel plate subjected to axial compression load using non-linear FEM using Abaqus CAE and comparing it with experimental results from literature. The static analyses were carried out on the plate where the effect of initial imperfection, boundary conditions and material properties were studied. In the numerical analyses both material and geometric non-linearity was considered. Dynamic structural response (load, plastic strain, deformations) of the steel plate was studied based on steel material properties (with and without strain rate effect) for various load rates. Abaqus implicit/explicit was used for the dynamic analyses so that it can capture the whole behaviour of the plate using very small increment sizes compared to Abaqus standard. The plate was then studied for different load applications and its responses for the type of amplitude curve used. The study shows that multi-linear curve is more appropriate to handle the dynamic effect on the steel plate. The strain rate was studied using different functions available in the software with different elements to test the function. Further, the plate was analysed with a lower slenderness to compare the behaviour with the thin plate.

Key words: Explosion, impulse load, nonlinear FE-analysis, Abaqus CAE, buckling, axial compression loading, plain steel plate, static loading, dynamic loading, parametric study.

Buckling av en stålplåt belastad axiellt med dynamiska laster av olika magnitud

Examensarbete inom masterprogrammet Konstruktionsteknik och byggnadsteknologi

RAIZA BERNADETTE FRANCIS GERARD

NATALIE LARSSON

Institutionen för arkitektur och samhällsbyggnadsteknik
Avdelningen för Konstruktionsteknik
Lättviktskonstruktioner
Chalmers tekniska högskola

SAMMANFATTNING

För att bemöta behovet av att förtäta det existerande samhället är det idag ett behov av att hantera ökade krav mot exceptionella laster så som explosioner. Som ett steg emot detta är den dynamiska bucklingsförmågan studerad för en tunn respektive tjock plåt. Detta är gjort genom att studera en axiellt belastad stålplåt med hjälp av en icke-linjär FEM-modell i Abaqus CAE samt jämföra resultatet med experimentellt resultat ifrån vetenskaplig litteratur. I den statiska analysen av stålplåten studerades effekten av initialkrokighet och geometriska imperfektioner, gränsvillkor och materialegenskaper. I den numeriska analysen beaktades materiel- och geometrisk icke-linjäritet. Dynamisk strukturell respons (last, plastisk töjning, deformationer) av stålplåten studerades baserat på stålmaterialegenskaper (med och utan töjningshastighetseffekt) för olika belastningshastigheter. För att kunna studera plåtens fullständiga beteende användes Abaqus implicit/explicit i den dynamiska analysen med mycket små beräkningssteg. Stålplåtens respons studerades även för olika lastapplikationer med varierad amplitud kurva. Studien visar att multi-linjär kurva hanterar de dynamiska effekterna av stålplåten på ett fördelaktigt sätt. Olika metoder för att applicera töjningshastighetseffekt i Abaqus CAE studerades för varierande elementtyp för att testa funktionen. Slutligen studerades en plåt med lägre slankhet för att jämföra beteendet med den ursprungliga stålplåten.

Nyckelord: Explosion, impulslast, icke-linjär FE-analys, Abaqus CAE, buckling, axiell trycklast, stålplåt, statisk belastning, dynamisk belastning, parametrisk studie.

Content

Contents

Preface

This Master thesis is handling a study of the buckling response of a thin steel plate subjected to axial compression load of various load rates. The study was carried out at the office of Norconsult AB in Gothenburg during the period January 2023 to June 2023. The thesis is a collaboration between Norconsult AB and the department of Lightweight structures at Chalmers University of Technology, Gothenburg, Sweden.

We would like to thank our supervisor Morgan Johansson, Norconsult AB, for taking his time to help us with this Master thesis. He has supported us during the whole process with priceless information and knowledge about the subject of explosions.

We would also like to thank the staff at the division of Bridges and analyses at the office of Norconsult AB in Gothenburg for being friendly to us and letting us be there and work on this Master thesis.

Our examiner Mohammad al-Emrani at the department of Lightweight structures has supported us with helpful knowledge about steel structures and guidance on how this work should be carried out.

Finally, we would like to thank our families for supporting us during the work with this Master thesis and throughout our whole education.

Gothenburg, June 2023

Raiza Bernadette Francis Gerard and Natalie Larsson

Notations

Roman upper case letters

A	Buckle constant
C	Material constant
D	Strain rate parameter (multiplier)
DIF	Dynamic increase factor
DIF_i	Dynamic increase factor for *i* numbers of strain intervals
DIF_u	Dynamic increase factor for ultimate strength
DIF_y	Dynamic increase factor for yield strength
DLF	Dynamic load factor
DLF_{cr}	Critical dynamic load
DLF_f	Dynamic failure load
E	Young´s modulus, energy
E_k	Kinetic energy
E_r	Energy absorption capability
F	Force
F_k	Kinetic force
F_e	External force
$F_{reaction}$	Reaction force
$F_{reaction,node}$	Reaction force in one node
$F_{plate,edge}$	Force applied on the plate edge
I	Impulse load, moment of inertia
I_k	Kinetic impulse load
L	Length
M	Moment
M_{el}	Elastic moment
M_{pl}	Plastic moment
N_{cr}^{dyn}	Dynamic buckling load
N_{cr}^{stat}	Static buckling load
$N_{crAbaqus}$	Buckling load from Abaqus
N_{dyn}	Dynamic load
N_f^{dyn}	Dynamic failure load
N_f^{stat}	Static failure load

N_x	Pulse load (x-direction)
N_{ref}	Reference load
P	Pressure
P_0	Ambient air pressure
R	Material constant, absorbed energy
R_m	Load capacity
T_P	Duration time of pulse loading
U_X	Degree of freedom, translation in x-direction
U_Y	Degree of freedom, translation in y-direction
U_Z	Degree of freedom, translation in z-direction
UR_X	Degree of freedom, rotation around x-axis
UR_Y	Degree of freedom, rotation around y-axis
UR_Z	Degree of freedom, rotation around z-axis
V_0	Initial velocity
W_{CSM}	Width, Corrugated sheet metal
W_y	External work
W_e	External work
W_i	Internal work

Roman lower case letters

a	Acceleration, length of the plate (unloaded edge)
b	Length of the plate (loaded edge)
b_{eff}	Effective plate width
b_{tf}	Width top flange
b_{bf}	Width bottom flange
f_u	Ultimate strength
$f_{u.d}$	Dynamic ultimate strength
f_y	Yield strength
f_{yd}	Design yield strength
h_w	Web height
h	Height
k	Spring constant
m	Number of buckles in longitudinal direction. mass
n	Number of buckles in transversal direction

q	Strain rate parameter (exponent)
t	Time, thickness
t_a	Arrival time
t_{cor}	Core thickness
t_{nom}	Nominal sheet thickness after cold forming
$t_{metallic\ coatings}$	Thickness of metallic coatings
t_{plate}	Thickness of the steel plate
t_r	Ramp-up time
t_{tot}	Total time
u	Deformation
u_{el}	Elastic deformation
$u_{el,1}$	Deformation where the material behaviour goes from elastic to plastic response
u_{pl}	Plastic deformation
$u_{pl,1}$	Plastic deformation for elasto-plastic behaviour
u_r	Ramp-up deformation
u_{tot}	Total deformation
v	Velocity
v_r	Ramp-up velocity (final value)
w	Width
w_{CSM}	Width of two webs together with top- and bottom flange
w_{0max}	Maximum initial deflection

Greek letters

α	Angle of the corrugate sheet metal web
δ	Displacement
ε	Strain
$\dot{\varepsilon}$	Strain rate
ε_{pl}	Plastic strain
ε_{tot}	Total strain
ϕ	Lateral displacement
λ	Slenderness ratio
$\lambda_{\#}$	Eigenvalue for # number of elements
λ_{2500}	Eigenvalue for 2500 number of elements
σ	Stress

σ_{cr}	Critical buckling stress
σ_{eff}	Effective stress
σ_L	Limit stress
σ_{max}	Maximal stress
σ_T	Ultimate tensile stress
σ_{ult}	Ultimate stress
σ_{ud}	Ultimate design stress
σ_y	Yield stress
σ_{yd}	Design yield stress
ω	Angular frequency, out-of-plane deflection

1 Introduction

1.1 Background

With the aim of making attractive land space available for further development, there is today a desire in many Swedish cities to densify the existing urban environment. However, such densification leads to a reduced free distance between buildings and transport route, which may result in increased requirements against exceptional accidents such as explosions. Hence it is becoming more common that new buildings located close to such transport routes are designed regarding a nearby explosion. Dynamic loading from explosions may put very different demand on the loaded structures and it is not certain that a structure designed to withstand static loading is also suitable to withstand the effect of such dynamic loads. Instead, in such structures a large energy absorption capacity is often more important than a large load capacity.

An often effective and cheap solution when handling static loads on a roof is to use load bearing corrugated sheet metal (CSM) to span between the roof's main girders. However, if subjected to dynamic loading from a nearby explosion, this concept theoretically has low capabilities to withstand the explosion load. The reason for this is that the corrugated sheet metal is stiff and strong but provides low deformation capabilities, which together results in low energy absorption capability. Steel is a ductile material, but the layout of the corrugated sheet metal means that its theoretical load capacity is limited by buckling of its compressed flanges, and hence, its deformation capacity also becomes very limited. However, the conventional design approach may prove to be too conservative, and it would be valuable to find a concept where it is possible to use a roof solution based on corrugated sheet metal when subjected to explosion loads.

1.2 Aim and objectives

The aim of this master thesis is to get a better understanding of the structural response of corrugated sheet metal when subjected to impulse loading. The focus is at a plain steel plate subjected to axial compression load of various load rates. Furthermore, the study was made to support the research in the field of impulse loaded structures at Chalmers, Structural Engineering. The specific objectives are,

- To study the influence of different material and geometrical parameters for a plain steel plate subjected to static and dynamic loading.
- To perform numerical analysis of plates loaded in compression and subjected to dynamic loading.
- To compare the numerical result with previous studies within the same field and to improve the understanding of the behaviour of such plates.

1.3 Method

The first phase of the study was a literature study where several scientific publications were studied to give a background knowledge about the topic of plate buckling under dynamic loading. Additionally scientific publications were reviewed to study the phenomena where a steel plate buckles when subjected to axial compressive load. Therefore, a plain steel plate was studied to replicate the compressive flange of the corrugated sheet metal where it buckles when affected by explosion loads. A certain experimental data was picked and based on which the same geometry was studied to reproduce the similar plate behaviour. This made it possible to compare the experimental and numerical results in the literature to the analytical result from this study. Furthermore, a numerical study was made using Abaqus CAE where nonlinear effects are considered on both geometry and material. Both static and dynamic analyses were made, and the impact of strain rate effects were also studied in the dynamic analysis. One geometry was included in the analytical and numerical analysis with varying value of the slenderness ratio, and the results were compared to each other and to the literature.

1.4 Limitations

The initial limitation of the study is that it was limited to looking at a plain steel plate and to understand the behaviour of it when subjected to dynamic loading. The work is limited to study plates loaded in uniform uniaxial compression. The effect of boundary conditions is studied where the plate's degrees of freedom are either fully fixed or free and various combinations are studied and compared to each other. Further, the effect of dynamic loading is studied within the range 0.05 mm/sec to 400 mm/sec. The effect of plate slenderness is studied by studying and comparing a plate with high slenderness and a plate with low slenderness. The plate studied was limited to replicating a dynamic test. Furthermore, the work is limited to numerical analysis where Abaqus CAE was used. To be able to compare the results from the study to previous results, the size of the geometry used in the study was limited to a geometry found in the literature survey. The same geometry was studied with two different thicknesses.

2 Background theory

2.1 Corrugated sheet metal

An often effective and cheap solution when handling static loads on a roof is to use load bearing corrugated sheet metal (CSM) to span between the roof's main girders. One type of a corrugated sheet metal is a trapezoidal sheet which is a CSM with trapezoidal shaped geometry. In this Section, the design of the material and the structural behaviour of it are described.

On the Swedish market, there exists several different producers of trapezoidal sheets for roofing, e.g., Lindab, Ruukki, Arcelor and Areco. Based on the span length and applied load on the roof, the used design of the trapezoidal geometry differs. The parameters that differ between the geometries is the plate thickness t, hight of the corrugation h_w, width of the top and bottom flange b_{tf} and b_{bf}, the angle of the web α and the width of two webs, top- and bottom flange w_{CSM}, see Figure 2.1. Additionally, the total width of the panel W_{CSM} and the length of the panel L is shown.

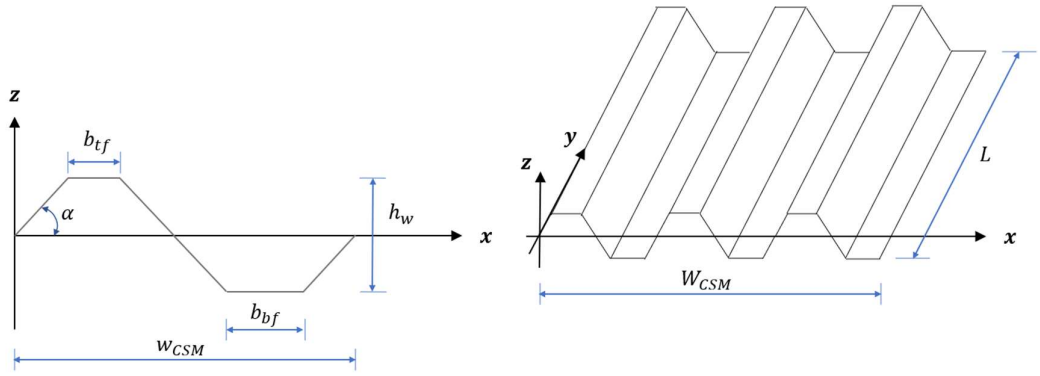

Figure 2.1 Geometry of a trapezoidal sheet where the different input parameters are marked.

Another thing that affects the dimensioning values of the different trapezoidal sheets is the steel property, the variety of the input parameters according to the producers mentioned above are shown in Table 2.1.

Table 2.1 Variety in input parameters for the trapezoidal loadbearing shells used on the Swedish market according to Lindab, Ruukki, Arcelor and Areco.

Input parameter	**Common values**
Steel quality	S280 - S420
Plate thickness t [mm]	0.6 - 1.5
Web height h_w [mm]	44 - 203
Top flange b_{tf} [mm]	60 - 201
Bottom flange b_{bf} [mm]	30 - 85
Width of two webs, top- and bottom flange w_{CSM} [mm]	151 - 427

There are two different kinds of trapezoidal steel plates used for roofing, one when having isolation and sheeting on top of the steel plate and one where there is no sheeting. The most common way is to have isolation and sheeting on top of the steel plate. Based on the geometry that the plate has and the steel quality, the maximum allowable span length and width varies.

The loadbearing trapezoidal sheet that is used for the roofing is in the static case loaded with transversal load. Transversal load comes from the self-weight of the isolation and sheeting material that is put on top of the steel plate, the wind load and the snow load. When studying a dynamic case of the structure with regards to explosion load, the steel plate is subjected to wave propagation, see Section 2.4.3 to read more how a structure is affected by an explosion.

The structural behaviour of corrugated sheet metal is affected by the boundary conditions of the plate. In a paper from Izabel et al (2016), a simply supported sinusoidal plate is subjected to distributed line loads. When studying the load-displacement relationship shown in Figure 2.2 it is seen that after the ultimate load is reached, the displacement keeps increasing with decreasing load.

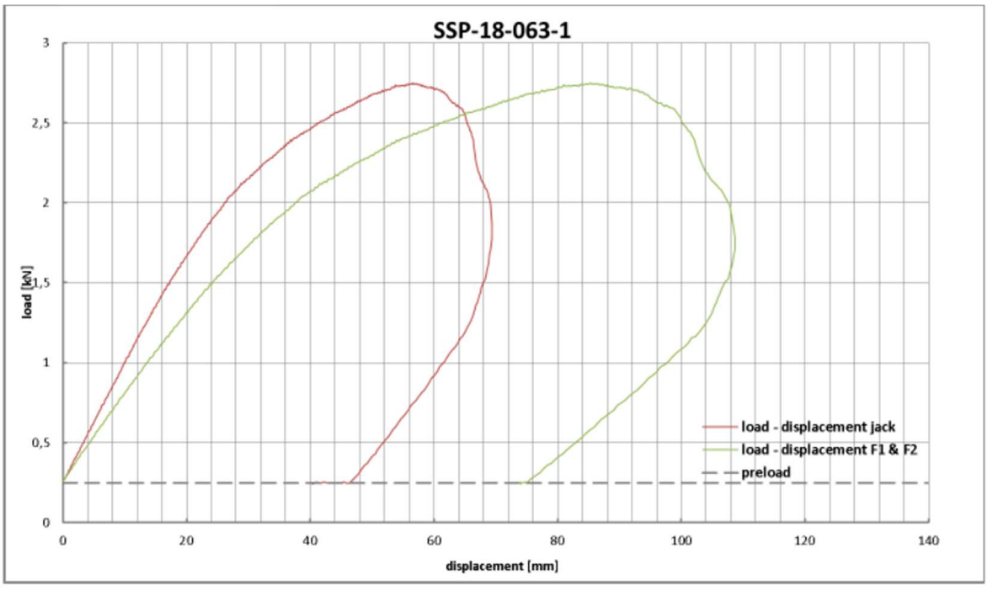

Figure 2.2 Load-displacement relationship of a test specimen subjected to distributed line loads (Izabel et al, 2016).

In Degtyarev (2020), a corrugated sheet subjected to point loads was studied in a finite element model, see Figure 2.3. The load deflection curve in Figure 2.4 is found for a trapezoidal deck where the load is applied at the bottom flange, top flange, and web respectively at the positions; length divided by eight, *L*/8, and at the mid of the plate, *L*/2. The steel plate that was modelled in this test was modelled to simulate a real plate with fixed deck attachment.

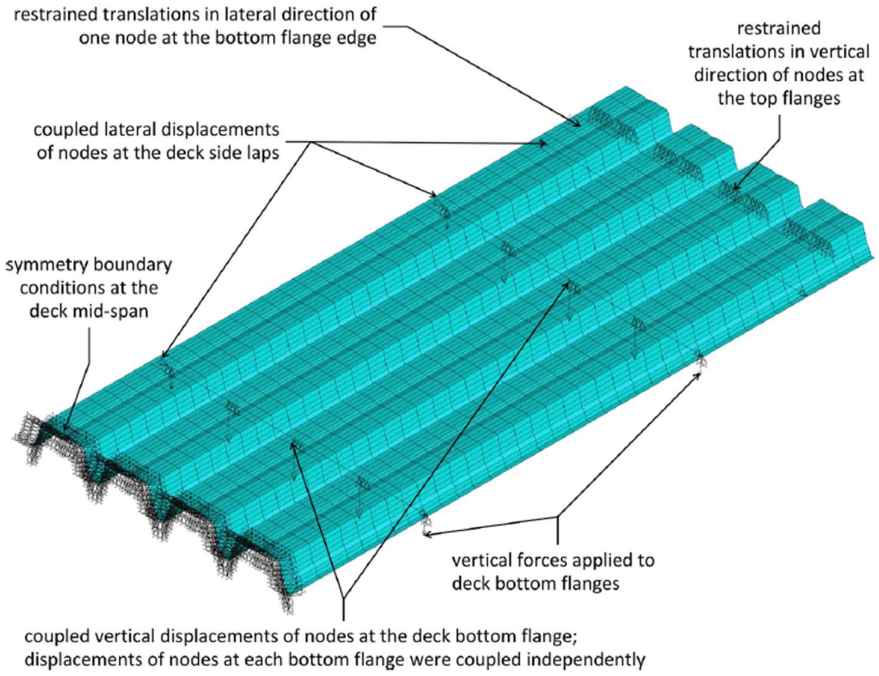

Figure 2.3 Single span steel deck with trapezoidal shape subjected to point loads (Degtyarev, 2020).

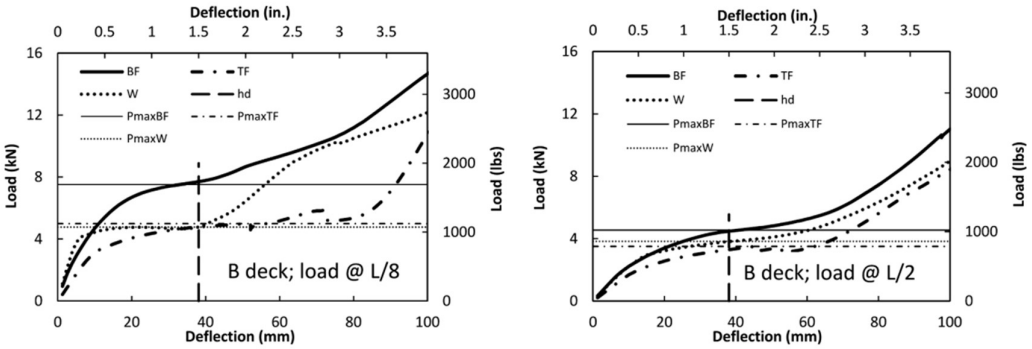

Figure 2.4 Load-deflection relationship for a trapezoidal steel plate subjected to point loads at two different places along the plate (Degtyarev, 2020).

In the results it is seen that there is no part or a negligible part where the load decreases when the displacement is increased instead the hardening effect comes directly after plasticity. According to Degtyarev this is due to the membrane action. In reality, if the behaviour should be like this it would put large demand on the anchoring of the plate and that it is strong enough to handle the forces.

2.2 Accidental limit state design

In ALS design according to Paik & Thayambali (2003a) it is important to achieve a design such that the main safety functions of the structure are not impacted during any accident or within a certain period after the accident. The main criteria for the ALS design are to limit the accidental consequences such as structural damage and environmental pollution. The possible accidents in structures are fire, explosion, foundation collapse or earthquakes and therefore the main functions to be considered in the ALS design are:

- Energy dissipation related to crashworthiness.
- Capacity of local strength members
- Global structure capacity
- Allowable tensile strains
- Fire protection

In ALS; design under predominantly impact oriented loading equation (2.1) may be rewritten using energy dissipation related criteria which is adopted in such a way that the safety of the structure is not lost.

$$W_e \leq W_i \tag{2.1}$$

Where W_e is external work and W_i is internal work.

2.3 Explosions

2.3.1 What is an explosion

An explosion is a sudden release of energy with a related volume of expansion that will lead to increase of light and temperature with a very high increase of pressure (Johansson & Laine, 2012a). For explosion in mid-air the pressure travels in spherical

motion and the pressure decreases with increased distance therefore distance is of utmost importance when the explosion load and the way to handle it is considered. The time it takes for the pressure to reach an object is called the arrival time, t_a. An ideal explosion consists of two phases, they are positive and negative phase. The positive phase is when the pressure is higher than P_0 which is the ordinary atmospheric pressure or the ambient air pressure. Due to the pressure wave, air is forced outwards creating a vacuum and this phase is called the negative phase since here the pressure is lower than P_0, see Figure 2.5.

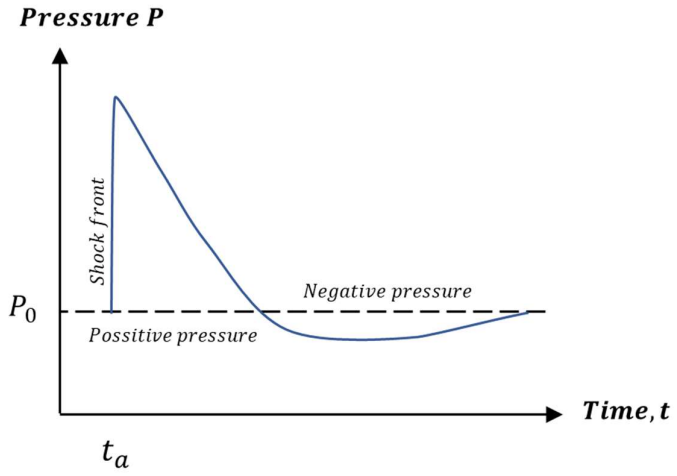

Figure 2.5 Schematic pressure-time relationship for where the positive- and negative pressure phases can be seen for an idealized shock wave. Graph based on Johansson & Laine (2012a).

2.3.2 Effect of explosions

There are two main aspects that effect the external energy from a given explosion acting on a structure and they are the distance to the source and the protective mass (Johansson & Laine, 2012b). The energy from the wave caused by the explosion is decreased when the distance is increased since the volume where the energy is increased. In the same way, the mass influences the energy that is needed to put a mass at work. For a larger mass, a larger amount of energy is needed and for a smaller mass, a smaller amount of energy is needed therefore the effect of an explosion of the same order impacts largely on a small mass and for increased mass the impact decreases.

The amount and type of explosive, distance to target and geometrical surrounding are important parameters that effects the magnitude and duration of an explosion (Johansson & Laine 2012a). The amount and type of explosive decides the energy release in the explosion and the resulting pressure obtained is a function of this and the volume affected. Generally, the pressure will decrease with increased distance and the duration will increase with increased distance. If the wave cannot propagate freely the pressure will not decrease as much with increased distance. Four phenomena important for final explosion loads are reflection, mirroring, diffraction and confinement, see Figure 2.6 to Figure 2.8 for schematic illustrations.

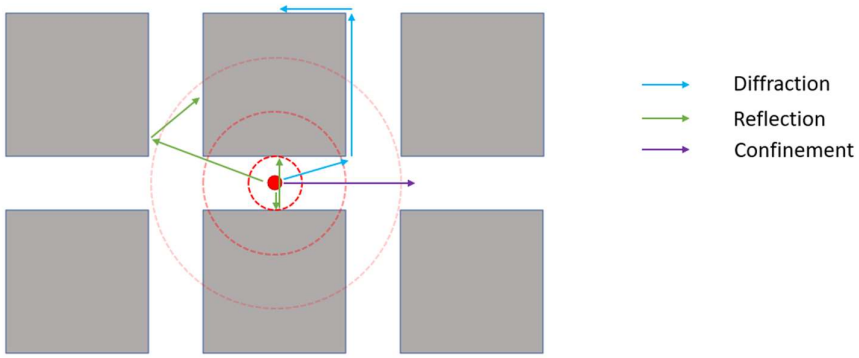

Figure 2.6 Illustration of three of the concepts affecting the magnitude and duration of the shock wave (Johansson and Laine, 2012b).

When studying the effect of the type of loadbearing structure, two definitions are considered. This is the reflecting pressure and the incident pressure (or unreflecting pressure) (Johansson & Laine, 2012a). The reflecting pressure is the pressure that effects the part of the structure that is facing the explosion while the incident pressure is the pressure that effects the part of the structure that are not facing the explosion, see Figure 2.7.

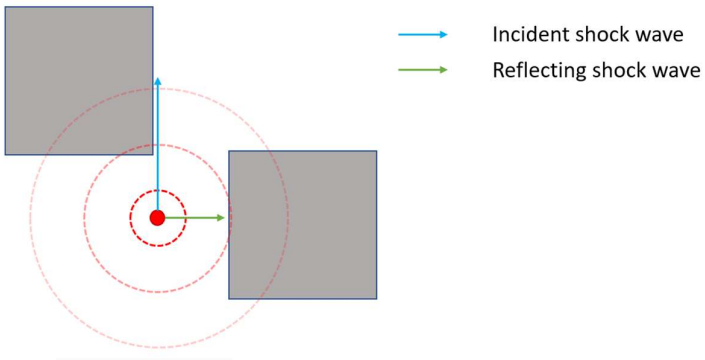

Figure 2.7 Illustration of the difference between an incident shock wave and a reflecting shock wave. Figure based on Johansson and Laine (2012b).

The concept of reflection occurs when the wave is reaching a reflective surface and this phenomenon is of extra importance when looking at explosions in urban environments and explosions close to a building (Carlsson & Kristensson, 2012).

The second concept, mirroring, is a type of reflexion which occurs when an explosion detonates close to the ground (Carlsson & Kristensson, 2012), see Figure 2.8. Not the full size of the mechanical wave is mirrored when reaching a mirroring surface instead there is some energy loss to the ground or the surface.

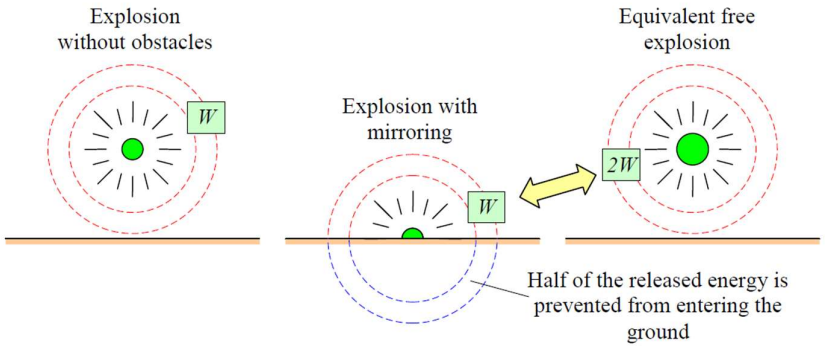

Figure 2.8 Illustration of mirroring's effect on the magnitude and duration of an explosion. Figure based on Johansson and Laine (2012a).

Diffraction describes how the explosion load is traveling around corners and it is a phenomenon that occurs when the blast wave is blocked by an intermediate object. Therefore, it needs to propagate around the corners of a building to reach the point on the other side (Carlsson & Kristensson, 2012), see Figure 2.6. Due to this, the direction of how the wave is propagating is changed and the distance that the mechanical wave is propagated through is increased.

Confinement of a blast wave from an explosion leads to increased impact from the blast wave. The reason for this is that due to the confinement, the energy from the blast wave will not disperse as it will if there is no confinement. One example of this is if an explosion appears at a street in an urban area with high buildings on both sides of the street, see Figure 2.6.

2.4 Impulse loading

2.4.1 Orientation

An impulse load is often a load with high pressure and short duration (Johannsson & Laine, 2012) in which the impulse rather than force determines the response of an affected structure. Impulse loading can be of various kind, it can either be as caused by an explosion or by the impact force obtained in a collision between two objectives. The size of the impulse load is equal to the force times the time, as shown in Figure 2.9 and calculated with equation (2.2).

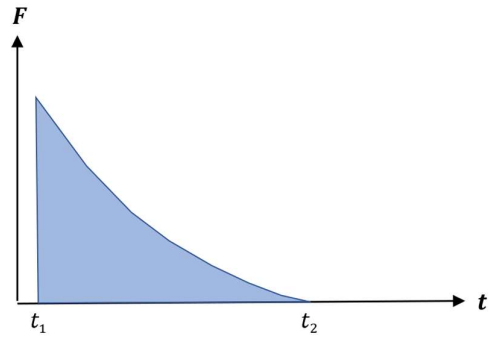

Figure 2.9 The impulse, I, is the area under the force-time graph.

$$I = \int_{t_2}^{t_1} F(t)dt \tag{2.2}$$

Where I is impulse load and $F(t)$ is force at given time, t_1 is the starting time and t_2 is the end time.

2.4.2 Difference in static and impulse load

The impulse load has higher velocity whereas the static load has less comparatively (Johansson & Laine, 2012b). Structures are usually designed to withstand static loads acting with a long duration, but an impulse load will affect the structure with high pressure during a short duration of time. The pressure from an impulse load can be considerably higher than the pressure from the static load that a structure can withstand. In case of static load, it is of normal interest that it can withstand the given load with limited deformation. In this case stiffness and load capacity is important to fulfil the requirements. For impulse loaded structures it is often more important to exhibit a good deformation capacity with the possibility of high energy consumption, than high stiffness and load capacity. In addition to the large difference of load magnitude, the duration of the impulse load is significantly shorter than a constant static load which leads to a considerable difference in the structural responses due to impulse load and static load, see Figure 2.10.

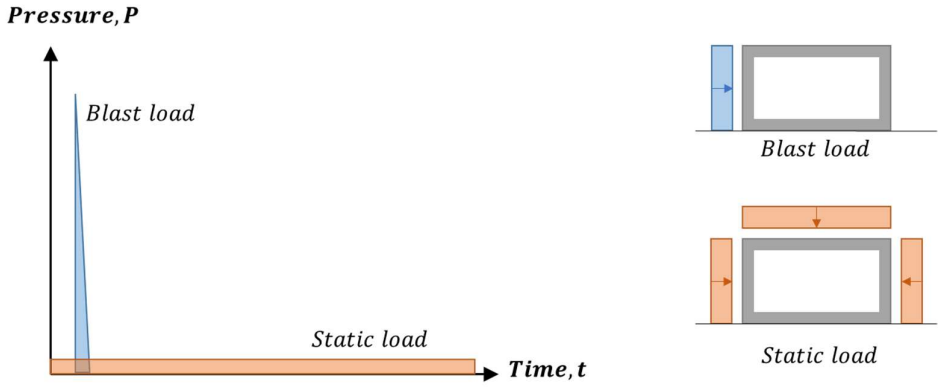

Figure 2.10 Shows the effect of blast load and static load in terms of pressure and time. Figure based on Johansson & Laine (2012b).

2.4.3 Structural response caused by Wave propagation effect

Any structure affected by external load, takes a certain amount of time to transfer the effect through the material (Johannsson & Laine, 2012). This type of phenomenon is called wave propagation effect and it might make the structure to differ a lot from the response obtained at a corresponding loading. Due to this effect, the boundary conditions for the structure can be seen as time dependent parameter in the initial phase and there is also a risk for other types of failure mechanisms to appear during this time, like local failures.

The effect caused by the wave propagation effect is dependent on the speed of the mechanical waves in the structure (Carlsson & Kristensson, 2012). Figure 2.11

illustrates a case where time dependent boundary condition is obtained due to wave propagation effect.

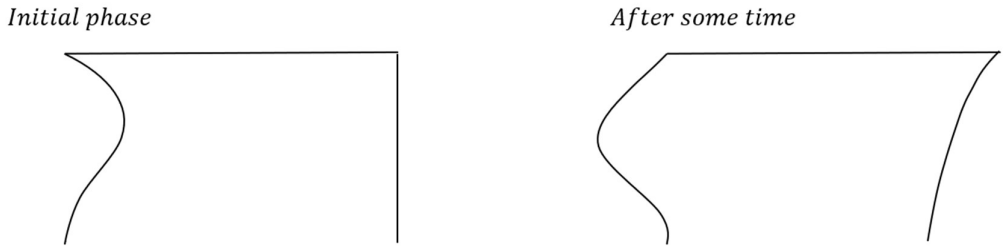

Figure 2.11 Initial structural response of a structure subjected to impulse loading and after some time.

As shown in the figure to the left above, only the closest region of the structure exposed to the load is affected in the initial phase while the rest of the structure is still unaffected. After some time, the rest of the structure will also have an impact from the load. Depending on the properties of the structure it takes different amount of time for the global structure to be affected. This phase is illustrated to the right in Figure 2.11, and this can be after like 50-100 ms. At this time, it can also be seen that there is a rebound of the left column that was affected in the initial phase.

Depending on the loading velocity, there might be an influence of the material properties of the member (Johansson & Laine, 2012a). Depending on the material of the member, the sensitivity for these phenomena, so called strain rate effect, differs.

2.4.4 Characteristic impulse loading and pressure loading

According to Johansson & Laine (2012b), a characteristic impulse load is a load with high intensity and very short duration, see Figure 2.12. An example of this kind of load is a load with a short distance to the source and when looking at weak structures with a large mass.

According to Johansson & Laine (2012b), a characteristic pressure load is a load that is added to a structure with low intensity and with long duration, see Figure 2.12. Depending on the type of structure the definition of a short or long duration is different, this is based on the time to reach maximum displacement compared to duration of load.

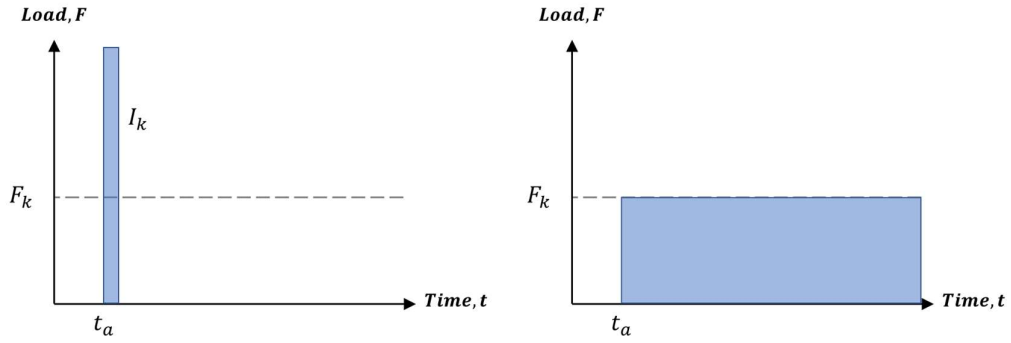

Figure 2.12 Force-time relationship for an impulse load (left) and a characteristic pressure load (right). Figure based on Johansson & Laine (2012b).

An example of this kind of load may be a gas explosion where there is small intensity of pressure. The overpressure is low and duration long. For this type of loading to appear, the structure should be stiff and light weighted. An example of a structure where this is true is corrugated sheet metal.

2.4.5 Energy balance

This Section is based on Carlsson & Kristensson (2012) where they refer that the external work that move the body through space or the impact transferring kinetic energy into potential energy in the body and momentum which based in equation (2.3) and (2.4) gives equation (2.5).

$$E_k = \frac{mv^2}{2} \tag{2.3}$$

$$I_z = m \cdot v \tag{2.4}$$

$$W_y = E_k = \frac{{I_z}^2}{2m} \tag{2.5}$$

Where E_k is kinetic energy, m is mass, v is velocity, I_z is moment of inertia about z-axis and W_y is external work.

The structures geometry and material behaviour are dependent of the internal work that arises as a response to the load. The definition for internal work is the structure's absorbed energy over the deformation and is given by equation (2.6), where *R(u)* is the resisting force.

$$W_i = \int_0^u R(u)du \tag{2.6}$$

Where W_i is internal work and *R(u)* is the absorbed energy at the deformation u.

To have a structure where there is equilibrium, the internal and external work needs to be in equilibrium to each other. The energy balance equation between external and internal work is shown in Figure 2.13.

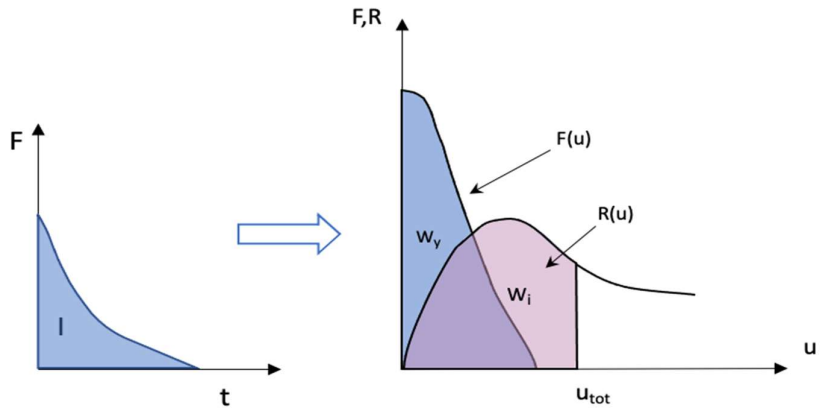

Figure 2.13 Illustration of the internal and external work. Figure based on Johansson & Laine (2012b).

The response of loaded structures and their behaviour can be simplified as e.g. linear elastic, ideal-plastic and elasto-plastic response as they give close approximations to the actual response in various structures. The deformations for elastic and ideal-plastic behaviour can be given by equation (2.7) and (2.8).

$$u_{el} = \frac{I_k}{\sqrt{km}} = \frac{I_k}{m\omega} \tag{2.7}$$

$$u_{pl} = \frac{I_k^2}{2m \cdot R_m} \tag{2.8}$$

Where u_{el} is elastic deformation, I_k is kinetic impulse load, k is spring constant and R_m is the load capacity. Additionally, ω is the angular frequency and can be calculated by using equation (2.9).

$$\omega = \sqrt{k/m} \tag{2.9}$$

For the elasto-plastic behaviour the structure is first deformed from u=0 with elastic behaviour until the load reaches the limit R_m. This happens at $u_{el,1}$ and if the load is greater than or equal to this limit, deformations will be plastic until u_{tot}, see Figure 2.14.

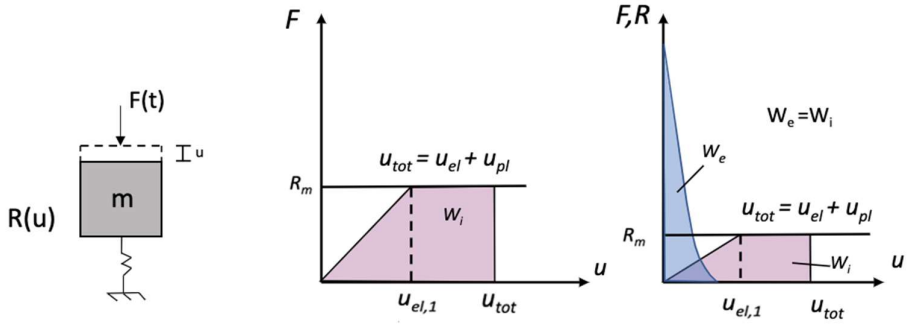

Figure 2.14 System with elasto-plastic response: (a) single degree of freedom system, (b) force-displacement relationship, (c) energy equilibrium relationship between external and internal energy. Figure based on Johansson & Laine (2012b).

The internal work for the elasto-plastic behaviour can be written as

$$W_i = \frac{R_m}{2} \cdot (u_{el,1} + 2u_{pl,1}) \tag{2.10}$$

Where $u_{el,1}$ is the limit where the material behaviour goes from elastic to plastic response and is defined as

$$u_{el,1} = \frac{R_m}{k} \tag{2.11}$$

By combining equation (2.5) and (2.10), the plastic deformation for the elasto-plastic behaviour $u_{pl,1}$ can be expressed as below.

$$u_{pl,1} = \frac{I_k^2}{2mR_m} - \frac{u_{el,1}}{2} = u_{pl} - \frac{u_{el,1}}{2} \tag{2.12}$$

Where u_{pl} is the material behaviour for the ideally plastic response and the total deformation is given by the following equation.

$$u_{tot} = u_{el,1} + u_{pl,1} = u_{pl} + \frac{u_{el,1}}{2} \tag{2.13}$$

If the pressure load (see Figure 2.12) is applied to a structure with elasto-plastic behaviour the plastic deformations can be reached even though the magnitude of the load is lower than the response limit, R_m. This is due to fulfilling the work equilibrium and the fact that the external work from the pressure load has a rectangle shape whilst the internal work initially has a triangular shape during elastic deformations, see Figure 2.15.

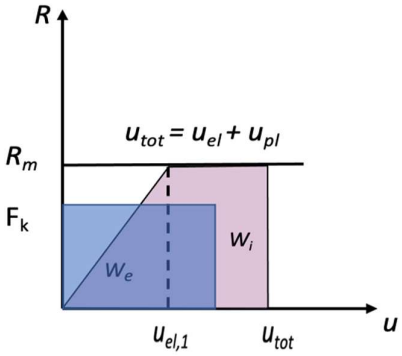

Figure 2.15 System with elasto-plastic response. Plastic deformations are formed even though the load is lower than the response limit due to the energy equilibrium. Figure based on Carlsson & Kristensson (2012).

2.4.6 Effect of mass

According to Johansson & Laine (2012b), the size of the mass affects the amount of effect introduced into the structure by the explosion, see equation (2.5). The reason for this is that the amount of mass effects the amount of energy needed to put it in movement. The larger the mass, the more energy is needed to make it move. This means that the effect that an explosion has on a structure depends on its mass. For the same size of the explosion, the effect on the structure will be decreased if the mass is increased.

2.4.7 Effect of stiffness

The inner work of a structure is based on the inner force that is within the structure (Johansson & Laine, 2012b). Depending on the material that is used and the shape of the structure, the size and intensity of the inner energy is changed. Although, a relationship is seen that stiffer structure leads to less deflections with high forces and more durable structures lead to larger deformations and small forces.

The stiffness of a structure is affecting the ability of a structure to absorb energy and the way in which the energy is stored in the structure (Johansson & Laine, 2012b). A structure that is allowed to deform more can absorb the energy in a more effective way than a structure that only allows small deformations. An increase in allowed deformation also means that the structure is more able to spread the energy inside the material.

2.4.8 Effect of strength capacity

In general, the response of a structure with high stiffness is identified by less deformation and high resisting force whereas for structures with low stiffness the opposite is valid (Johansson & Laine, 2012b). In case of static load, it is favourable when the structure has more stiffness with higher load capacity whereas in case of impulse load it is good to have structures with lower stiffness, lower load capacity and higher deformation capacity. As shown in Figure 2.16 the blue region indicates a

structure with higher stiffness and load capacity and the red region denotes the latter. The internal work W_i can be calculated using equation (2.6).

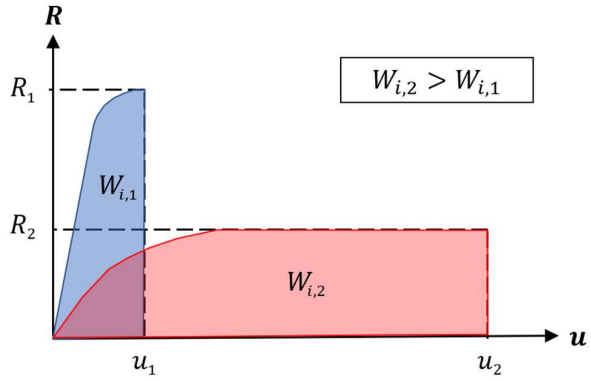

Figure 2.16 Resisting force-load relationship for two different types of structures where the blue area indicates a favourable structure in a static case while the red area is favourable for a structure subjected to impulse loading. Figure based on Johansson & Laine (2012b).

2.4.9 Effect of ductile behaviour

The ductility of a steel material effects the behaviour of a steel structure. Either the material can fail in brittle or ductile manner, see Figure 2.17, where the steel ideally fails in ductile manner where the internal stresses are redistributed within the material which will delay the global failure of the structure and by doing that, collapse may be avoided.

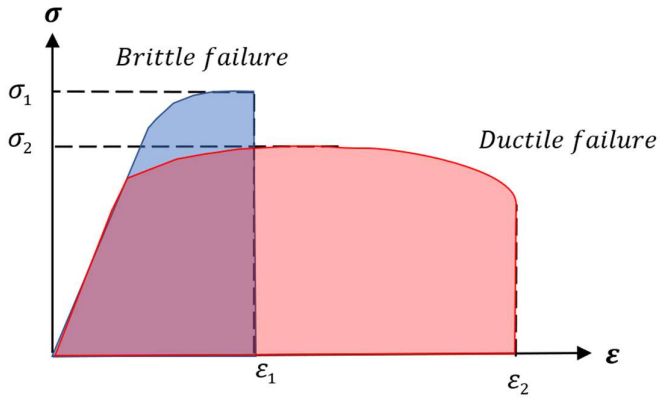

Figure 2.17 Stress-strain relationship for a structure with brittle- and ductile failure.

The structural response of a plate is affected by the properties of the structure. In steel structures, buckling may occur and depending on the risk of local buckling to appear in a steel plate they are divided into four different cross-section classes, class 1-4 where class 4 is where the risk is the highest (Al-Emrani & Åkesson, 2020). Based on the cross-section class that a steel specimen is in, the ductile behaviour is affected (Dubina et al, 2012). The ductility of a material is affecting the load-displacement relationship of the steel after the linear elastic response. One of the aspects that effects the ductility of a material is the cross-section class of the steel. The lower cross-

section class there is, the less ductile the steel is. This means that if the piece is in cross-section class 3 or 4, the ductility is low, and these pieces are generally not allowed to be designed using plastic behaviour. If the steel has low ductility, the ability for the steel structure to dissipate energy is reduced.

2.4.10 Inertia effects

Inertia effect is that the more mass the object has the object tends to have greater tendency to resists changes in its state of motion. Inertia effects may have an influence in case of fast load application, e.g., due to impact or when subjected to an explosion load (Paik & Thayambali, 2003a). Due to the inertia effects and stress wave propagation phenomena within the structures during impact loading, the strain distribution or the deformation pattern at any moment in time would be non-homogeneous. It is considered that when the strain rate is greater than 0.1 s^{-1} the inertia effects become more important.

2.4.11 Equivalent static load

The use of an equivalent static load is a way to transform the dynamic load to a static load, which is easier to use in design for most engineers (Johansson & Laine, 2012b). The equivalent static load is commonly used for dynamic loading such as explosions and impacts. Using the equivalent static load enables the use of a simplified calculation of the dynamic load. According to Johansson & Laine (2012b) the equivalent static load can be defined as "The static load that performs the same work as a dynamic load". If the studied load case is of linear elastic response, the calculated maximum deformation will be the same when using the equivalent static load as the actual impulse load. Due to this, the maximum potential energy from the static load should be equal to the maximum potential energy from the dynamic load.

The size of the equivalent static load depends on the characteristics on both the dynamic load and the structure subjected to the load. The characteristics include load type, the maximum load, the load duration and impulse impact of the incoming body. The impulse impact depends on properties like mass, stiffness and load capacity. The characteristics of the support, its mass, its stiffness and its load capacity also influence the size of the load. One thing that is very important to consider is that it is generally not possible to determine the equivalent static load only based on the dynamic load. The static dimensioning should consider the possible rebound of the structure and the designer needs to also have information about the structure on which the dynamic load is applied to be able to know which equivalent static load to use.

2.5 Steel structures

2.5.1 Mechanical properties of steel

The mechanical properties of steel are very important in determining the quality of steel (Paik & Thayambali 2003a) and some of the important properties are ultimate strength, yield strength, toughness, hardness of steel and elongation, see Figure 2.18. The mechanical properties of steel vary with the amount of work and heat treatment

applied during the rolling process. Typically plates that receive more work have higher yield strength than the plates that do not.

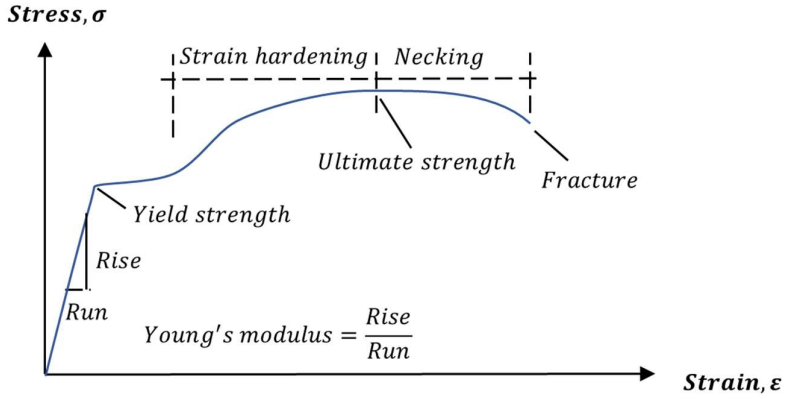

Figure 2.18 Schematic figure of properties used to determine the quality of steel.

2.5.2 Plastic hinges

When steel is subjected to a certain amount of load, the yielding point of the material will be reached, and it starts to yield (Al-Emrani & Åkesson, 2020). Depending on the material properties and the shape of the steel member several plastic hinges may be created. This will happen where the elasto-plastic material reaches plasticity and deformation in these points will remain when unloading the structure. When plastic hinges are created, redistribution of forces within the material will start and due to this, the material can still be loaded with additional load until the final (ultimate) load is reached.

2.5.3 Thickness

The provisions for design given by part 1-3 of EN1993 may be used for steel within given ranges of core thickness t_{cor} (Dubina et al, 2012). The following values are recommended:

- For sheeting and members: 0.45 mm ≤ t_{cor} ≤ 15 mm
- For connections: 0.45 mm ≤ t_{cor} ≤ 4 mm

Thicker or thinner material may also be used, provided the load bearing resistance is determined by design assisted by testing.

The steel core thickness t_{cor} should be used as design thickness, where,

$$t = t_{cor} \qquad if\ tol \leq 5\% \tag{2.14}$$

$$t = t_{cor} \cdot \frac{(100 - tol)}{95} \qquad if\ tol > 5\% \tag{2.15}$$

With

$$t_{cor} = t_{nom} - t_{metallic\ coatings} \tag{2.16}$$

Where *tol* is the tolerance expressed in % and t_{nom} is the nominal sheet thickness t_{nom} after cold forming.

2.5.4 Strain rate

When a structure is subjected to high strain rate the material property might be affected. The strength or capacity of the material will increase, and the material will have less ductility.

The strain rate sensitivity according to Yang et al (2022) is an important property in the formability of sheet metal. The strain rate effect is quantified by three indices in structural steels:
DIF_y is the dynamic increase factor for the yield strength f_y,

$$DIF_y = \frac{f_{yd}}{f_y} \tag{2.17}$$

DIF_u is the dynamic increase factor for the ultimate strength, defined as the ratio of the dynamic ultimate strength $f_{u,d}$ to the static ultimate strength f_u.

$$DIF_u = \frac{f_{u.d}}{f_u} \tag{2.18}$$

Among the three indices, DIF_y is widely used but can result in inaccurate predictions if applied as a stress amplification factor to the full quasi-static stress-strain curve for the following reasons (Yang et al, 2022):

- When subjected to impact or explosion, steel deforms into the strain-hardening range, which is beyond the yield point.
- The dynamic increment in $f_{y,d}$ is generally higher than that of other points on the stress-strain curve, leading to an overestimation of the predicted constitutive response when using DIF_y.
- Measured DIF_y reported in the literature can be sensitive to the system errors associated with stress nonuniformity during the elastic stage.

DIF_u is mostly lower than DIF_y thereby leading to an underestimation of the constitutive response. Therefore, the use of DIF_y is not always suitable for characterizing the dynamic properties of structural steel.

2.5.5 Strain rate effects in Abaqus CAE

Strain rate is one aspect that significantly effects the material's mechanical properties and therefore this is a parameter which is important to consider when looking at the buckling behaviour of steel structures subjected to fast dynamic loading (Paik & Thayamballi, 2003a). The strain rate or loading speed $\dot{\varepsilon}$ can be calculated based on the initial velocity, V_0, and the average displacement, δ, see equation (2.19).

$$\dot{\varepsilon} = \frac{V_0}{\delta} \tag{2.19}$$

There exist various types of methods to describe the strain rate effect of a material and one of these are Cowper Symonds power equation.

Strain rate effect can be included in the model using three methods in Abaqus CAE where the material non-linearity can be established with the stress strain relationship, and they are the following.

2.5.5.1 The power law

The dynamic yield strength σ_{yd} of the material can be studied using the power law also known as Cowper-Symonds power equation (Yang et al, 2022). The Power law equations is given by:

$$\sigma_{yd} = \sigma_y \left(1 + \left(\frac{\dot{\varepsilon}}{D}\right)^{1/q}\right) \tag{2.20}$$

Where σ_y is the yield strength and the strain rate parameters *D* and q are values which can be calculated with equation (2.21) and (2.22) which are based on the yield strength f_y of the material. The parameters *D* and q are based on DIF_y, described in Section 2.5.4.

$$D = 1000\left(\frac{f_y}{235}\right)^{3.8} \tag{2.21}$$

$$q = 5\left(\frac{f_y}{235}\right)^{-0.5} \tag{2.22}$$

2.5.5.2 Yield ratio

The yield ratio is another method that can be used in Abaqus CAE to include the strain rate effect in the model. When using this method, the dynamic increase factor and the plastic strain is calculated manually and given by the user directly for different strain rate.

2.5.5.3 Johnson-Cook

The Johnson-Cook method is another method where the strain rate effect can be added to the model. This method is suitable only for hight strain rate deformation of metals. This method is referred to as "Johnson-cook dynamic failure model". This is a recommended technique for progressive damage and failure of materials. The method is based on the value of equivalent plastic strain of the element integration points and failure is assumed to occur when damage parameter reaches 1.

$$\varepsilon_{pl} = \varepsilon_{EXP}\left(\frac{1}{C}(R-1)\right) \tag{2.23}$$

Where ε_{pl} is plastic strain, ε is strain and the parameters R and C are material constants. However, this method is not used here for further study of strain rate effect as the stress strain curve is rather smooth compared to the actual curve.

2.5.6 Buckling

When a steel plate is subjected to a load the stress will start to distribute within the cross-section of the member (Al-Emrani & Åkesson, 2020). Based on the slenderness of the parts used in the cross-section, there might be a risk for local buckling in the cross-section before the plastic capacity of the cross-section is reached. The slenderer the cross-section is, the larger risk there is for this phenomenon to appear and if the plate is very slender, local buckling can even appear in the elastic range, i.e., before yield strength is reached at any point in the cross-section. When designing a plate based on the buckling load three components are considered, the slenderness of the plate, the boundary conditions, and the load that the steel member is subjected to. Both the boundary conditions and the loading condition is considered in the buckling coefficient k, while the slenderness is considered in the cross-section class of the plate.

In the Eurocode there are four different cross-section classes (CSC) that a steel member is divided into to define the risk of local buckling, class 1 to 4 (Al-Emrani & Åkesson, 2020). Which cross-section class a member belongs to depends on the slenderness ratio λ that each individual plate within the cross-section belongs to. Based on the cross-section class, the critical buckling stress of a plate is affected, see Figure 2.19.

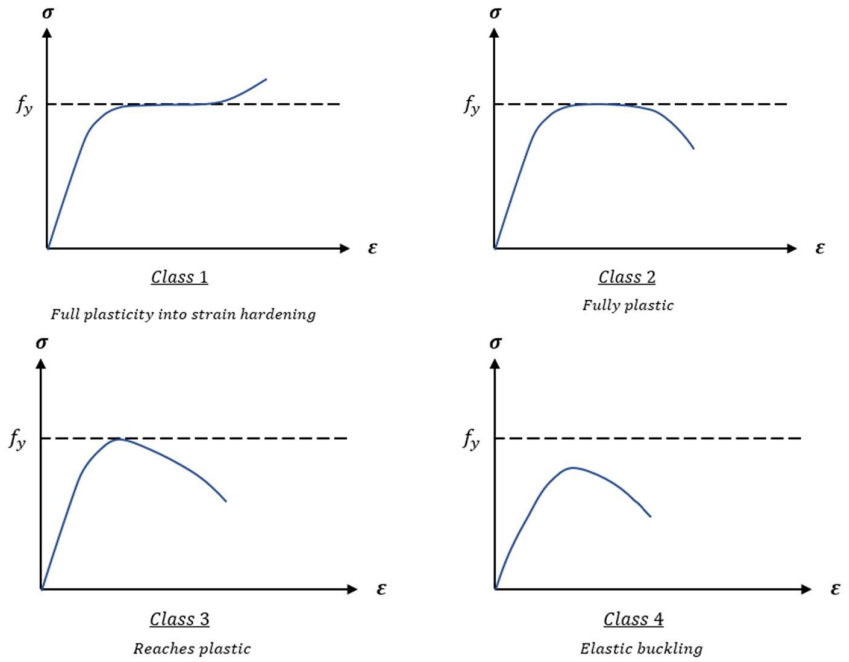

Figure 2.19 Stress-strain relationship for the plates with four different cross-section classes. Figure based on Al-Emrani & Åkesson (2020).

If the steel member is in class 1 or 2 (compact sections) full plastic distribution can be achieved for the cross-section. If instead the member is in CSC 3, only elastic stress distribution is allowed. In cross-section class 4, the buckling of the plate will appear within the elastic range, see Figure 2.20.

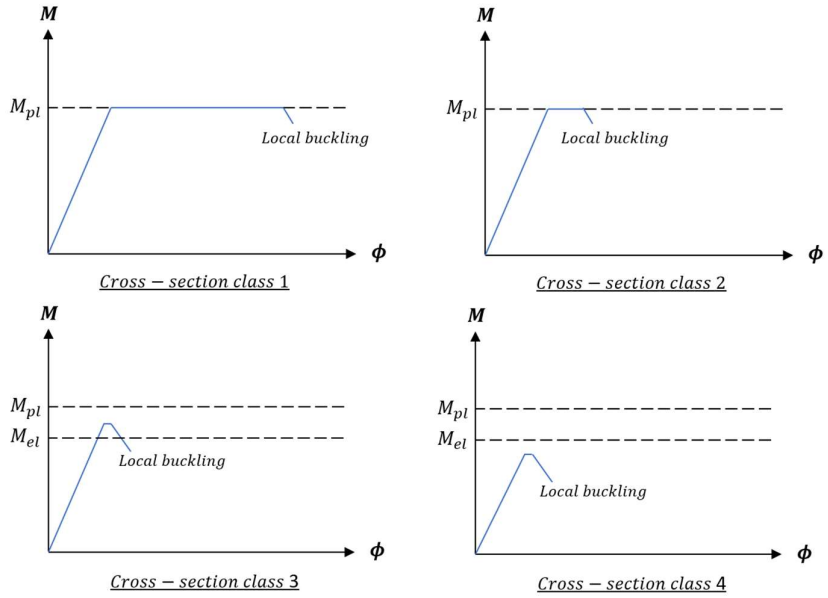

Figure 2.20 Cross-section resistance in bending for different cross-section classes. Figure based on Al-Emrani & Åkesson (2020).

When comparing Figure 2.19 and Figure 2.20 it is seen that for cross-section class 1 there is a high cross-section resistance since here it reaches full plasticity into strain hardening. If instead looking at cross-section class 4 low resistance is seen, local buckling appears before elastic moment is reached which also is shown in Figure 2.19 where the curve doesn't reached yielding.

2.5.7 Initial imperfections and residual stresses

When steel members are constructed, there is always some kind of imperfections that will make the steel member behave in a different way than an ideally perfect piece would have done (Al-Emrani & Åkesson, 2020). There can be effects like a column that are not straight, or some geometrical deviation and these aspects may strongly affect the ultimate load capacity of the column. To allow for these imperfections, so called initial imperfections are considered when designing a steel structure. When designing a steel beam accordingly to EN 1993-1-1, the effect of the initial imperfections is already included in the different buckling curves which are dependent on the geometry of the cross-section.

The effect that the initial imperfections have on the structure is dependent on the magnitude of the imperfections (Al-Emrani & Åkesson, 2020). The more initial imperfection there is, the larger effect it has on the buckling capacity of the structure and therefor the buckling capacity σ_{cr} needs to be reduced more, see Figure 2.21. As seen in the plot, unlike the buckling capacity, the initial imperfections have a negligible impact on the maximum load-bearing capacity σ_u which is the same for

both curves. When studying the figure, it is also seen that the transition at the bifurcation point, the point where σ_{cr} is reached, is smoother when initial imperfections are included. This transition is smoother, the more initial imperfections there is since the ultimate load-carrying capacity is not affected. Based on this, out-of-plane buckling will not appear dramatically for plates with initial imperfections and residual stresses, instead the buckling will appear in a gradual manner.

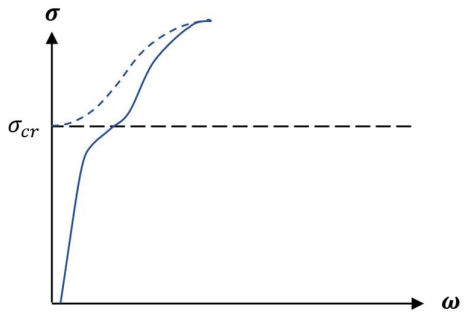

Figure 2.21 Schematic plot of the stress vs. lateral displacement which shows the influence that the initial imperfection has on the critical and ultimate stress of a plate subjected to compression. The dotted line is for an ideally perfect plate and the solid line is for a plate with initial imperfections.

The effect of the residual stresses is similar to the effects that the initial imperfections have and hence the effect is often hidden by the effect from the initial imperfections. Due to this, there might be a problem if there is of interest to separate the influence form residual stresses and initial imperfection. Therefore, the influence are considered in a combined effect in the codes that are used.

2.5.8 Post-buckling behaviour

A plate buckles at its critical load, the load that results in a loss of stability (Kubaik, 2013). When a plate buckles, it means that the plate has reached a system transition and the plate goes form one equilibrium (unbuckled plate) to another (buckled plate). If the load is still increased after buckling has occurred, the plate can behave in two different post-buckling equilibrium paths. If the displacement is increased when the load is increased, then the plate behaves in stable post-buckling equilibrium path. If instead the plate displacement increases with decreased load, then the plate behaves in an unstable post-buckling equilibrium path. The type of behaviour that occurs depends on the type of plate, type of loading, geometry, and size of initial imperfections.

The buckling behaviour of a thin-walled structure can be divided into four different stages, see Figure 2.22. The first stage is the unbuckled stage, prebuckling behaviour. Here the slope of the curve in the graph is related to the initial imperfections. If the initial imperfections are zero, then the shortening is zero and if the initial imperfections are increased, then the shortening is increased. At point A the stress has reached the buckling load and local buckling occurs. The second stage is the stable post buckling equilibrium path, here the plate can sustain further load and the displacement will increase. At point B, the stress has reached the yielding point and

the plate starts to plasticize or global buckling is reached (bifurcation point). If global buckling is reached, then it means that the behaviour of the plate is unstable and reaches a postcritical equilibrium path. The third stage is where the plate has an elastic-plastic post critical behaviour. This stage continues until the maximum load is reached (point C), this is the load carrying capacity of the steel structure. After point C is reached, the remaining phase is the failure stage (phase four).

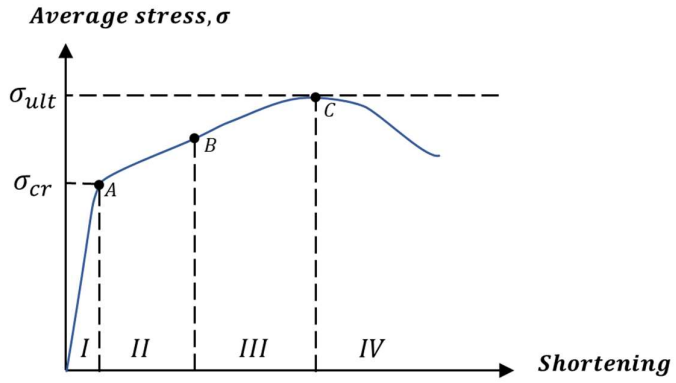

Figure 2.22 Stress-displacement relationship for a thin-walled structure. Figure based on Kubiak (2013).

2.5.9 Buckling modes

When looking at a beam or column with corrugated sheet metal, there is a risk for buckling for both the plate and for the web (Al-Emrani & Åkesson, 2020). Depending on the shape and boundary condition, the buckling mode and buckling magnitude are affected. To understand the behaviour of how the steel will deform, a plate is studied.

When a plate is subjected to compressive force it will remain straight until the buckling load is reached. After this load, some additional load can still be applied after buckling has occurred thanks to the post-critical reserve strength, shown in Figure 2.23.

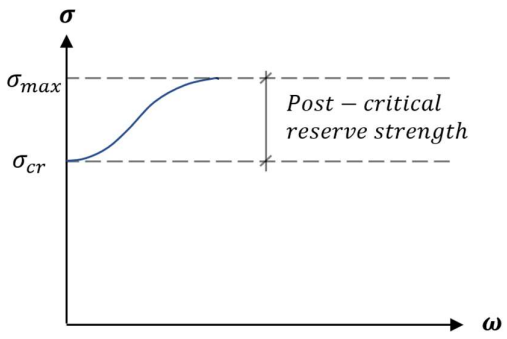

Figure 2.23 Stress-deformation relationship for a steel plate and the effect of post-critical reverse strength.

The reason that the plate can carry additional load once reaching the buckling load is that membrane forces are formed which stabilizes the buckle through a transverse tension band. The area that has buckled loses a major part of its stiffness and due to

this, the force in the plate needs to be spread around the buckle, to the unbuckled area which is stiffer (Al-Emrani & Åkesson, 2020). When the compressive force is spread to the edges of the plate, a transversal membrane in tension is created through the buckle to keep force equilibrium in the plate, see Figure 2.24.

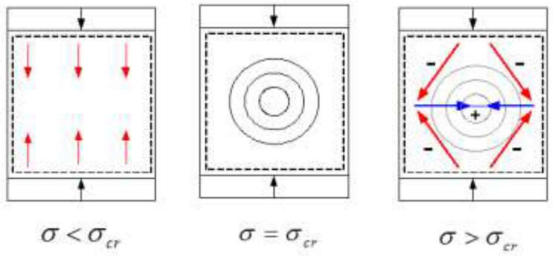

Figure 2.24 Schematic figure of how the force is spread in the plate before and after the plate has buckled (Al-Emrani & Åkesson, 2020).

How the plate will behave when subjected to compressive force is depending on the boundary conditions (Al-Emrani & Åkesson, 2020). The boundary conditions effects both the location of the buckle, the shape of it and the magnitude of it, see examples in Figure 2.25.

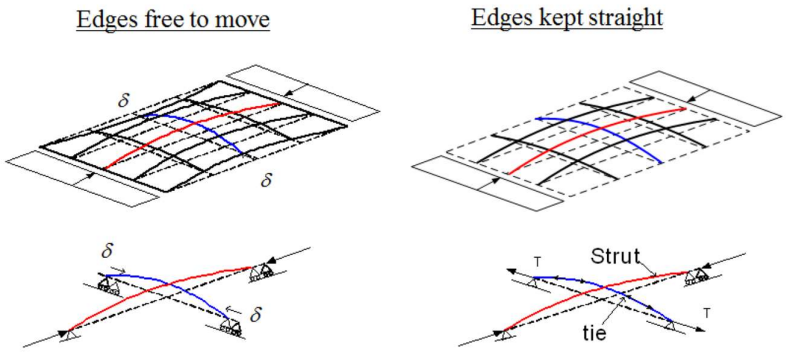

Figure 2.25 Behaviour of a steel plate subjected to compressing force, two different types of boundary conditions (Al-Emrani & Åkesson, 2020).

To calculate the deformation ω in a general solution, equation (*2.24*) is used where A is a constant, m is the number of buckles in the longitudinal direction, n is the number of buckles in the transversal direction, a is the length of the plate (unloaded edge) and b is the width of the plate (loaded edge).

$$\omega = A \cdot \sin\frac{m \cdot \pi \cdot x}{a} \cdot \sin\frac{n \cdot \pi \cdot y}{b} \tag{2.24}$$

When looking at a slender steel web plate subjected to patch loading, there is three different kinds of failure modes that may appear (Al-Emrani & Åkesson, 2020). The failure modes are crushing, web crippling and web buckling, see Figure 2.26 for illustrations of the failure modes.

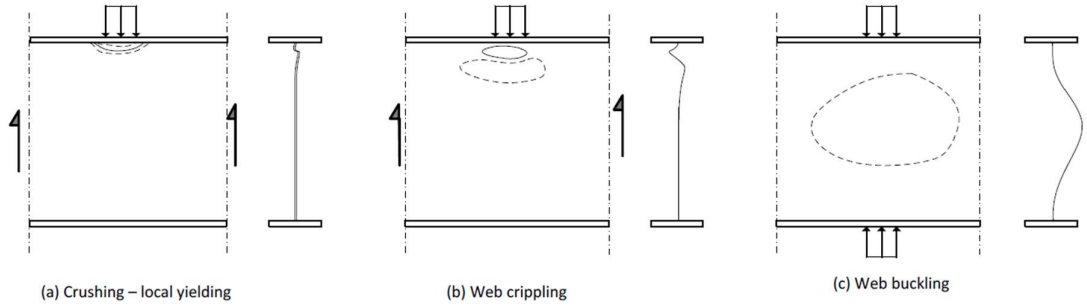

Figure 2.26 Three different kinds of failure modes that may appear for a slender steel web plate (Al-Emrani & Åkesson, 2020).

The buckling mode crushing occurs when there is local yielding of the web and therefore there is plastic collapse of the web (Al-Emrani & Åkesson, 2020). This case appears when the web is compact with a slenderness ratio *b/t*, plate width *b* divided by plate thickness *t*, which is sufficiently small. The second buckling mode, web crippling, is when there is local buckling under the applied load. In this case local buckling is reached in the web closest to the place where the load is applied. If instead looking at the third buckling mode, web buckling, this occurs when the entire web underneath the applied load buckles. Both web crippling and web buckling appears when the web is very slender which leads to buckling due to instability. Web crippling is the mode that appears when the web is intermediate slender.

2.5.10 Forms of stability loss

A stability loss can happen in different kinds of forms where interactive buckling or coupled buckling is the most dangerous form (Kubaik, 2013). The reason for this is that interactive buckling often causes the structure transition from the equilibrium path to unstable equilibrium path. This makes the structure collapse even when the load is lower than the critical load. The phenomenon interactive buckling appears when the critical load corresponding to (two or more) different buckling modes almost have the same magnitude.

2.5.11 Stiffeners

To increase the maximum load bearing capacity of a plate, stiffeners can be added. By adding stiffeners in the zones where the expected maximum amplitude of the buckling would appear, the risk for normal stress buckling is prevented or delayed (Al-Emrani & Åkesson, 2020).

There are two different types of stiffeners that can be added to a plate, transverse stiffeners, and longitudinal stiffeners. Transverse stiffeners are added vertically on the plate while longitudinal stiffeners are added longitudinally on the plate.

When studying slender plates subjected to compressive load, the ultimate load-carrying capacity depends on the effective width b_{eff} of the plate and hence the effect of an increasing width is small. If instead adding a longitudinal stiffener, a larger influence is seen on the capacity of the plate, see Figure 2.27.

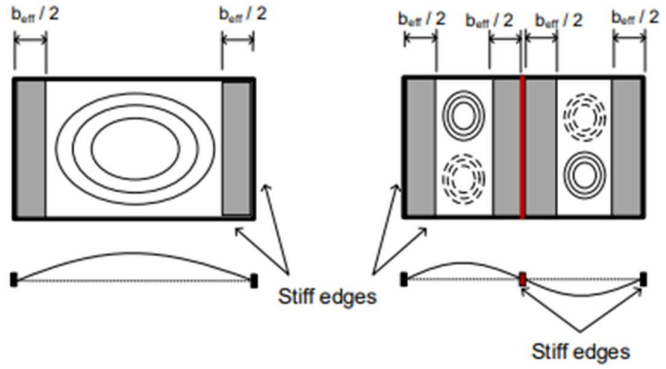

Figure 2.27 Effective with of a plate subjected to compressive force with and without a longitudinal stiffener (Al-Emrani & Åkesson, 2020).

For the plate to have the full impact on the effective width, the stiffener needs to fulfil the following two conditions stated by Al-Emrani & Åkesson (2020):

- "The stiffener should not buckle locally (i.e., should not be in class 4)"
- "The stiffeners (along with an effective part of the plate on both sides of the stiffener) should not buckle globally, e.g., column-type of buckling or torsional buckling".

If both conditions are not fulfilled or if they are only partly fulfilled, the effect from the stiffener will not be maximally utilized and therefore capacity needs to be reduced.

If adding a longitudinal stiffener to a plate the critical stress capacity can be increased while the impact from the post-critical strength is reduced. This means that the proportion between the ultimate load and the critical stress is decreased when the buckling load is increased, see Figure 2.28. If the increase in buckling load is increased large enough, the influence from post-critical strength might be negligible and the plate will have a column like behaviour. This is the case for heavily stiffened plates. Based on this, a stiffened plate should be designed both regarding column-like behaviour and plate-like behaviour.

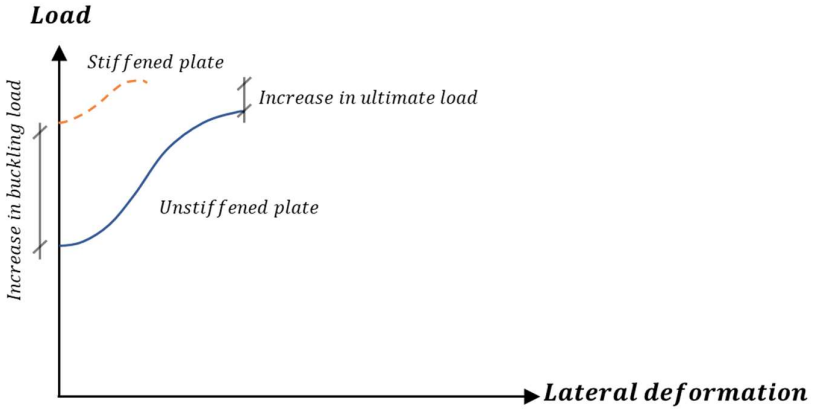

Figure 2.28 Load-displacement relationship for an unstiffened- and stiffened plate.

2.5.12 Dynamic loading and dynamic critical load

Based on previous studies it is seen that there is some difference between the buckling in the dynamic case and the static case (Kowal-Michalska & Mania, 2008). The dynamic behaviour of how a steel plate is affected by an in-plane pulse loading depends on the quantity of pulse intensity, the amplitude and duration of the load.

According to Kowal-Michalska & Mania (2008), the dynamic critic load is the amplitude of pulse force that causes the dynamic buckling of the steel plate. This load is affected by the degree of initial imperfections and the load increases when the initial imperfections are decreased. To determine the dynamic critical load, this needs to be made based on one of the criteria that exist. Three of the most popular criteria to use are Volmir´s, Budiansky & Hutchinson, and Petry-Fahlbusch Criterion (Kubiak, 2013). How these three different Criterions are defined and how they differ are described below based on Kubiak's text.

Volmir´s Criterion is based on a work where he looked at how a simply supported rectangular plate behaved when it was subjected to different impulse loads (Kubiak, 2013). In the work, Volmir studied the pulse of infinite- and finite duration. The type of pulses that he took into consideration was of a rectangular and exponentially decreasing shape. Bubnov-Galerkin method was used to solve the dynamic buckling problem and solve the buckling and post buckling state for statically loaded structures. Volmir created a relationship where he looked at the load and deflection over time and by doing that, he obtained the equations of motion which are solved by using a numerical method. Both the tensile load pulses and the shear type were considered in the analysis. Based on the results, Kubaik presented a method to calculate the critical dynamic load which is simple to use but time consuming.

When using the method, the buckling mode was assumed and the dynamic response calculated (Kubiak, 2013). For each critical mode, a dynamic load factor (DLF) was determined which was defined as the ratio of the dynamic buckling load N_{cr}^{dyn} divided by the critical static load N_{cr}^{stat}, see equation (2.25).

$$DLF = \frac{N_{cr}^{dyn}}{N_{cr}^{stat}} \tag{2.25}$$

Based on the results that Volmir saw, he stated his Criterion for the dynamic stability loss and in this criterion, he assumed that the loss of stability that occurs in a plate subjected to pulse loading appears when the maximum deflection reaches the same magnitude as the assumed constant value. The Buckling criterion that Volmir formulated is according to Kubaik (2013) as follows:

> *"The dynamic buckling occurs at this mode for which the deflections grow the most rapidly and the dynamic buckling load corresponds to the pulse amplitude at which the maximal deflection equals some chosen vale".*

Budiansky & Hutchinson Criterion is one of the initial displacement criterions that was formulated which involves both the effect from geometrical imperfections and the unstable post-buckling equilibrium. In the study, a cylindrical shell and rods which was axially loaded was studied. The type of pulse load that was considered in the study was both of finite- and infinite duration. They then derived the relation

which allowed them to determine the critical load which corresponded to the inflection point when looking at the relationship between the load and the deflection, see Figure 2.29. Based on the results Budiansky and Hutchinson defined according to Kubaik (2013) the following criteria:

> *"A loss of stability of structures subjected to pulse loading occurs when there is an unlimited increase of deflection for small increments of load."*

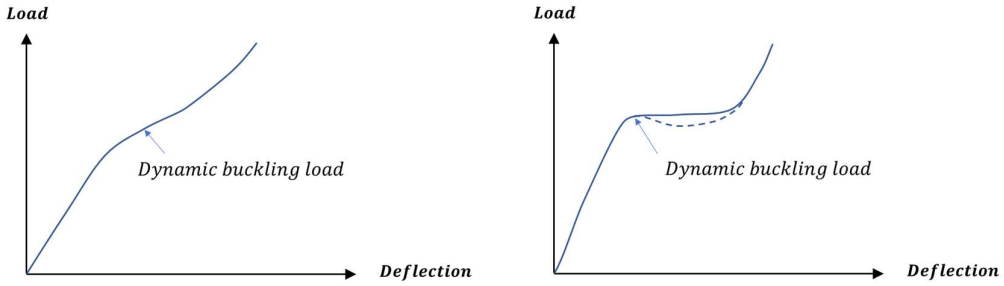

Figure 2.29 Load-deflection relationship where the point for the dynamic buckling load can be seen for both large (left) and small (right) initial imperfections. Graphs based on Kubiak (2013).

Furthermore, a dynamic failure criterion is defined by Petry and Fahlbusch which is valid for linear elastic – perfectly plastic materials (Kowal-Michalska & Mania, 2008). In the criterion it is said that a dynamic response for an isotropic plate is dynamic stable when the following conditions are fulfilled for all the locations in the structure, all the time. The effective stress σ_{eff} should be equal to or smaller than limit stress σ_L. Based on this criterion, the dynamic failure load can be calculated, using equation (2.26) or (2.27). When looking at the dynamic failure criterion, it is strongly influenced by the material data and the applied failure criterion.

$$DLF_{cr} = \frac{N_{f_{cr}}^{dyn}}{N_{cr}^{stat}} \tag{2.26}$$

$$DLF_{f} = \frac{N_{f_{cr}}^{dyn}}{N_{f_{cr}}^{stat}} \tag{2.27}$$

Where $N_{f_{cr}}^{dyn}$ is the dynamic failure load and $N_{f_{cr}}^{dyn}$ is the static failure load.

2.5.13 Parameters affecting dynamic response of steel plates

The geometric imperfections, shape of pulse loading and, and duration time of pulse loading are factors that strongly affect the dynamic behaviour of steel plates (Kowal-Michalska & Mania, 2008). Kowal-Michalska & Mania studied a plate subjected to axial pulse loading, see Figure 2.30. The influence of pulse shape was investigated under the assumption of equal amplitude at constant duration time for different pulses and then the rectangular pulse always causes the largest deflections. When looking at pulses of short duration, the deflections caused by rectangular loading grow more rapidly but for duration time equal to the period of natural vibrations larger deflections correspond to a sinusoidal pulse.

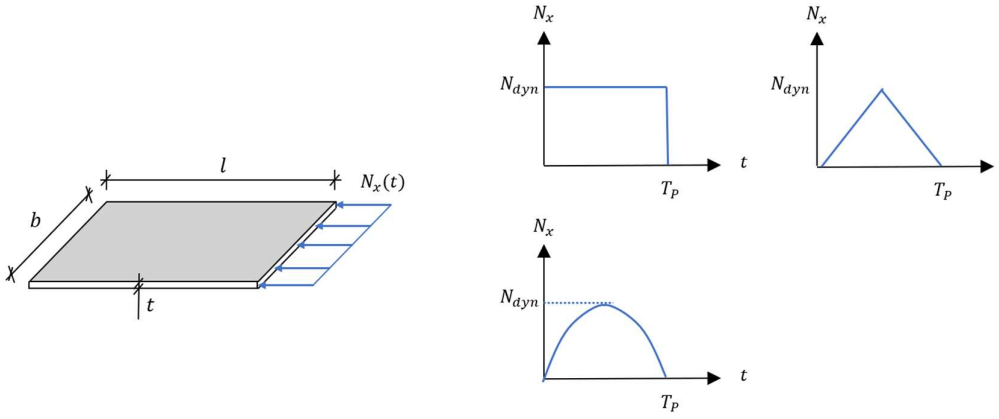

Figure 2.30 Plate geometry and loading of the plate with corresponding shapes of pulse loading. Figure based on Kowal-Michalska & Mania (2008).

2.5.14 Dynamic buckling

When a structure is subjected to dynamic loading, dynamic buckling may occur (Kubaik, 2013). How this phenomenon will occur and when depends on the so-called pulse intensity, the duration of the pulse load and the amplitude of it. If the load has a very short duration in combination with a load amplitude that has a magnitude which is relatively high, then an impact phenomenon is observed. If instead looking at a case where the duration time corresponds to the time period of natural vibrations and where the load amplitude has a average magnitude, then this is when dynamic buckling occurs. Furthermore, if looking at the same magnitude of load amplitude but now the duration is a long period, then it is quasi-static load. When comparing the static buckling load with the dynamic critical load for a short pulse duration, then the dynamic critical load can be of a higher magnitude than the static buckling load. Kubaik (2013) is mentioning that when looking at the dynamic critical load in the elastic range, the damping effect can be neglected due to the size of the response which will be less than 1 %.

Kubaik (2013) are also mentioning that since dynamic stability loss only appears for a structure with initial imperfections, the dynamic bifurcation load does not exist. Instead, when looking at a structure without geometrical imperfections (ideal structure) the critical dynamic buckling load tends to infinity. This phenomenon can be seen like it is strengthening the imperfections, the effect from the dynamic buckling increases the effect that the initial imperfection causes. The load when dynamic buckling occurs for a structure should be defined based on one of the criterions that exists, which these criterions are and how to calculate are described in Section 2.5.12.

2.6 Solving nonlinear problems using FEM

The Finite element method (FEM) is one of the most effective approaches to analyse the non-linear behaviour of structures. In general, the method requires a lot of computation effort due to large number of unknown mainly as it involved several numerical integration procedures. The problem is nonlinear when the stiffness matrix

varies as the applied load increases and when the load vector depends on the displacement. There are namely two non-linearities and they are the geometric non-linearity and the material non-linearity. Geometric nonlinearity is associated with changes in geometric configuration and material nonlinearity is associated with changes in material properties. The following methods can be used to solve nonlinear problems.

When solving a nonlinear problem using FEM, there is two different kinds of numerical approaches that can be used to solve the load increments (Plos et al, 2021). These two approaches are Implicit solution method and Explicit solution method. In the Implicit solution method, the result is based on information from the current increment and the previous ones. When using this method, an iteration procedure needs to be used for each increment to be able to find equilibrium. This method can be used both when studying a static case and when studying a case with dynamic load. If instead using the Explicit solution method, the result is based only on the information from the previous increments and hence, no iteration procedure is needed. This method is mainly used when studying a case with dynamic load even though the method also can be used when studying the effects from a static load. When using Explicit method there is a "cost" since the load increment has to be very small to fulfil the requirements for it to be used while for the implicit method much larger load increments can be used. The need of a small timestep is also a reason why explicit method is effective to use for structures subjected to impulse loading since the time step in such cases need to be small anyway.

When solving a problem with implicit method three different iteration methods can be used, tangent stiffness method, initial stiffness method and secant stiffness method, see Figure 2.31. Which method to use depends on both the problem that is investigated and the used material model.

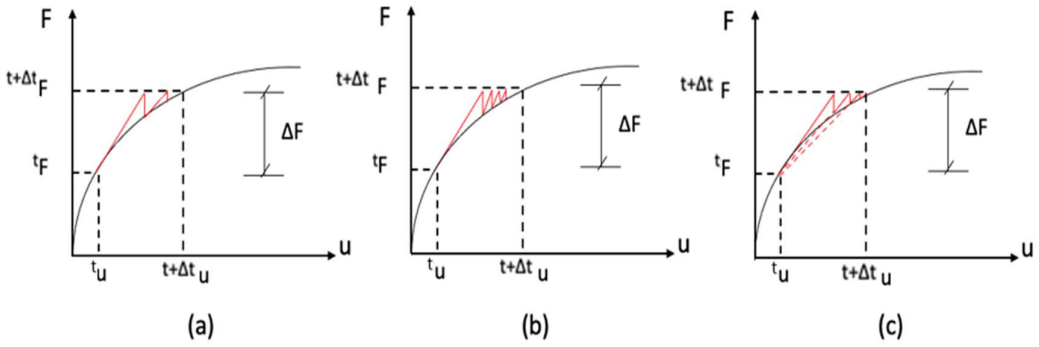

Figure 2.31 Three different iteration methods to use in an implicit solution method, (a) tangent stiffness method, (b) initial stiffness method and (c) secant stiffness method. Based on Plos et al. (2021)

The value of the tolerance for when the solution is seen as good enough depends on the type of iteration method that is used. The method also influences the type of tolerance and the number of iterations that is needed to find the solution. To achieve a stable converging analysis, there can be a need of using a bigger tolerance. This type of solution can still be reliable but if possible small tolerance is preferably used since that might improve the overall convergence.

When using iterations to solve a problem, three different methods to calculate the load-displacement relationship can be used. These three methods are load-controlled, displacement-controlled and arch length method, see Figure 2.32. The simplest method to use is the load-controlled where the force is increases step by step. Due to this, it is not possible to detect the response when the force is decreased with increasing displacement, instead the part where this happens will be kept out of the results and there may instead be a considerable big increase in the displacement between two iteration points. If the load capacity do not increase again beyond the current load point no solution will be found. If instead using displacement-controlled method, decrease in loading with increase in displacement will be included. However, the part where the decrease in both force and displacement will still be missing in the achieved result, the so-called snap-back part. If using the arch-length method, both these parts will be included in the solution and if the iteration steps are small enough, the full response may be captured.

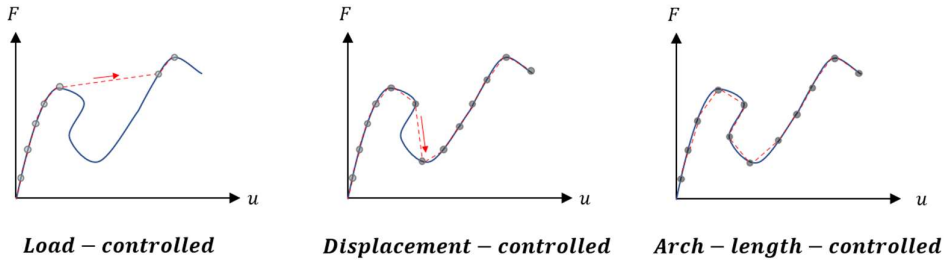

Figure 2.32 The three different iteration methods that can be used when studying load application on a structure. The dots are the solution from the stated method and the solid line is the actual solution. Figure based on Plos et al. (2021).

3 Previous studies

3.1 Orientation

In the past, several studies, e.g., Paik & Thayamballi (2003b) and Yang et al (2018), have been made which is related to this study. When looking at blast loaded plates, most of the experiments that have been done is where the plate is subjected to the blast load transversally. In the studies, different geometries have been studied to see the impact of it. Some parameters where the impact has been analysed is slenderness of the plate, distance to the explosion and if they are unstiffened or stiffened. When looking at stiffened plates, different geometries of the stiffener have been studied (horizontal, transversal, round etc.) and the number of stiffeners.

When looking at previous research of this type, it is seen that the software Abaqus CAE is commonly used, e.g. Yang et al (2018). It is also seen that in most of the cases, shell elements are use when modelling the plate.

3.2 Paper 1 – Experimental study of a steel plate

One experimental study that has been performed is where a ship plate is loaded with axial dynamical loading (Paik & Thayamballi, 2003b). In this study the dynamic ultimate compressive strength of the plate was investigated by applying an axial compression load of various load rates.

The tested plate was simply supported along all edged to keep the edges straight. The compression load was applied by using a hydraulic dynamic testing machine with capacity of 100 kN. The test setup is shown in Figure 3.1 and the material properties of the test specimen are shown in Table 3.1.

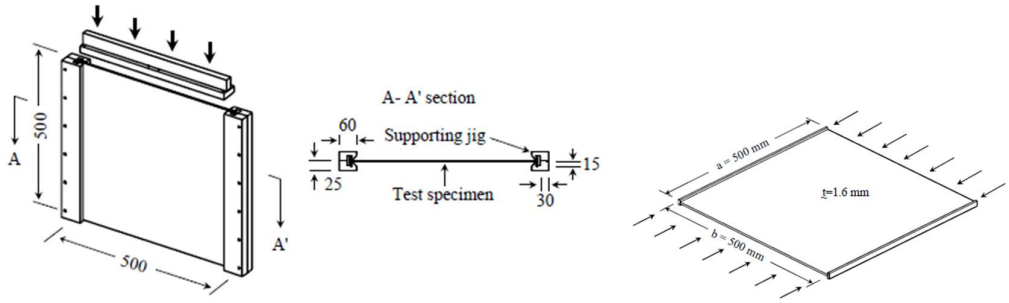

Figure 3.1 The test setup, the geometry of the test speciment and the loading situation (Paik & Thayamballi, 2003b).

Table 3.1 Material properties of the test specimen.

Yield stress, σ_y [MPa]	252
Ultimate tensile stress, σ_T [MPa]	360
Young's modulus, E [GPa]	198
Elongation [%]	39.5

The rate of which the load was applied, was controlled by a personal computer and the speed was kept constant during each test period. When the tests were performed, the computer was documenting the in-plane displacement and out-of-plane deflection for each timestep. The experimental study was performed for varying loading speeds v_0 within the range 0.05 mm/s to 400 mm/s. The test lasted until the ultimate strength of the plate was reached and sometime after.

According to the authors of the paper, the results from the experiments showed that an increase in loading speed results in an increase in ultimate compressive strength and in-plane stiffness. The reason they saw for this is that when the loading speed is increased, the strain rate of the material is increased. Another thing that the results from the experiment shows is that the lateral displacement and axial deflection up to the ultimate limit state increases rapidly when the loading speed is increased, see the plots in Figure 3.2. When studying the graph, Paik & Thayamballi (2003b) also states that the unloading behaviour is more rapid when the loading speed is increased. Due to this, an increase in loading speed will result in a more unstable behaviour for the material after the ultimate state is reached.

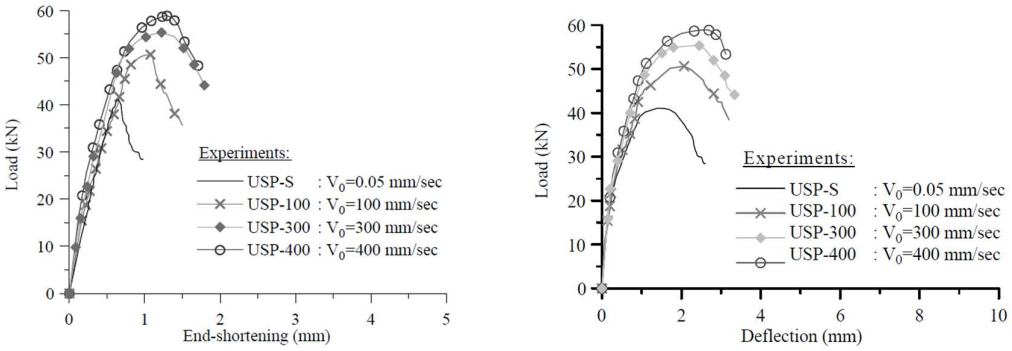

Figure 3.2 Relationships between load and displacement/deflection when varying the loading speed (Paik & Thayamballi, 2003b).

Furthermore, the authors studied the relationship between the strain rate and the ratio between the ultimate design stress and the ultimate stress. Here the strain ratio is defined as the applied velocity divided by the length of the plate. To describe the strain rate relationship, he Cowper-Symonds equations is used with the parameter D=40.4 s^{-1} and q=5. The results from the experiment showed a good fit to the curve created based on the empirical formulation, see Figure 3.3.

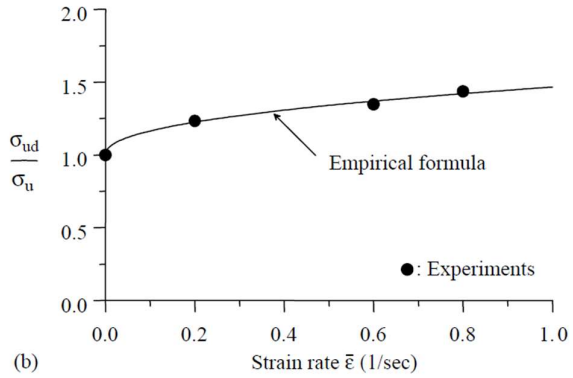

Figure 3.3 Relationship of ratio of stress and strain rate for the experimental plate (Paik & Thayamballi, 2003b).

3.3 Paper 2 – Finite element study of a steel plate

This paper from Yang et al (2018) includes the extensive non-linear FE analysis of ship plates and the determination of their dynamic ultimate strength and comparing it to the results from experimental tests and then formulating an empirical formula for calculating the ultimate strength of rectangular plates under in-plane compressive loading.

The applicability of the FE analysis is verified using Abaqus CAE with the experimental results of Paik & Thayambali (2003b) done on a simply supported rectangular steel plate keeping all four edges straight, see Figure 3.4 for overall deflection shape and Section 3.2 for a brief description of the experimental paper. The strain rate is expressed as a function of loading speed V_0 and based on the loading speed the ultimate strength and the end-shortening from the numerical method was compared to the results that Paik achieved in his experiment, see Table 3.2.

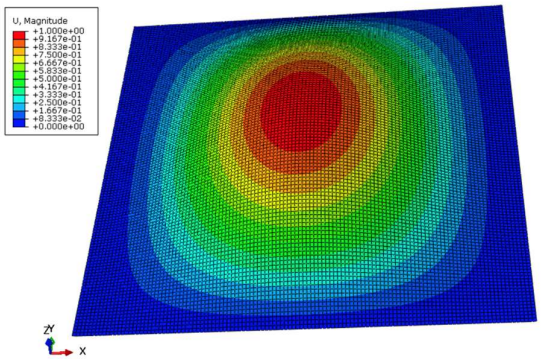

Fig. 2. Initial deflection shapes: Overall deflection shape.

Figure 3.4 Shows the contour plot of the initial overall deflection shape from the numerical analysis (Yang et al., 2018).

Table 3.2 Comparison between the test- and numerical results (Yang et al., 2018).

Loading speed [mm/s]	Test results		Numerical results		Error
	Ultimate strength [kN]	In-plane displacement [mm]	Ultimate strength [kN]	In-plane displacement [mm]	Ultimate strength error
0.05	41.2	0.63	38.0	0.60	7.6 %
100	50.6	1.07	45.7	0.62	9.7 %
300	55.6	1.23	54.0	1.01	3.0 %
400	59.2	1.27	58.1	1.28	1.9 %

In this paper the plate buckling mode is regarded as the initial deflection of the ship plating with an average level ($w_{0max} = b/200$). Various plate geometries, plate slenderness ratios and different yield stresses were studied for different strain rates.

3.4 Input for the analytical- and numerical analysis

3.4.1 Basic geometry and boundary conditions

Based on the two papers a recreation of the same type of study is made using static and dynamic analyses, see Chapter 4 and 5. The basic geometry, boundary conditions and material properties used in Abaqus CAE are based on the information given in the two papers from Paik & Thayamballi (2003b) and Yang et al (2018).

To verify the model used in Abaqus CAE and make sure that the load and the boundary conditions are applied in a way that replicates the actual case of the plate, the geometry that is modelled is the same geometry as the one used in the two previous studies from Paik & Thayamballi (2003b) and Yang et al (2018). This geometry has the geometry shown in Figure 3.5 and the geometrical properties is shown in Table 3.3.

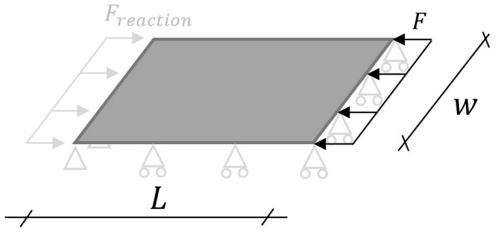

Figure 3.5 Illustration of the plate geometry showing the location of the applied edge load and the boundary conditions.

Table 3.3 Geometrical properties for the basic plate.

Width, w [mm]	Length, L [mm]	Thickness, t [mm]
500	500	1.6

Several different boundary conditions are studied and compared to find the best way to describe the actual behaviour of the plate studied in the articles. In some models the rotation of the plate is fixed along two or more edges and in some of the studied models the unloaded edges are fixed in y-direction. Based on the results the following boundary conditions are picked.

The plate is free to rotate and fixed in z-direction along all edges. The load is applied along one edge and the opposite edge is fixed in x-direction which creates a reacting force $F_{reaction}$ in the same size as the applied load F, see equation (3.1).

$$F = F_{reaction} \tag{3.1}$$

3.4.2 Material properties

The material properties that are mainly used for the plate are picked based on the papers from Paik & Thayamballi (2003b) and Yang et al (2018) and are shown in Table 3.4.

Table 3.4 Material properties of the basic plate for material A. Partly based on the papers from Paik & Thayamballi (2003b) and Yang et al (2018).

Young's modulus [GPa]	Poisson's ratio [-]	Yield stress [MPa]	Ultimate tensile stress [MPa]	Plastic strain [-]	Density [kg/m^3]
199	0.3	252	360	0.19	7 800

$$\varepsilon_{pl} = \varepsilon_{tot} - \frac{\sigma_s}{E_s} \tag{3.2}$$

Where ε_{pl} is the plastic strain, ε_{tot} is the total strain, σ_s is the steel stress and E_s is the Young's modulus of the steel.

The plastic strain is determined with equation (3.1). The plastic behaviour of the material is shown in Table 3.5 and a stress-strain graph is shown in Figure 3.6. As seen in the figure, the relationship is simplified as linear between the specified points.

Table 3.5 Plastic properties of the material used in Abaqus CAE for the test material, material A.

Yield stress [MPa]	252	253	303	337	351	359	360
Plastic strain [-]	0.000	0.011	0.025	0.045	0.069	0.099	0.190

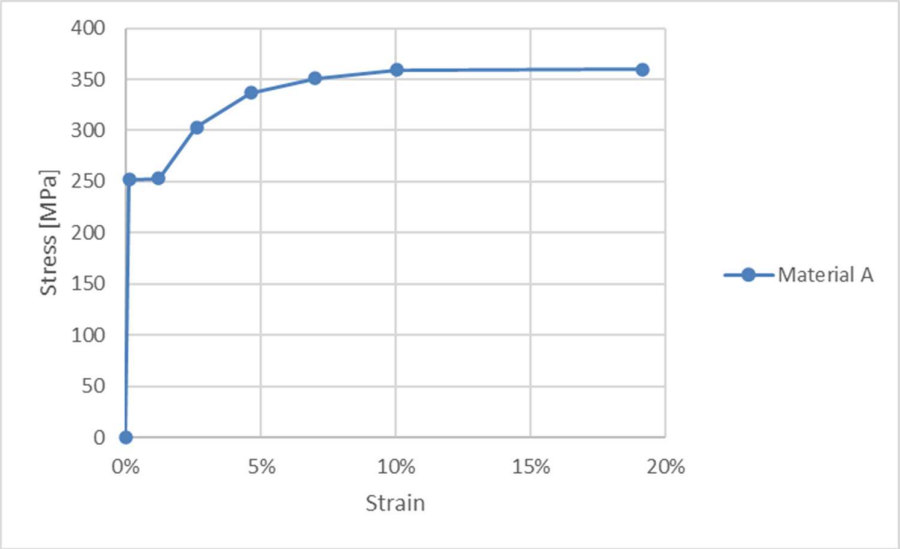

Figure 3.6 Stress-strain relationship for the steel material used in the Abaqus CAE model, material A.

Geometrical imperfections are applied to the model to consider the 2nd order effects in the analysis. Different geometrical imperfections are compared to investigate the effect of the initial imperfection. Further, when studying this effect, the position where the maximum out-of-plane deflection and the position where the maximum in-plane displacement appears are studied. This is further described in Section 4.3.

To simulate the effect of various yield and ultimate strength, which is an approximate way to simulate the potential effect of high strain rates, the material is adjusted according to equation (3.3) to (3.6).

$$f_{y,B} = 1.2 \cdot f_{y,A} \tag{3.3}$$

$$f_{u,B} = 1.05 \cdot f_{u,A} \tag{3.4}$$

$$f_{y,C} = 1.4 \cdot f_{y,A} \tag{3.5}$$

$$f_{u,C} = 1.1 \cdot f_{u,A} \tag{3.6}$$

A linear relation of the increased stress is used for the strain values between the yield strain f_y and the ultimate strain f_u which gives plastic properties to material B and C as shown in Table 3.6.

Table 3.6 Plastic properties of the material used in Abaqus CAE for the adjusted materials, material B and C.

Material B

Yield stress [MPa]	0	302	303	342	365	373	377	378
Plastic strain [-]	0.000	0.010	0.017	0.029	0.048	0.074	0.12	0.220

Material C

Yield stress [MPa]	0	352.8	353.5	381	392	394.9	395.9	396
Plastic strain [-]	0.000	0.010	0.017	0.029	0.048	0.074	0.12	0.220

The results are also compared to material B_2 and C_2 where the yield strength is the same as in material A and the ultimate strength is increased according to equation (3.4) and (3.6). Following this, a linear relationship is used between the increase in ultimate strength and zero increase for the yield strength which gives the following plastic properties shown in Table 3.7. Young's modulus, Poisson's ratio and the density of the material is kept the same for all the materials, see Table 3.4.

Table 3.7 Plastic properties of the material used in Abaqus CAE for the adjusted materials, material B_2 and C_2, where only the ultimate strength is increased.

Material B_2

Yield stress [MPa]	0	252	235	310	350	367	377	378
Plastic strain [-]	0.000	0.010	0.017	0.029	0.048	0.074	0.12	0.220

Material C_2

Yield stress [MPa]	0	252	253	317	364	383	395	396
Plastic strain [-]	0.000	0.010	0.017	0.029	0.048	0.074	0.12	0.220

To compare the plastic properties of the five materials, the stress strain relationship is plotted for each of the steel materials and a comparison is shown in Figure 3.7 .

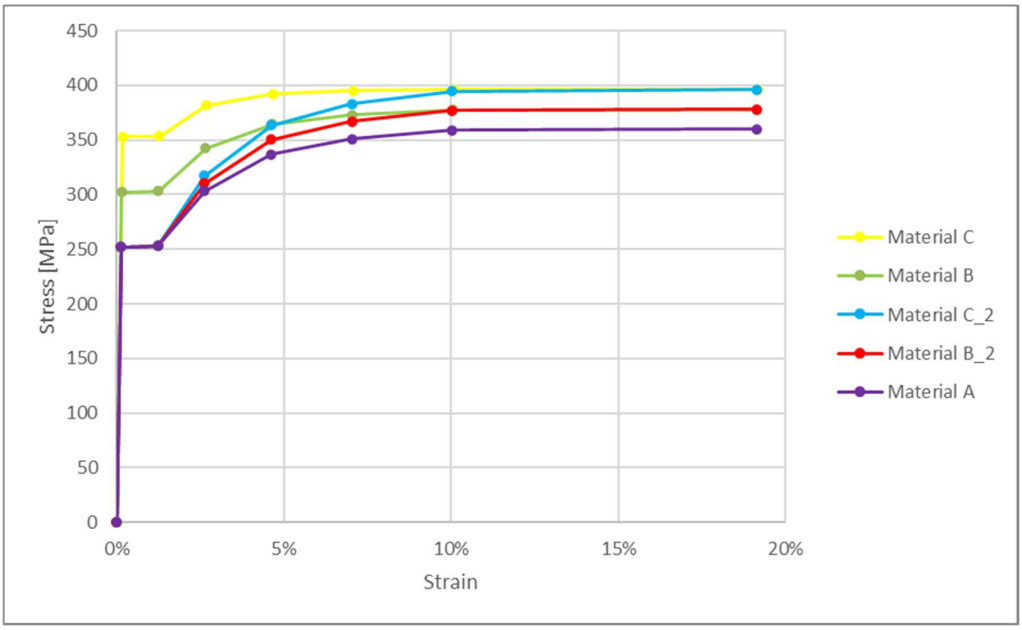

Figure 3.7 Stress vs. strain relationship of the studied steel materials.

3.5 Abaqus CAE model

- Geometry:
  The plate was modelled in Abaqus CAE using shell elements S4R: A 4-node doubly curved thin or thick shell, reduced integration with hourglass control, finite membrane strains with 5 thickness integration points.

- Main boundary conditions:
  The plate as explained in the experimental paper from Paik & Thayamballi (2003b) is simply supported initially in all four sides and then the load was applied initially on one side of the plate axially as a uniformly displacement along one side of the plate which then replicated the actual static case. In dynamic analysis the same load was applied as velocity controlled with a defined amplitude.

- Buckling analysis of the plate:
  The eigenvalue buckling is generally used to estimate the critical buckling loads and they can provide useful estimates of the different collapse mode shapes of the plate. Abaqus/Standard offers two eigenvalue extraction iteration methods, and they are Lanczos and Subspace iteration method. In this case the default Subspace iteration Eigen solver was used and the maximum number of iterations was set to 30.

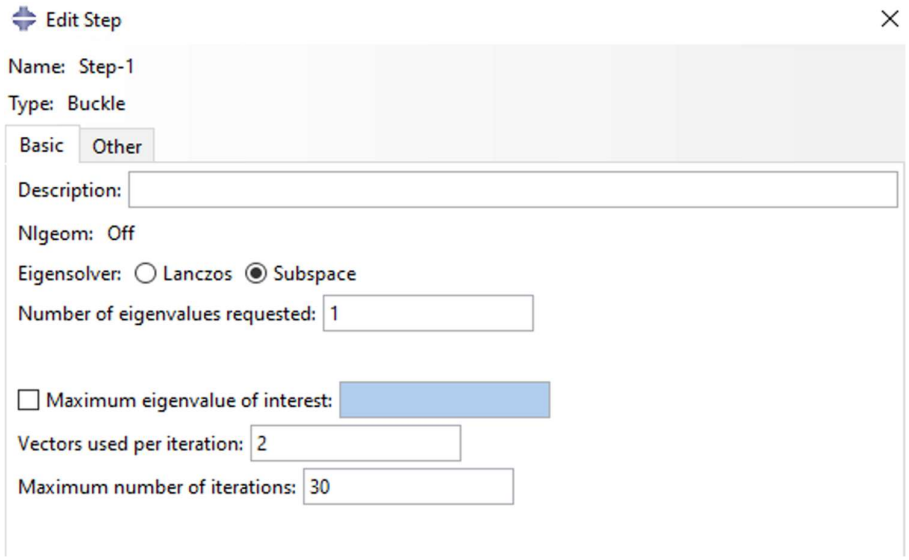

Figure 3.8 Step settings used in Abaqus CAE for buckling calculation.

- Static analysis:
  The Non-linear static analysis was done using the general static method in Abaqus CAE with nonlinear geometry. Here the default time period "1" was chosen and the automatic time stepping scheme is chosen as shown in the plot where the maximum number of increments and increment size chosen is shown. In the static analysis the load is applied as a prescribed displacement which is put to 1mm. Further, in some parts of the study, a total displacement of 2 mm is used.

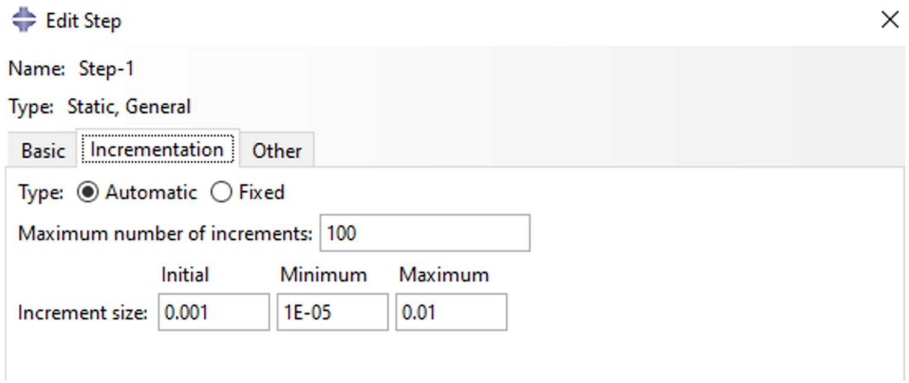

Figure 3.9 Increment settings for static analysis in Abaqus CAE.

- Dynamic/Explicit analysis:
  The explicit dynamics procedure performs a large number of small times increments efficiently. The default incrementation scheme in Abaqus/Explicit is fully automatic and does not require user intervention. The explicit dynamics procedure is suitable for analysing high-speed dynamic events but many of the advantages are also applicable for analyses with slower processes.

Within the study, described in Chapter 4 and 5, several different input parameters were tried and studied, they are as mentioned in the brief description of the study below (the final values are presented using bold font).

A mesh convergence study is made where several different mesh sizes were used to find an appropriate mesh size. The mesh size was varied from coarse to very fine with the following values {2, 5, **10**, 20, 50} mm.

The influence of different sizes of the initial imperfection are studied where the initial imperfection of the plate is varied as follows {1.5, 2.0, **2.5**, 3.5, 5} mm.

Different material properties are studied where the ultimate strength of the material is changed {**360**, 378, 396} MPa. In parts of the study, also the yielding strength of the material is changed for the material {**252**, 302, 353} MPa in combination with increased ultimate strength.

Different settings are used for the boundary conditions to see the influence of fixing different parameters. The case which is mainly studied in this study is where the plate is seen as simply supported along all edges. This case is compared to the settings used in the paper from Yang et al (2018) and additionally 5 more cases.

To see the influence of applying small edge beams to the unloaded edges of the plate, like the one seen in Figure 3.1, a study is made with varying sized of beams like this. In all cases the thickness of the beams is used as 1.6 mm and then the height is varied with the values {**0**, 10, 20, 30} mm.

The static analysis of the plate is followed by a dynamic study. In the dynamic study of the plate, both implicit and explicit model is used. In the dynamic analysis the load is applied as a velocity with varying magnitude {0.05, 1, 5, 10, 20, 50, 100, 200, 400} mm/s. Different kind of load applications were studied where the load is applied as constant or with linear or multi-linear ramp-up of various time rates.

The result of the case where a velocity of 0.05 mm/s are compared to the static results to examine if this dynamic load case can be regarded as static loading.

Further, a damping study is made where damping is applied to the plate using coefficients based on calculations using Rayleigh damping.

A strain rate study is made where strain rate is added to the plate using power law and the prescribed values for the variables according to the paper from Yang et al (2018). In the paper Yang et al calculates the strain rate based on the rate between velocity and the length of the plate, only the in-plan strain is considered. Based on the results from this study, the strain rate application in Abaqus CAE is studied by looking at a single element rod subjected to an axial force. The strain rate is extracted from the element and therefor both buckling strain and in-plain strain is included. The effect of the strain rate application is studied using both the function Power law and the function Yield ratio available in Abaqus CAE. In the study the values of the parameters are changed where D is set to {40.4, 1000, **1304**} and the exponent q to {5, 2, **4.83**}. Based on the strain rate study for the rod, the parameters and method used to apply strain rate is picked which later is used in the strain rate study of the plain plate.

3.6 Buckling analysis of the plate

In the static and dynamic analyses, the calculations are made based on a file which is created based on the buckling mode for the specific case. For each load case the specific boundary conditions were picked and the Abaqus procedure *Linear perturbation – Buckle* is used. One buckling mode was picked as the number of requested eigenvalues and by running the job, the linear buckling load capacity was estimated. This value was then compared and confirmed with hand calculations, shown in Appendix A.

To save the shape of the buckling mode as a *.fil extension the following two lines were added to the keywords in the model. The lines were added in Abaqus CAE just before the line END STEP.

```
* NODE FILE, GLOBAL=YES, LAST MODE=1
U
```

When the buckling file is run after the two lines are added, a text file with the same name as the job will be generated. This file is later used in both the static and the dynamic analysis.

4 Static analysis

4.1 Orientation

The static analysis of the steel plate was studied for the quasi-permanent load case and the following studies was done on the plate based on the input described in Chapter 3. Based on the static model, a convergence study was made to find an appropriate mesh size and except that, the following parameters were studied: initial imperfection, material properties, load application and boundary conditions of the plate.

4.2 Mesh convergence

A convergence study was made on the plate for different mesh sizes to make sure that the mesh size was sufficiently small. The study is made for two different cases, one where the eigenvalue from the buckling analysis is studied and one case where the force versus in-plane displacement is studied. For each case, several different mesh sizes of various sizes are used and compared see Table 4.1 for relationship between mesh size and number of elements.

Table 4.1 Relationship between mesh size and number of elements.

Mesh size [mm]	Number of elements
50	100
20	625
10	2 500
5	10 000
2	62 500

When studying the convergence of the calculated eigenvalue based on the buckling analysis, it is seen that the change in result when using mesh sizes finer than 20 mm is negligible and even for 50 mm there is a very small change in result, see Figure 4.1.

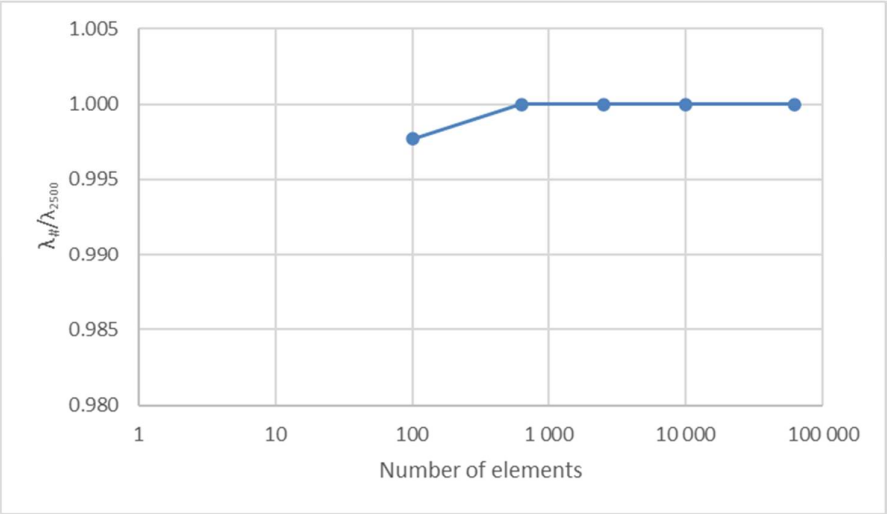

Figure 4.1 Convergence study of the mesh size of the plate based on the buckling analysis.

The last mesh convergence study which is made is where the force vs. in-plane displacement for the plate when loading the plate with static loading. This convergence study is made using four different mesh sizes within the range 5 mm to 50 mm, see Figure 4.2. In the plot it is seen that the result is influenced by what mesh size is used, and it is seen that when using a mesh size of 10 mm or finer the result has converged.

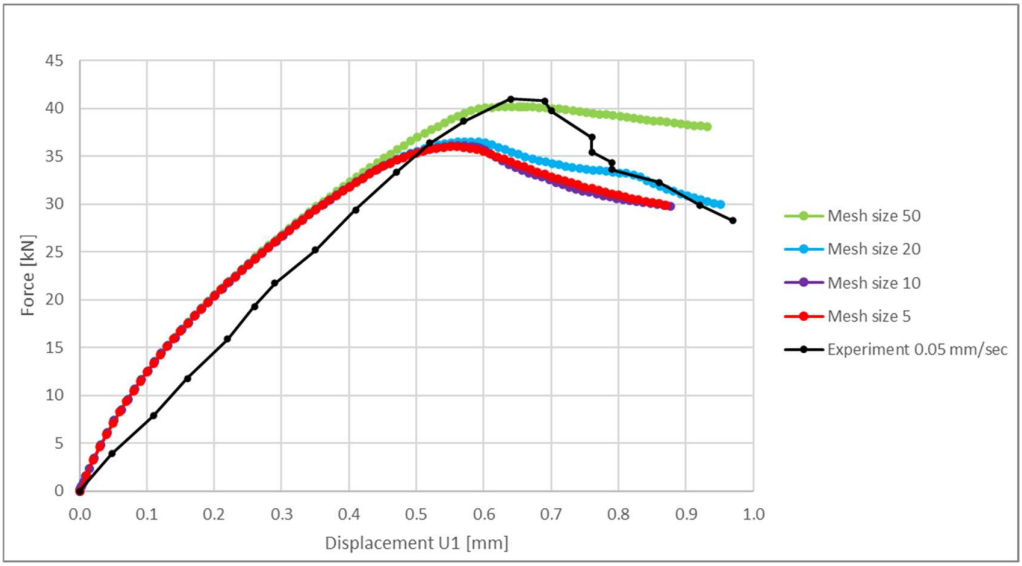

Figure 4.2 Convergence study of the plate based on the force vs. in-plane displacement relationship when using different mesh sizes.

Based on the two different convergence studies it is seen that all the results of interests have converged when using a mesh size of 10 mm or finer. The finer mesh size, which is used, the more time it takes for the computer to run the calculations, therefore it is of interest to use as coarse mesh as possible. Based on this, the mesh size used in this study is set to 10 mm.

4.3 Initial imperfections

A study of the initial imperfections can be done for the post buckling response in Abaqus CAE for various imperfection values. This can be done in three different ways: linear superposition of the buckling eigenmodes, from the static analysis displacements or by specifying the node number and the imperfection value directly to the input file. In this study, the third option was used, in which different imperfection values were used in a static load application. For each case the load displacement curve was studied to see what influence the initial imperfection of the plate has, see Figure 4.3.

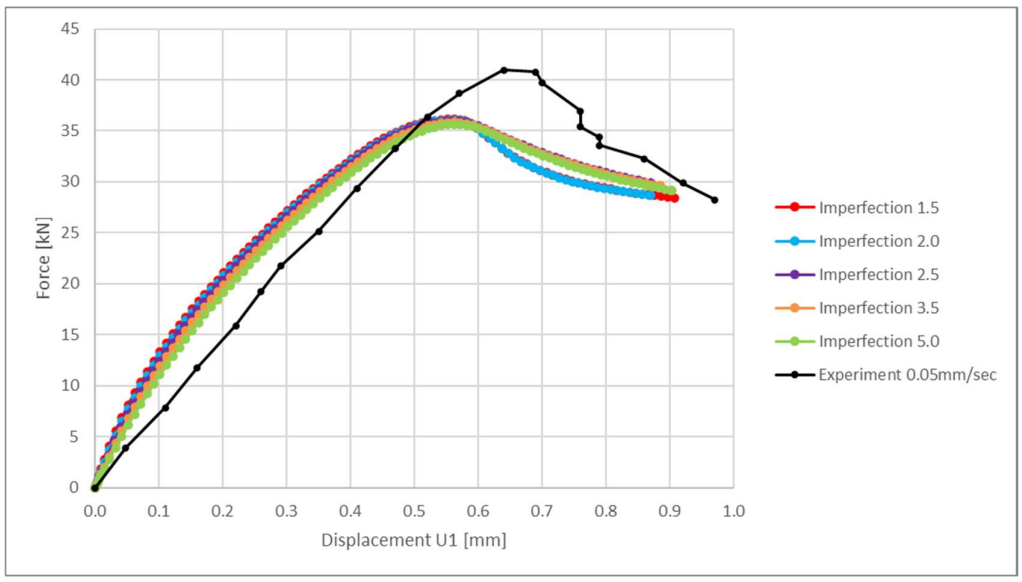

Figure 4.3 Force vs. in-plane displacement relationship for the plate when using different initial imperfections, given in mm.

By comparing the different curves, a small change in initial plate stiffness can be seen. However, the change in ultimate load is negligible between the different curves. Based on the plot, it is seen that the influence of the initial imperfection of the plate is very small and therefore can be regarded as negligible. Based on this, the initial imperfection used in this study is of the same size as mentioned in the paper from Yang et al (2018): i.e. an initial imperfection size 2.5 mm.

It is not shown here but the out-of-plane deflection for different initial imperfections were also studied, which showed similar result as the in-plane displacement; i.e. that the difference in result was negligible.

4.4 Material properties

To study the influence of the yield strength and the ultimate strength of the material, the five different materials described in Subsection 3.4.2 are studied. Where material A is the original material, material B and C have both increased yield strength and ultimate strength. Material B_2 and C_2 have the same yield strength as material A and increased ultimate strength. See Subsection 3.4.2 for material parameters of each material. A comparison of the material properties is shown in Figure 3.7.

The different materials are studied in the static case and the responding force vs. in-plane displacement are plotted in a graph with the result from the experiment when using the velocity 0.05 mm/s, see Figure 4.4.

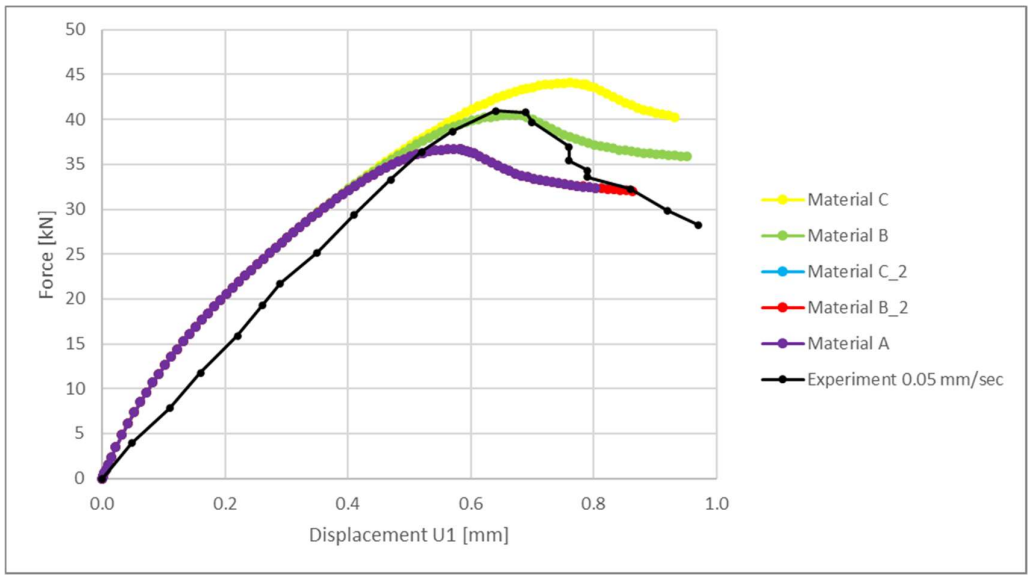

Figure 4.4 Force vs. in-plane displacement relationship for a plain plate when using different steel materials where material A, B_2 and C_2 gives the same result.

When studying the plot, it is seen that the ultimate force is increased for material B and C while material B_2 and C_2 have the same force vs. displacement relationship as material A. Based on the result it is seen that the ultimate strength of the material has a negligible influence of the ultimate force in the static case. The reason for this is that the maximum stress in the studied plate is reaching just above yielding and therefore the extra capacity in ultimate strength does not influence the result. If instead looking at material B and C where the yield strength is increased, it is seen that the resulting maximum force is increased with the same magnitude from material A to material B as from material B to material C. The ultimate force of material A is 37 kN, for material B it is increased with 8 % to 40 kN, and for material C the ultimate force is increased with 19 % to 44 kN. Based on this it is seen that there is a relationship between the yield strength of the material and the ultimate force of the plate. Based on the result shown in Figure 4.4 it is also seen that the initial slope of the curves is not affected of the change in plastic properties of the material. Since there is no difference in input data until a specific strain all results should have the same initial behaviour.

4.5 Load application

In the static analysis the load is applied as a uniformly distributed displacement on all the nodes along one side of the plate which increases linearly from zero to the desired value. In the experimental paper from Paik & Thayamballi (2003b), they use velocity-controlled loading where the slowest velocity is 0.05 mm/s. The static calculation is

an approximation of this velocity and later in Section 5.3 a comparison between the results is made to see if the approximation is suitable.

As mentioned in Subsection 3.4.1, the side which is parallel to the side where the load is applied is fixed in x-direction, see Figure 3.5. This creates a reaction force and by summing up the reaction force from each node along the side $F_{reaction,node}$, the total applied force is calculated, see equation (4.1).

$$F = F_{reaction} = \sum F_{reaction,node} \tag{4.1}$$

4.6 Boundary conditions

Seven different boundary conditions were tested on the steel plate to study how the response on the force-deformation relationship was affected and to find the buckling mode of interest, the same buckling mode as studied in the analytical paper from Yang et al (2018), see Section 3.3. In the study, only extreme cases were studied where the degrees of freedom are either fixed or free. In reality the boundary conditions are probably somewhere in between these two extreme cases. In the different models, different combinations of boundary conditions are combined and in all the load cases the load is applied as a uniformly distributed load along the side B_1B_2, described in Section 4.5.

The Abaqus CAE settings for each of the seven cases have varying boundary conditions for the translation and the rotation of the edge nodes, where more or less degrees of freedom are fixed. The settings for each load case are described based on Figure 4.5 and shown in Table 4.2.

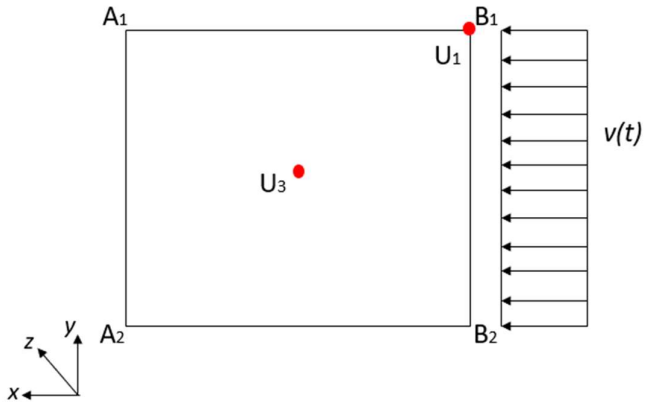

Figure 4.5 Definitions of the edges of the steel plate and the locations of U1 and U3.

Table 4.2 Boundary conditions for each of the different cases studied in Abaqus CAE, the degrees of freedom which is marked with a dot is put as fixed.

	Locations	Translations			Rotations	
		U_X	U_Y	U_Z	UR_X	UR_Y
Case 1	A_1B_1 & A_2B_2			●		
	A_1A_2	●		●		
	B_1B_2			●		
	Mid-nodes of A_1B_1 & A_2B_2		●			
Case 2	A_1B_1 & A_2B_2		●	●		
	A_1A_2	●		●		
	B_1B_2			●		
	Mid-nodes of A_1B_1 & A_2B_2					
Case 3 (As in numerical paper)	A_1B_1 & A_2B_2		●	●		●
	A_1A_2	●		●	●	
	B_1B_2			●	●	
	Mid-nodes of A_1B_1 & A_2B_2					
Case 4	A_1B_1 & A_2B_2		●	●		
	A_1A_2	●		●	●	
	B_1B_2			●	●	
	Mid-nodes of A_1B_1 & A_2B_2					
Case 5	A_1B_1 & A_2B_2			●		
	A_1A_2	●		●	●	
	B_1B_{12}			●	●	
	Mid-nodes of A_1B_1 & A_2B_2		●			
Case 6	A_1B_1 & A_2B_2			●		
	A_1A_2	●		●		●
	B_1B_2			●		●
	Mid-nodes of A_1B_1 & A_2B_2		●			
Case 7	A_1B_1 & A_2B_2			●	●	
	A_1A_2	●		●		●
	B_1B_2			●		●
	Mid-nodes of A_1B_1 & A_2B_2		●			

Static calculations are made for each of the boundary condition cases and force-deformation curves are shown in Figure 4.6 and Figure 4.7.

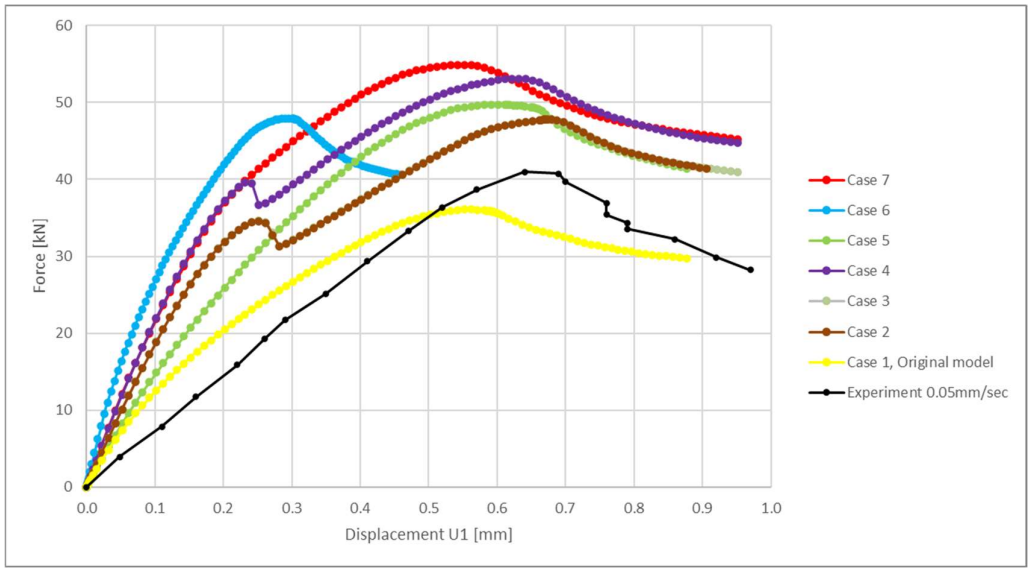

Figure 4.6 Force vs. in-plane displacement relationship for the plate when using different boundary conditions.

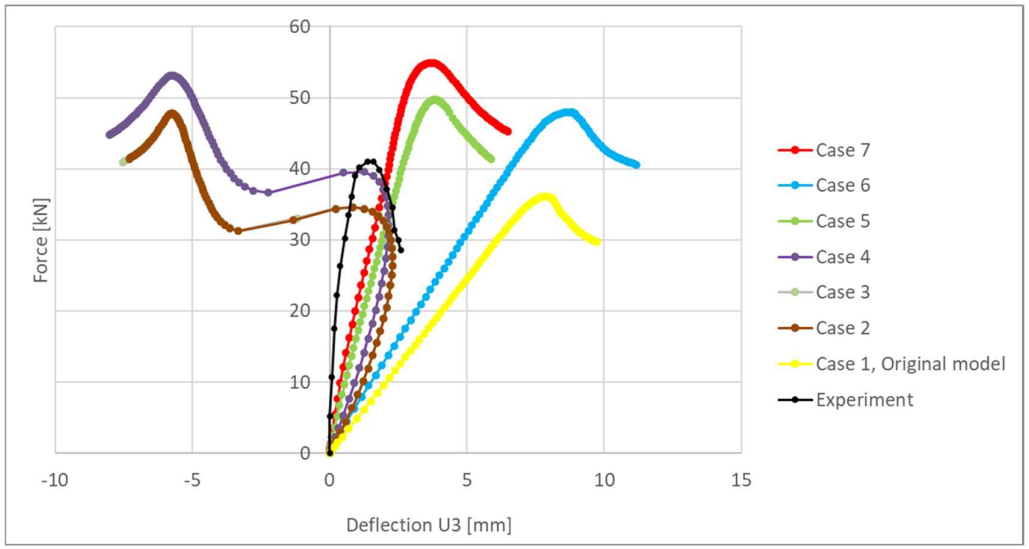

Figure 4.7 Force vs. out-of-plane deflection relationship for the midpoint of the plate when using different boundary conditions.

Based on the plot of the force vs. in-plane displacement relationship it is seen that when more degrees of freedom are fixed than in the original model, case 1, the ultimate force of the plate is increased. The reason for this is that when more degrees of freedom are fixed, the stiffness of the plate is increased and therefor more loads can be applied to the plate. When studying the in-plane displacement where the ultimate load is reached and furthermore the slope of the curves, it is seen that the stiffer the plate the steeper the curve gets. Furthermore, it is seen that for most of the cases the difference in in-plane displacement where the ultimate load is reached is similar

which means that the effect from the boundary conditions is small on this result. Only for case 7, a marginally change in the in-plane displacement can be seen. Additionally for the same case, the stiffest behaviour of the plate is seen.

When studying Figure 4.6 it is also seen that for some of the graphs, a jump can be seen in the graphs where the force is decreased when the in-plane displacement is increased. This jump indicates a snap-back behaviour in the plate. The cases where this behaviour appear is case 2, 3, and 4, which is all the cases where the translation along the unloaded edges in y-direction are fixed. Case 2 and 3 even have identical result. When studying the deformation plots for the part where the snap-back behaviour appears, it is seen that the buckling mode changes from one buckle to two and later to three, see Figure 4.8. When studying the buckling mode with different boundary conditions it is seen that for all the studied boundary conditions the initial buckling mode is as for case 1 in Figure 4.8. This mode is also the same as seen in the paper from Yang et al (2018).

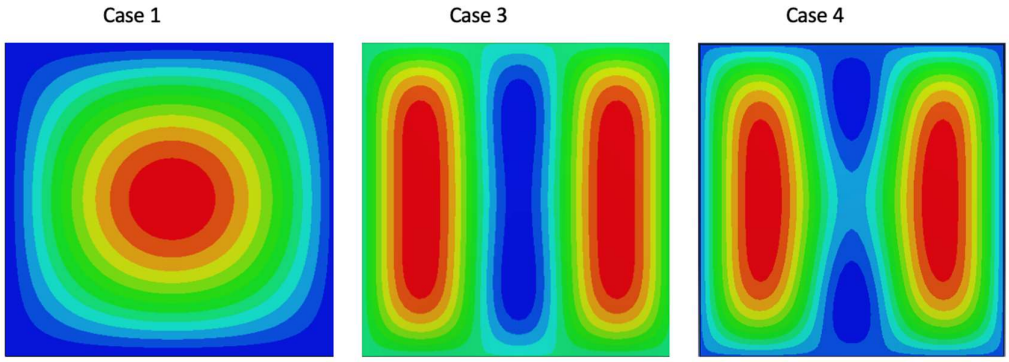

Figure 4.8 Buckling mode for the plate for the case 1 and buckling modes for case 3 & 4 when there is a snap back behaviour when using different boundary conditions.

The snap-back behaviour is also indicated in the curves of the out-of-plane deflection shown in Figure 4.7. Here it is seen that when the snap-back appears in the plate, the deflections go from positive values to negative. In the same graph, force vs. out-of-plane, it is seen that the result from all the studied boundary conditions shows a weaker stiffness than the experimental results.

Based on the result in the study of the boundary conditions of the plate, it is seen that the case where the buckling mode of interest appears in the original model, case 1. For this case, the buckling mode is similar to the one studied in the paper from Yang et al (2018) and the ultimate load is not greater than the measured value in the experiment in the paper from Paik & Thayamballi (2003b). When comparing the results with the results from Yang et al (2018) it is concluded that it was not able to reproduce the same results. When using the same boundary conditions as Paik & Thayamballi (2003b) are presenting, a different response is achieved (3rd buckling mode) and the achieved load capacity is considerably higher than what Paik & Thayamballi presents. However, when assuming boundary condition in accordance with Case 1, the achieved load capacity is similar to the presented value by Paik & Thayamballi and the achieved buckling mode is reproducing the one-mode buckling shape that Paik & Thayamballi presents. The out-of-plane deflection could not be

compared with results from Paik & Thayamballi since they did not report such results. Based on this, the boundary conditions used in the rest of this study is as described for Case 1.

4.7 Edge beams

Based on drawings in the experimental paper from Paik & Thayamballi (2003b) it can be seen that there is some kind of small edge beam along the two unloaded edges on the plate, see Figure 3.1. Apparently, this configuration was used to ensure the wanted boundary condition in the experimental set-up. To investigate the influence of this kind of beams, two beams of various sizes are added on the plate in the Abaqus CAE model. The geometry of the beams can be seen in Figure 4.9 and the input parameters for the different edge beams are shown in Table 4.3. The beams are studied to change the boundary condition of the plate, not to add any axial capacity. Therefor the beams are modelled as single elements and tie interactions are used to connect the plate to the beams.

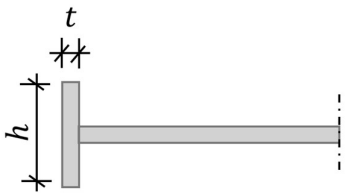

Figure 4.9 Geometry of the edge of the plate with an added beam along the two unloaded edges.

Table 4.3 Geometry input for the studied edge beams.

	Height, h [mm]	Thickness, t [mm]
Edge beam 1 (original geometry)	0	1.6
Edge beam 2	10	1.6
Edge beam 3	20	1.6
Edge beam 4	30	1.6

The beams are modelled in Abaqus CAE by using a 3D deformable beam elements with a rectangular cross-section. The same material properties as used for the plate are used for the beams. The plate is connected to the beams by using tie intersections and the boundary condition in z-direction along the edges where the beams are applied are moved to the beams instead of the plate. The rest of the boundary conditions are kept as before, where the loaded edges are fixed in z-direction, additionally the left side of the plate is fixed in x-direction and the mid nodes of the loaded sides are fixed in y-direction.

For each geometry of the edge beam the load vs. deformation is plotted for the static loading[1], shown in Figure 4.10 and Figure 4.11.

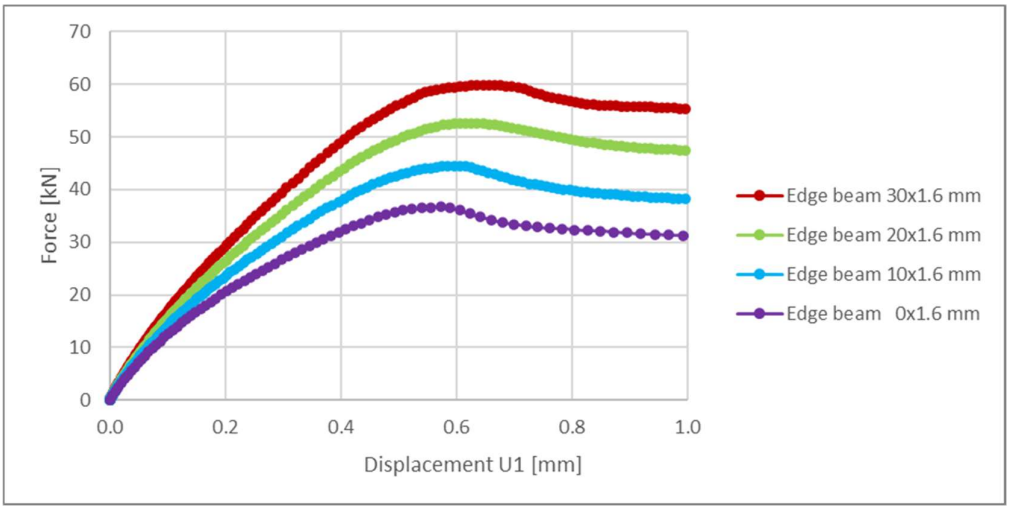

Figure 4.10 Force vs. in-plane displacement when using different sizes of the edge beams along the unloaded edges of the plate.

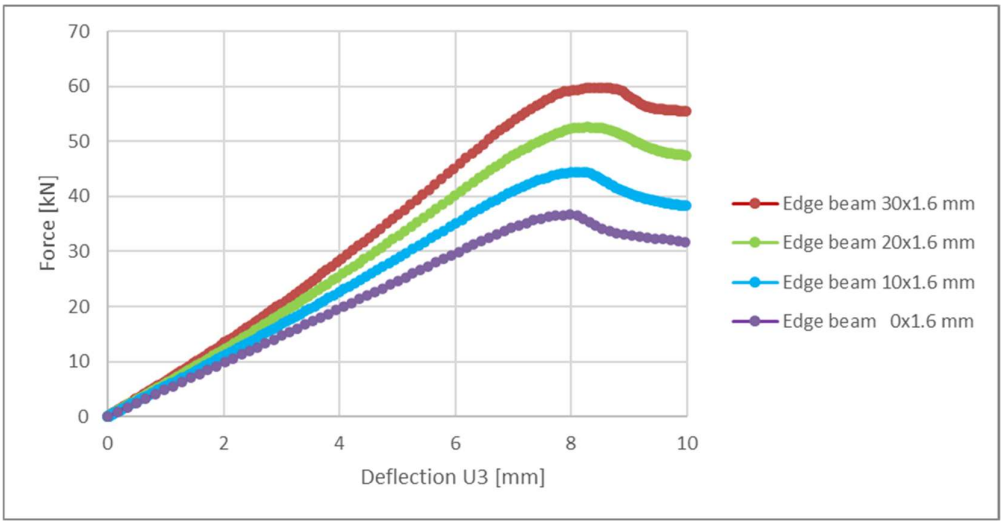

Figure 4.11 Force vs. out-of-plane deformation when using different sizes of the edge beams along the unloaded edges of the plate.

Based on the plots it is seen that by adding an edge beam along the unloaded edges, the plate stiffness is increased. Further, the force capacity of the plate is increased accordingly. The same type of increase and behaviour is seen both when looking at the in-plane displacement and when looking at the out-of-plane deformation.

[1] When studying the cases with edge beams with a height of 20 and 30 mm there was a convergence problem in Abaqus. Due to this, explicit dynamic calculations with a multi-linear ramp up according to Subsection 5.4.4 and a velocity of 1 mm/s was used instead for these two cases. To make sure that the dynamic results are representative, the case with 10 mm of the beam was made using both static and dynamic calculations and based on this it was seen that dynamic affects were negligible.

5 Dynamic Analysis

5.1 Orientation

Dynamic analysis is a method where the model is analysed using Implicit and Explicit methods where the model is subjected to transient dynamic events as it is designed to solve highly discontinuous high-speed dynamic problems. In Abaqus initially implicit methods were used for constant and linear load velocities. For multi-linear load velocities Explicit method was used to capture smaller increment sizes in the analyses to achieve a smoother curve. The total step time in this method is specified and the increment size is chosen automatically from the program based on the used mesh size.

When looking at the velocity 0.05 mm/s with multi-linear ramp-up, calculations are made using Abaqus Explicit except for the case where a total displacement of 2 mm is studied. In this case the calculation takes long time due to the small time step and therefor Abaqus Implicit is used instead.

5.2 Dynamic modelling

During the study both implicit and explicit models have been used in Abaqus CAE. The result from both the models are compared to see the different parts of the result that each model manages to collect. The reason for this is that pros and cons have been seen with both methods. When using implicit model in Abaqus CAE, there is a problem with running the calculation with increments which is small enough to capture the behaviour of all parts of the calculation and to achieve the smooth shape of the curve. An example of this is that there is a problem to run the model with a significantly small initial increment size, which is needed to capture the behaviour of the plate when it is initially loaded. Instead for this type of calculations, a larger initial increment size is used to avoid error messages in Abaqus CAE. Based on this, explicit model is better since then the increment step is decided based on the mesh size and it is therefore possible to run small increment steps.

In the dynamic analysis of the plate the load is applied as a uniformly distributed velocity on all the nodes along one side of the plate. The velocity is achieved by deriving the displacement, see Figure 5.1. When applying the load like this, a certain acceleration is applied to the plate in the beginning of the calculation. This was found to cause problems later on and therefor different load ramp-up was used.

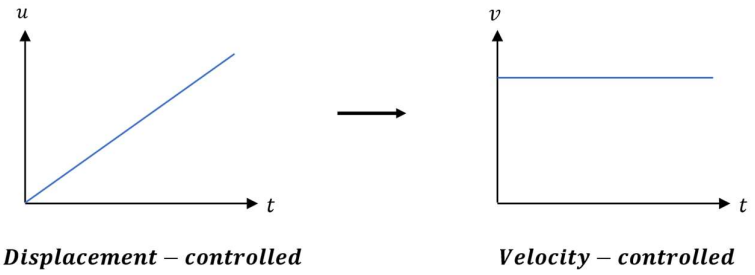

Figure 5.1 Load application when applying it as a displacement and when applying it as a velocity.

The velocity-controlled load was applied on the plate as a uniformly distributed velocity along one side of the plate. By changing from displacement-controlled loading to velocity-controlled loading it was also possible to easily control both the velocity and the ramp-up of the velocity in the dynamic study. To see the influence of different loading speeds, both the velocities studied in the paper from Paik & Thayamballi (2003b) are used together with some additional velocities. The velocities that are studied later on in the dynamic analysis are stated in Section 3.5.

For the case when looking at the velocity 0.05 mm/s, there is a problem with the small increment size which the explicit model uses. The problem is that analysis takes very long time due to the small time step. Due to this, implicit model is used for calculations using a velocity of 0.05 mm/s when a total displacement of 2 mm should be captured. To ensure that this does not affect the result, the result from explicit method is compared to implicit method. Based on the results, it was concluded that the two methods produce the same result.

In the end, based on the achieved results, explicit model is the type of model which is mainly used in the dynamic study. Therefore, if not otherwise mentioned in the text, the part of the study is based on this type of model.

5.3 Comparison to static case

To ensure that the model behaves in the same way no matter if static or dynamic calculations are made on the plate, a comparison of the result from the slowest velocity, 0.05 mm/s and the static result is made, see Figure 5.2.

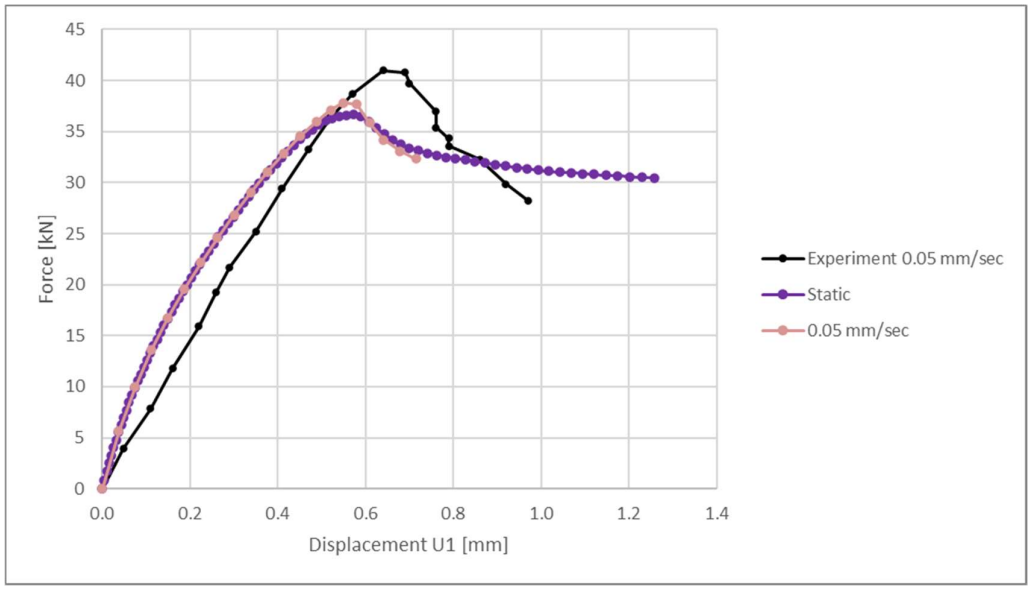

Figure 5.2 Comparison of force vs. in-plane displacement for a static load case and when applying a dynamic load of 0.05 mm/s.

Based on the figure it is seen that the same stiffness can be seen in the plate for both type of calculations and it is also seen that the maximum force is reached for the same in-plane displacement. A difference can be seen in the region closest to the point where the ultimate load is reached. In this region the dynamic calculations reach an

ultimate load which is approximately 1 kN greater than when doing a static calculation. Since the difference is small it can be seen as negligible and based on this, the results when using a velocity of 0.05 mm/s is regarded as a static load.

5.4 Initially dynamic study

5.4.1 Orientation

When modelling in Abaqus CAE the load can be applied in several different ways. In the dynamic study, the load is applied as a velocity which can be determined by looking at the slope of the displacement curve shown in Figure 5.3, and the applied force can be found by looking at the reaction force for all the nodes on the parallel side.

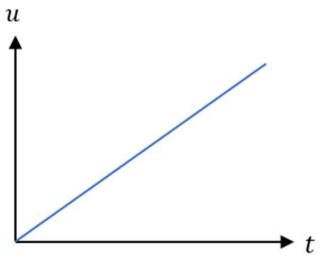

Figure 5.3 Displacement controlled loading where the slope of the curve is the applied velocity.

When studying dynamic results, the applied velocity and the acceleration is of interest and therefor the link between the time dependent displacement, velocity and acceleration are considered, shown in Figure 5.4.

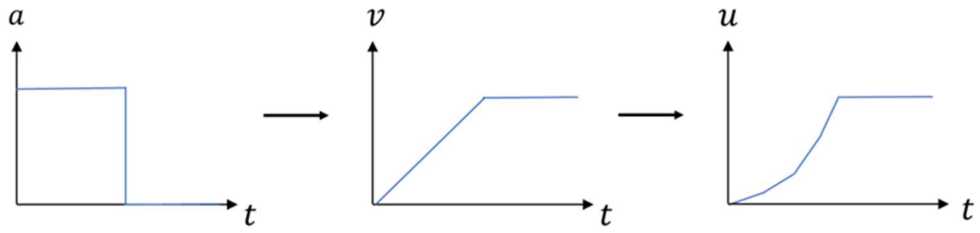

Figure 5.4 Link between time dependent acceleration, velocity, and displacement.

Based on the figure above it is seen that the shape of the velocity is affected by the shape of the acceleration. This link is used in the following Subsections where the effect of different load applications is studied.

5.4.2 Constant velocity

The dynamic analysis of the plate was carried out on the steel plate using Abaqus CAE Implicit for different load velocities and the force vs. in-plane displacement curve was studied. Initially the load was applied as a constant velocity, as described in Section 5.2, which means that at the first load step the required final velocity was used. However, based on the resulting curves it was seen that the graphs were not as

desired, instead of producing one smooth peak a sinusoidal curve was produced and for some velocities the curve had several local peaks, see Figure 5.5 and Figure 5.6.

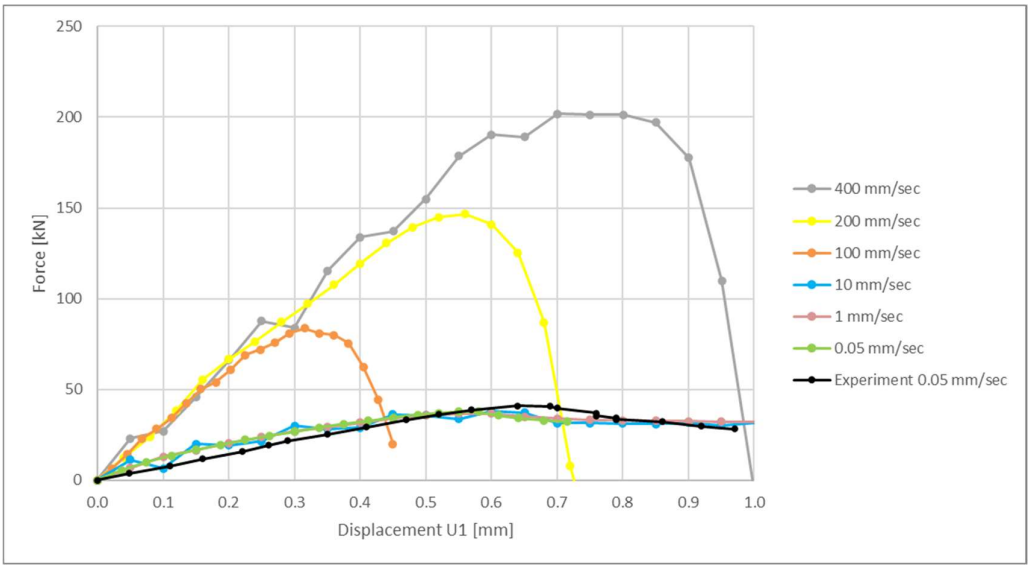

Figure 5.5 Force vs. in-plane displacement for the steel plate when the load was applied as a constant velocity.

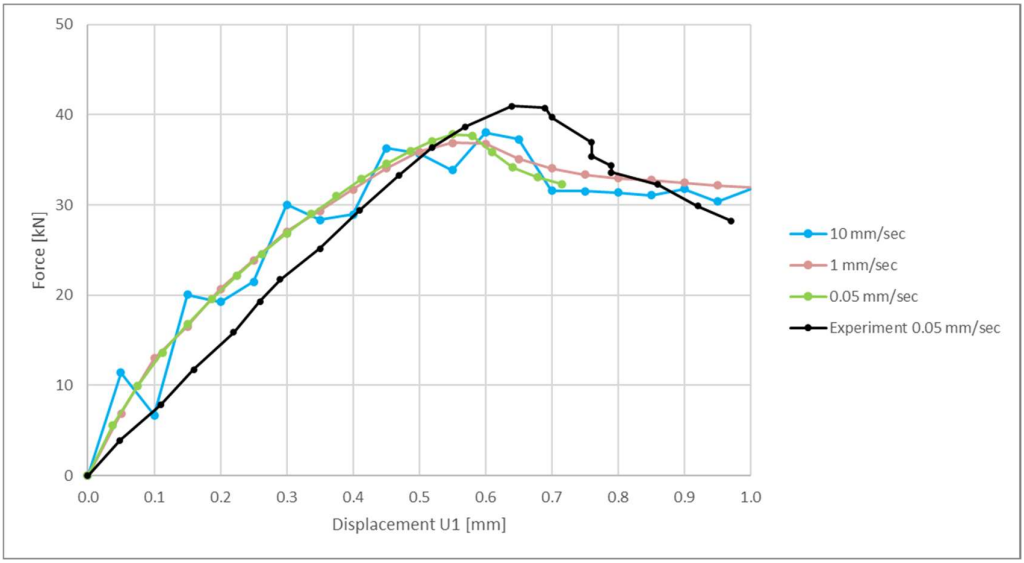

Figure 5.6 Zoomed plot of the force vs. in-plane displacement relationship for the plate when the load was applied as a constant velocity.

Based on the graphs it is seen that the magnitude of the dynamic effect differs depending on the applied velocity. When studying the result from the velocity of 10 mm/s, it is seen that the shape of the curve is a sinusoidal shape but at the same time the curve is still following the shape of the result the slower velocities. Unlike this, when studying the result of the velocities 100 mm/s, 200 mm/s and 400 mm/s, a considerable dynamic effect can be seen. For these results, a very stiff behaviour is seen, much greater than the static case. Based on the fact that the curves for the

velocities 100 mm/s, 200 mm/s and 400 mm/s have the same slope of the curve it is concluded that the same stiffness due to dynamic effects is seen for all three cases.

In the dynamic study above and the rest of the study no damping is applied to the plate. To see what influence such an input would have had on the results and in an attempt to decrease the sinusoidal shape, a damping study was made where a small amount of damping was applied.

This was done using Rayleigh damping, according to Rayleigh (1877), with a damping of 2 % between the frequencies 4.9 Hz and 40.3 Hz used to calculate the input parameters. The load capacity results are compared to the case where no damping is used, and it is seen that for this case there is a negligible change in the results. Based on this it is shown that a usage of damping of this magnitude does not affect the results in this study.

5.4.3 Linear velocity ramp-up

To get rid of the sinusoidal shape and for the program to handle the dynamic effect in a better way, a linear ramp-up of the velocity is used. By applying the load in this way, it is more similar to a real loading in which it is not possible to directly apply a constant load. The tabular data in Abaqus CAE Implicit was used to define the amplitude curve for the model for desired points on the time scale. The resulting force vs. displacement plots are shown in Figure 5.7 and Figure 5.8.

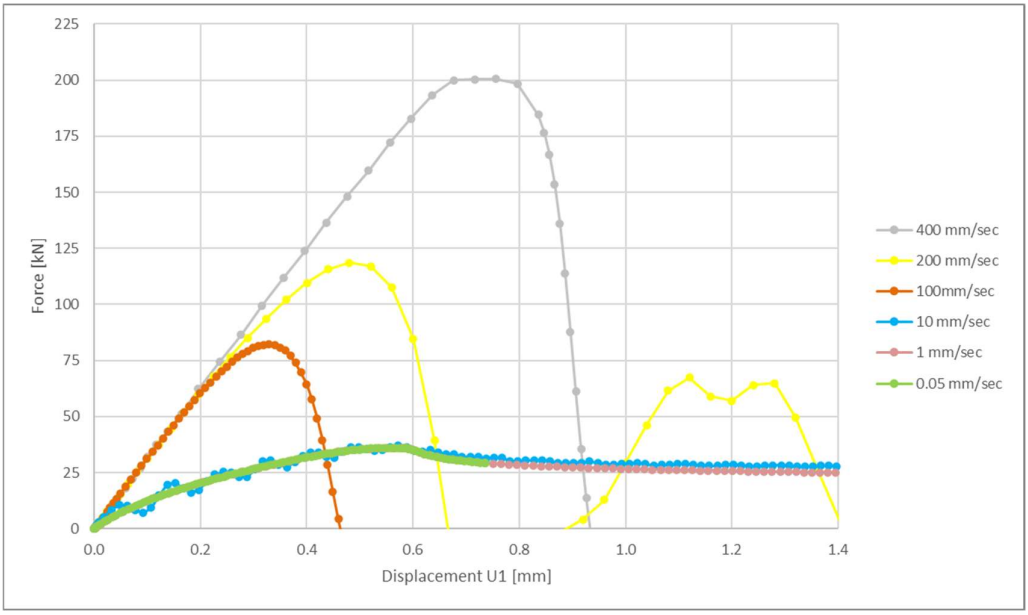

Figure 5.7 Force vs. in-plane displacement relationship for the plate when subjected to a velocity with linear ramp-up.

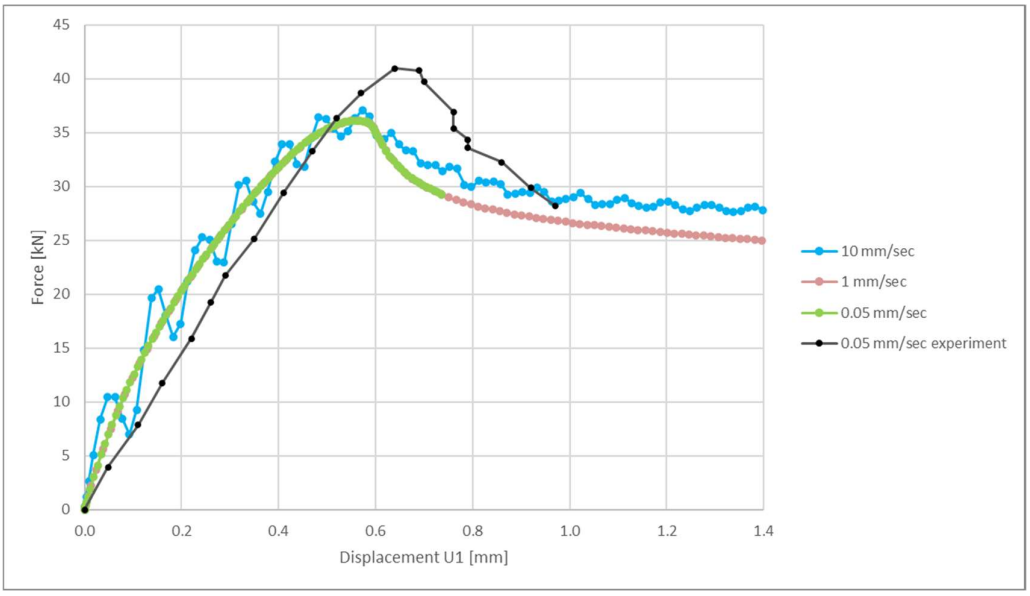

Figure 5.8 Force vs. in-plane displacement relationship for the plate when subjected to a velocity with linear ramp-up.

Based on the two plots above, it is seen that when applying the load with a linear ramp-up the sinusoidal shape of the curves are decreased a bit. This indicates that a smoother loading helps reducing the dynamic effects in the plate. To examine how the influence changes with different time periods of the ramp up, four different time periods were applied to the plate. The velocity which is studied mainly is 20 mm/s since this is the slowest velocity where the sinus shape of the curve was observed. To decide what time periods to look at the time until the ultimate load is reached was studied for each velocity. Based on this time, the ramp-up periods were picked for each load case as a percentage of this value, according to Figure 5.9. The force vs. in-plane displacement is plotted for each load case shown in Figure 5.10.

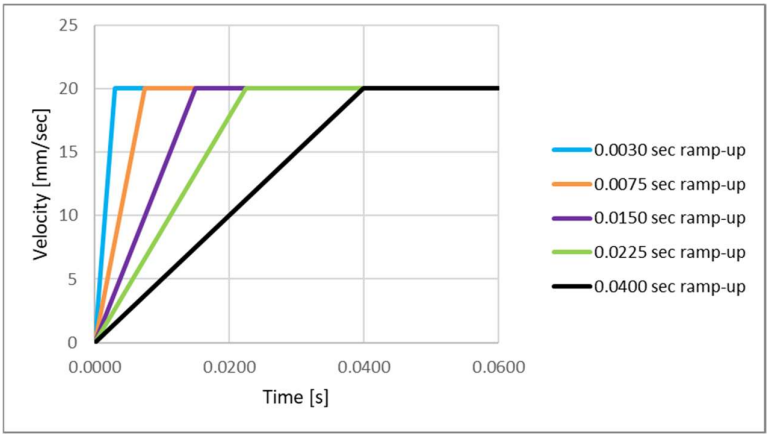

Figure 5.9 Different time periods used for the linear ramp-up of the velocity 20 mm/s applied to the plate.

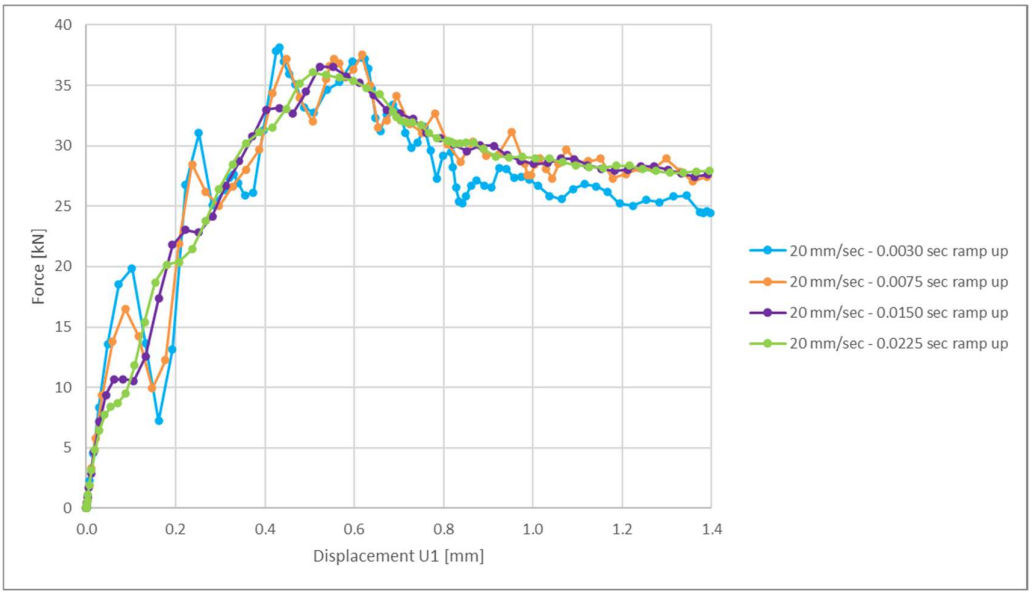

Figure 5.10 Force vs. displacement relationship for the plate subjected to a dynamic load with the final velocity 20 mm/s and different linear ramp-up.

By comparing the curves in Figure 5.10 it is seen that the ramp up time considerable affects the sinusoidal shape of the curve for the load case 20 mm/s. When applying the load with a short ramp-up time, the curve obtained a sinusoidal shape with a large amplitude and for increased ramp-up time, the oscillating amplitude decreased, and a smoother curve was obtained.

Later on, the ramp-up time is increased even more so that the ramp-up for the velocity 20 mm/s is 0.04 sec which gives the result shown in Figure 5.11. For this load case it is seen that the sinusoidal shape of the curve is small and there is a negligible change in ultimate load between the two load cases. For each load case, it is ensured that the required velocity is reached before the ultimate load is reached.

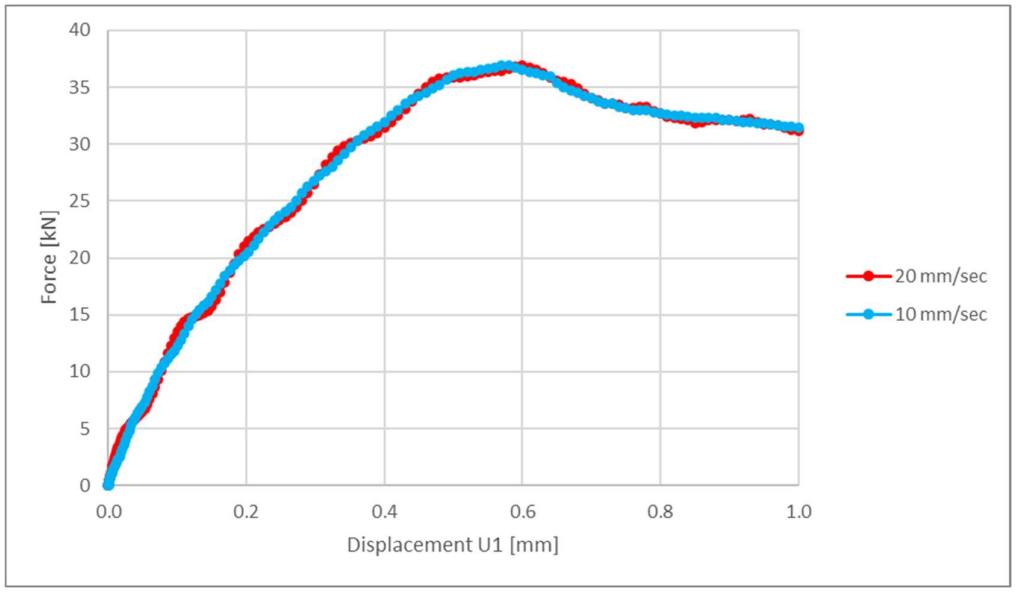

Figure 5.11 Force vs. displacement relationship for the plate subjected to linear ramp-up of the velocities 20 mm/s and 10 mm/s. The velocity 0.05 mm/s gives very similar result to 10 mm/s.

Based on the ramp-up for 20 mm/s, the ramp-up for the other velocities with the same magnitude are calculated as shown in Table 5.1.

Table 5.1 Settings for linear ramp-up of the velocity where the data gave u_r=0.4 mm and u_{tot}=2.0 mm.

v_r [mm/s]	t_r [s]	t_{tot} [s]
1	0.8000	2.4000
10	0.0800	0.2400
20	0.0400	0.1200
50	0.0160	0.0480
100	0.0080	0.0240
200	0.0040	0.0120
400	0.0020	0.0060

When studying the results, it is seen that the curves for velocities up to 20 mm/s are quite smooth when using a linear ramp-up but still the faster velocities result have a big dynamic influence. Since a sinusoidal shape still can be seen in the force vs. deformation plots, it is decided to look into multi-linear ramp-up instead.

5.4.4 Multi-linear velocity ramp-up

Since the results for velocities higher than 20 mm/s are still not smooth, additional studies of the load application are made where the load is applied as a multi-linear load instead of linear. When using both a linear- and multi-linear ramp-up a total time period of the calculation is picked so that the final in-plane displacement is

approximately 2 mm. The multi-linear shape of the velocity ramp-up is made to symbolise a linear acceleration of the load, according to Figure 5.12.

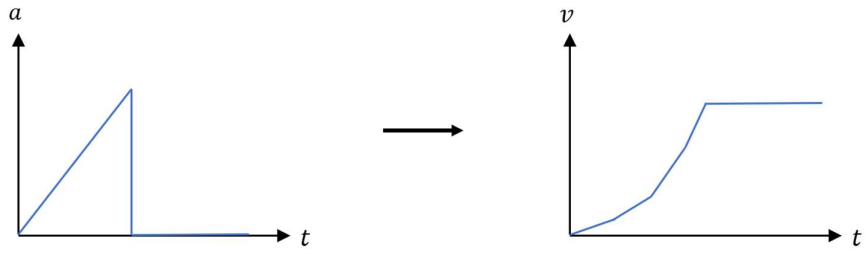

Figure 5.12 Illustration of how linear acceleration is seen as a velocity.

The force vs. in-plane displacement were studied for each of the load cases and based on the results the final shape of the ramp-up was decided, coefficients described in Table 5.2 and shown in Figure 5.13.

Table 5.2 Input used in Abaqus CAE to model the multi-linear ramp-up where the factors are the slope of each segment. The data gave u_r=0.34 mm and u_{tot}=2.0 mm.

	Factors					
	10	2	1.2	1.1	4	1.33
v_r [mm/s]	$v_{r,1}$ [mm/s]	$v_{r,2}$ [mm/s]	t_r [s]	t_{tot} [s]	$t_{r,1}$ [s]	$t_{r,2}$ [s]
1	0.100	0.500	0.9600	2.6400	0.2400	0.7200
10	1.000	5.000	0.0960	0.2640	0.0240	0.0720
20	2.000	10.000	0.0480	0.1320	0.0120	0.0360
50	5.000	25.000	0.0192	0.0528	0.0048	0.0144
100	10.000	50.000	0.0096	0.0264	0.0024	0.0072
200	20.000	100.000	0.0048	0.0132	0.0012	0.0036
400	40.000	200.000	0.0024	0.0066	0.0006	0.0018

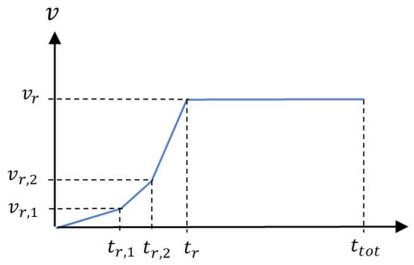

$$u_r = \frac{v_{r,1} \cdot t_{r,1}}{2} + \frac{(v_{r,1} + v_{r,2}) \cdot (t_{r,2} - t_{r,1})}{2} + \frac{(v_{r,2} + v_r) \cdot (t_r - t_{r,2})}{2}$$

$$u_{tot} = v_r \cdot (t_{tot} - t_r) + u_r$$

$$v_{r,1} = \frac{v_r}{10} \qquad v_{r,2} = \frac{v_r}{2} \qquad t_{r,1} = \frac{t_r}{4} \qquad t_{r,2} = \frac{3 \cdot t_r}{4}$$

Figure 5.13 Final shape of the multi-linear ramp-up of the velocity used in Abaqus CAE with corresponding equations.

Based on the final shape of the multi-linear ramp up of the velocity, the final force vs. in-plane displacement is created, see Figure 5.14 and Figure 5.15.

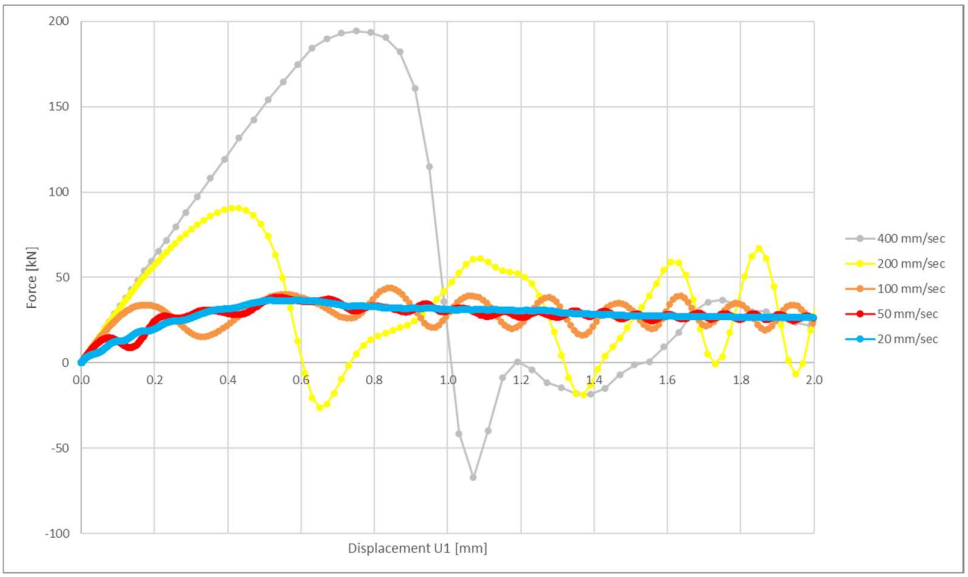

Figure 5.14 Force vs. in-plane displacement relationship for the plate subjected to multi-linear ramp-up of the velocity. The velocities slower than 20 mm/s has negligible difference in this scale and therefor they are not shown in this graph.

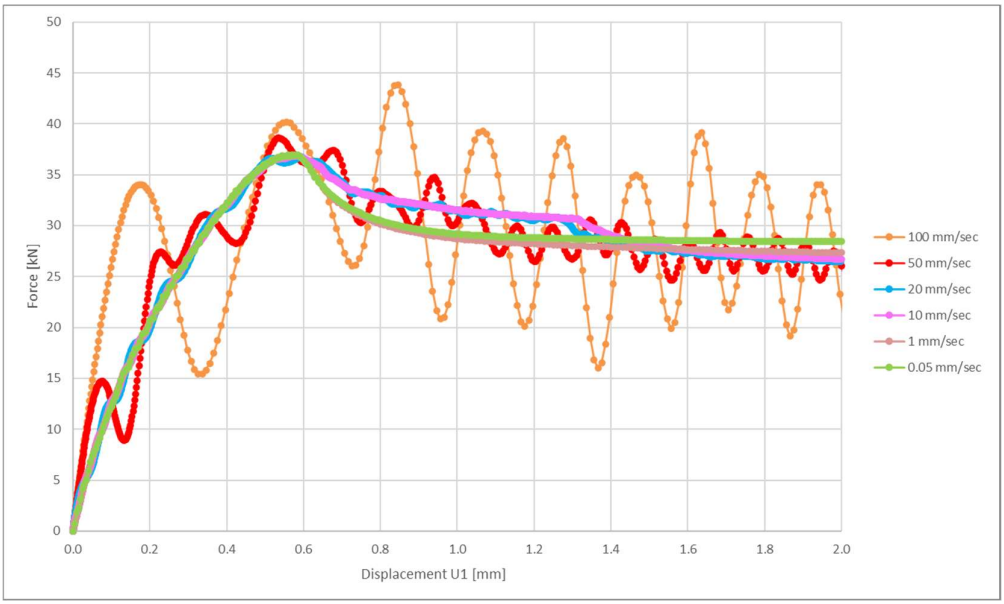

Figure 5.15 Zoomed-in plot of the force vs. in-plane displacement relationship for the plate subjected to multi-linear ramp-up of the velocity. Here the negligible difference in results for load velocities < 20 mm/s can be seen.

Based on Figure 5.14 and Figure 5.15 it is shown that less dynamic effect is seen when applying the load in this way compared to constant and linear ramp-up. The curves are still not smooth for all velocities but for velocities up to 100 mm/s, they are smoother, and they are also following the general shape obtained at static loading.

Based on all three different kinds of loading, constant, linear ramp-up and multi-linear ramp-up, the calculations where the lowest dynamic effects are seen is where multi-linear ramp-up is used. Based on this, the multi-linear ramp-up is the type of loading used in this study.

When comparing the results for different dynamic velocities to the result obtained by Paik & Thayamballi (2003b) shown in Figure 3.2, the same result cannot be produced for the velocities 100 mm/s to 400 mm/sec for any of the three different types of loading, constant, linear or multi-linear. The obtained force vs. displacement relationship from this study results in a significant increase in initial plate stiffness for higher velocities which is not seen in the result from the experiment. Furthermore, the ultimate force obtained by Paik & Thayamballi is around 50 kN for the velocity 100 mm/s and around 60 kN for the velocity 400 mm/s which is significantly lower than the values obtained in the Abaqus model which is 90 kN for 100mm/s and 195 kN for the loading 400 mm/s.

5.5 Strain rate effect of the steel plate

To study the influence of strain rate effect on the model, calculations in Abaqus CAE are initially made using no strain rate effect, see Subsection 5.4.4, and later strain rate is applied to the numerical model and the results are compared to each other.

There are different types of strain rate effects that can be used. In the studied model the same equation is used as in the empirical paper from Yang et al (2018), the so-called Cowper-Symonds power equation, see equation (2.20) in and Section 2.5.5 for more details.

$$\sigma_{yd} = \sigma_y \left(1 + \left(\frac{\bar{\varepsilon}}{D}\right)^{1/q}\right) \tag{5.1}$$

The dynamic analysis of the plate was carried out on the steel plate using Abaqus/Explicit for different load velocities with multi-linear load ramp-up of the load and the force displacement curve was studied. In Abaqus CAE there is a function to apply Cowper-Symonds power equation and to make sure that this function present the expected results, calculations are made both using the function and by manually adding the yield ratio for the plate. The calculations are made for the velocities 400 mm/s, 200 mm/s, 100 mm/s, 50 mm/s, 10 mm/s and 0.05 mm/s.

Based on the power law function and the parameters D=40.4 and q=5, given in the paper from Yang et al (2018), a graph of the dynamic increase factor, *DIF*, vs. strain rate is created, see Figure 5.16.

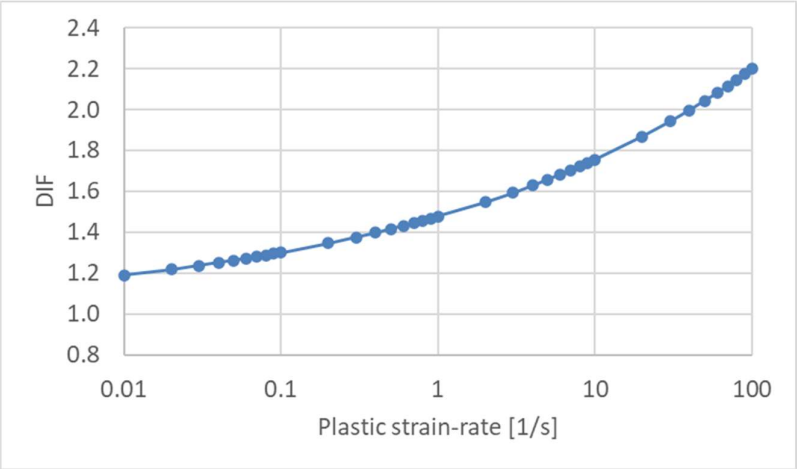

Figure 5.16 Expected relationship between the dynamic increase factor and the plastic strain based on the power law equation and the given parameters D and q.

The power law in Abaqus CAE was used to implement the strain rate effect and the input values were taken from the empirical paper for D and q as mentioned in Section 3.2. To find the element where the maximum plastic strain appears, colour plots are made at the force when plastic strain starts to appear in the plate and when the ultimate force is reached, see Figure 5.17.

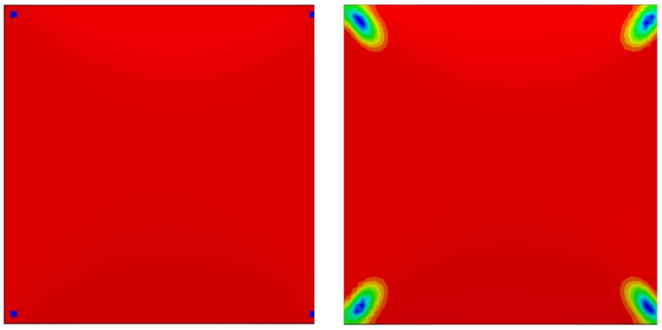

Figure 5.17 Plots of the plastic strain distribution in the plate at the force where plastic strain first appears in the plate (left) and when ultimate load is reached in the plate (right) for the velocity 1 mm/s. Red colour indicates zero plastic strain and blue colour indicates maximum plastic strain.

Based on the plot of the plastic strain distribution of the plate it is seen that the corners are interesting parts to study, since this is where the plastic strain first appears and where the maximum strain eventually is reached. Therefore, one element in this region is picked when the strain rate study is made, see Figure 5.18.

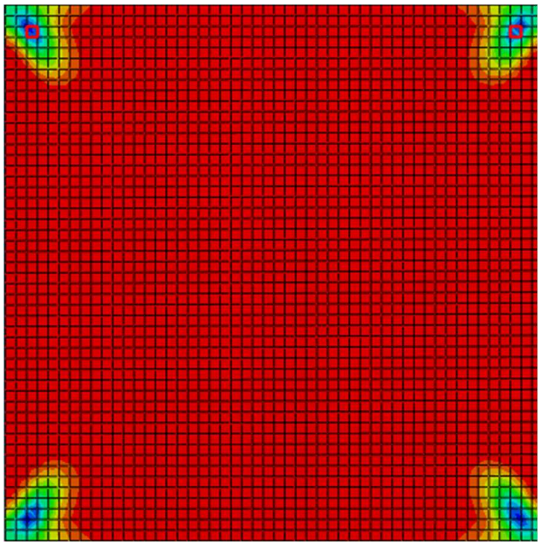

Figure 5.18 Location of the elements in Abaqus CAE where the strain effect was studied (red frame around element).

Based on the plastic strain, the dynamic increase factor, *DIF*, is calculated and later compared to the expected value based on the graph with the strain rate vs. *DIF* relationship, see Figure 5.19.

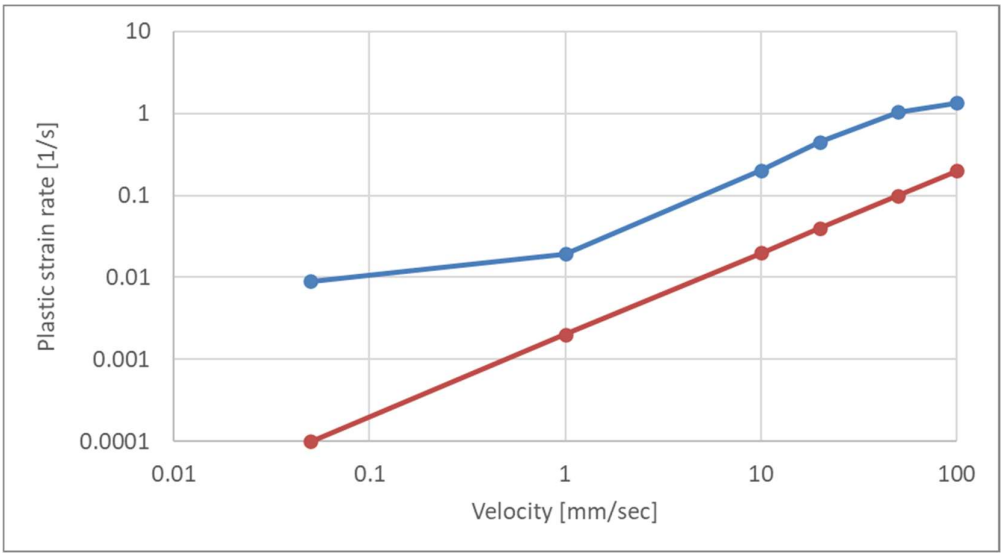

Figure 5.19 Plastic strain rate vs velocity for the steel plate without strain effect for velocities up to 100 mm/s where the blue curve shows the plastic strain extracted from the element in Abaqus and the red curve shows strain rate calculated as in the experimental paper from Paik & Thayamballi (2003b).

The resulting stress strain curves for 1 and 100 mm/s are shown in Figure 5.20 where the stress-strain relationship does not have much difference with or without strain rate but in reality, there should be an increase in capacity.

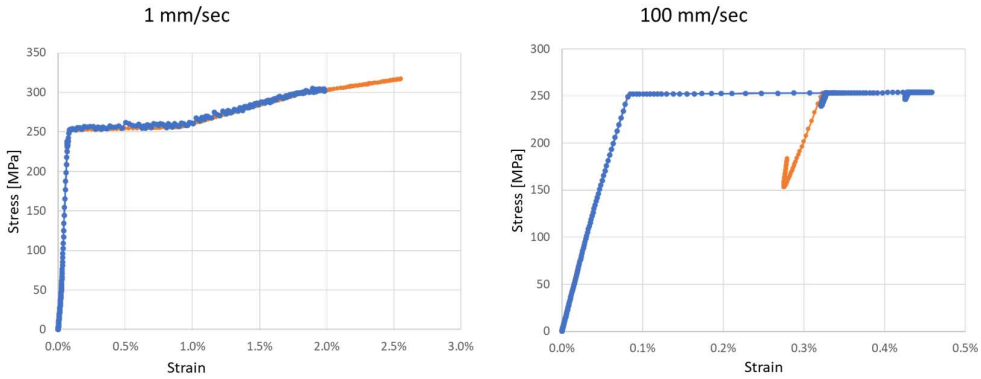

Figure 5.20 Stress vs. Strain relationship for the steel plate when applying D=40.4 and q=5, where the orange curve shows without strain rate effect and the blue curve shows with strain rate effect.

When studying the results of the stress-strain curve for the different velocities the increase in capacity is compared to the excepted value based on the resulting plastic strain and the corresponding *DIF* from Figure 5.16. As seen in this figure and based on the information given in Figure 5.19, the expected increase in capacity would be about 20 % for 1 mm/s and about 50 % for 100 mm/s. Based on these results it can be concluded that the effect on the result is not as expected based on the power law and the parameters given in the paper from Yang et al (2018), both in magnitude and it is also seen that for lower load velocities, a negligible effect is seen which is not as expected.

Based on this, a study is made where the strain rate behaviour in Abaqus CAE is studied in more detail, both when using the function power law and the function yield ratio, to better understand how the software is working. Initially this is done for a simplified case where a single beam element is modelled to study a rod subjected to a tensile force, described in Section 5.6.

5.6 Strain rate study on a simple rod

5.6.1 Orientation

The Dynamic analysis was carried out on a steel rod to examine the strain rate effect by using both the function power law in Abaqus CAE and by defining the strain rate effect manually by using the function yield ratio. The studied beam is modelled as a single 2D beam element with a length of 100 mm, see Figure 5.21. The beam is supported in both the edges of the beam where the left side is fixed in both horizontal and vertical direction. To make sure that no unintended rotation appears at the support, this edge is fixed in all directions. At the right edge of the beam, the beam is fixed in y-direction and here a horizontal velocity is applied to tension the beam. In the study, the size of the velocity is adjusted to different velocities to see the static and dynamic effect of the load. The calculations are made for the velocities 400 mm/s, 100 mm/s, 50 mm/s, 10 mm/s and 0.05 mm/s.

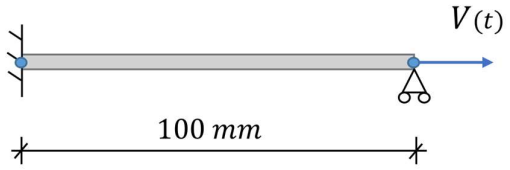

Figure 5.21 Geometrical properties and boundary conditions of the rod which is modeled as a simple beam element.

To start with, the same type of calculations was made for the rod as for the plate described in Section 5.5. The calculations were made for several velocities and the results for power law and yield ratio were plotted respectively. For each velocity, the stress and strain are taken from the result in Abaqus CAE for the integration points in the element. Based on this result, the stress ratio (Dynamic increase factor, *DIF*) and strain rate is calculated. The resulting values for strain rate are plotted in a graph to show the relationship between *DIF* and strain rate. Additionally, the value for the parameter q was changed to a value half and twice the original value to see what happens whether the parameter is changed, the results are shown in Figure 5.22 and Figure 5.23.

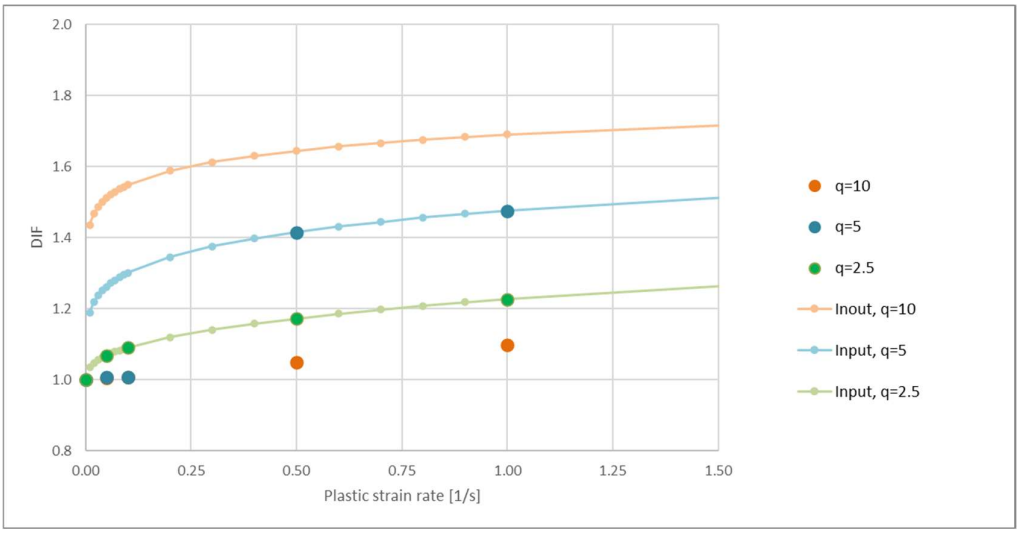

Figure 5.22 Relationship between plastic strain rate and the dynamic increase factor for different values of the parameter q using the Abaqus CAE function Power law. Additionally, the expected graphs based on the formula are shown.

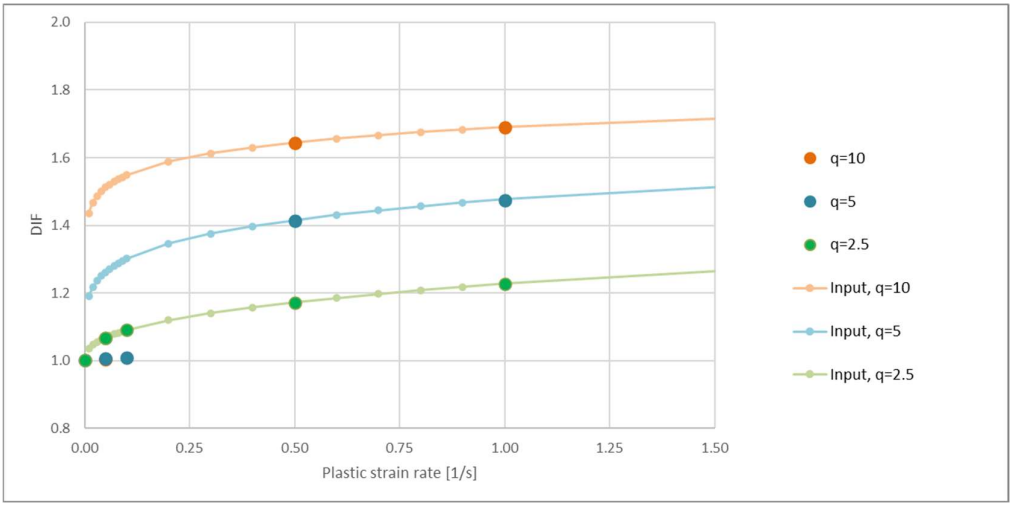

Figure 5.23 Relationship between plastic strain rate and the dynamic increase factor for different values of the parameter q using the Abaqus CAE function Yield ratio. Additionally, the expected graphs based on the formula are shown.

Based on the result shown in Figure 5.22 and Figure 5.23 it is seen than when using the values of D and q based in the information given in the research paper from Yang et al. (2018), the results were not as expected. Based on these values an increase in material strength could not be seen in the results for all the velocities studied. It was also seen that when using the power law function with q=10 (twice as original), none of the resulting points matched the expected curve when using the function Power law.

To make sure that there is no influence whether the rod is in tension or compression, the same type of calculation is made where the velocity acts in the opposite direction. By comparing the results when using the same amplitude of the velocity for a case where the rod is in tension and compression, it is concluded that there is no influence of the load direction when looking at a 2D beam element.

Based on this, a more detailed study was made where the power law function and the yield ratio in Abaqus CAE was studied. The below Subsections show the results of the detailed study of the two methods.

5.6.2 Power law method

Based on the result from the initial study of the power law, where the parameters q and D were based on the paper from Yang et al. (2018), an additional study was made where the values of D and q were then taken from Abaqus user manual (Dassault Systèmes Simulia Corporation, 2022) where D=1000 and q=2. This was made to test the method and to see if the generated results are equal to the calculated values of *DIF*. The resulting DIF vs. strain rate relationship when using both these input values are shown in Figure 5.24 and Figure 5.25.

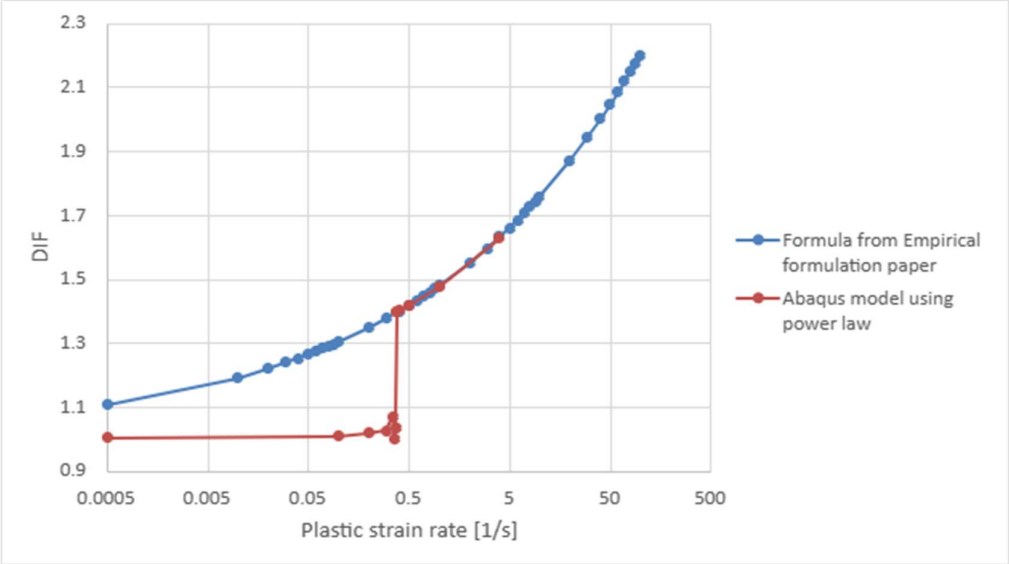

Figure 5.24 Relationship between Dynamic increase factor (DIF) and strain rate for a beam using the Cowper-Symonds power equation for D=40.4 and q=5.

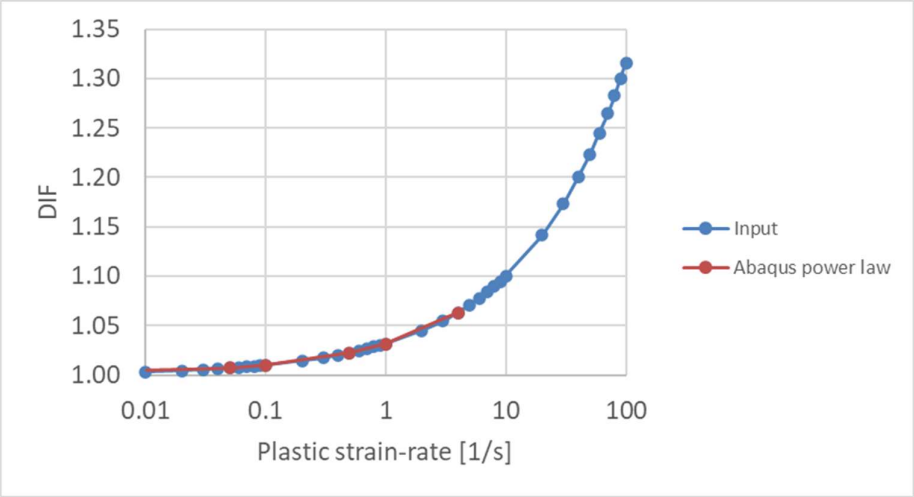

Figure 5.25 Relationship between Dynamic increase factor (DIF) and strain rate for a beam using the Cowper-Symonds power equation for D=1000 and q=2.

Based on the resulting curves it is seen that when using the initial values, a strain rate effect is seen when the strain rate is equals to 0.38 or more. If the strain rate is lower than this, then its effect is negligible. If instead looking at the case where the parameters are based on the Abaqus user manual, it is seen that for this case the result in Abaqus CAE is seen as equal to the calculated value based on the power law equation. This shows that for the given parameters D=1000 and q=2 the function Power law gives the expected result.

Following this, an additional study is made where the values of *D* and *q* are calculated based on the equations (2.21) and (2.22) and the material property given in Table 3.4. The resulting parameters are shown in Table 5.3 and the resulting DIF vs. strain rate curve is shown in Figure 5.26. In the same graphs, the relationship based on the formula is inserted so compare the values and conclude that the model does not behave as intended.

Table 5.3 Values of the two parameters used in Abaqus CAE.

Source	***D***	***q***
Research paper	*40.4*	*5*
Abaqus user manual	*1000*	*2*
Values used in the study	*1304*	*4.83*

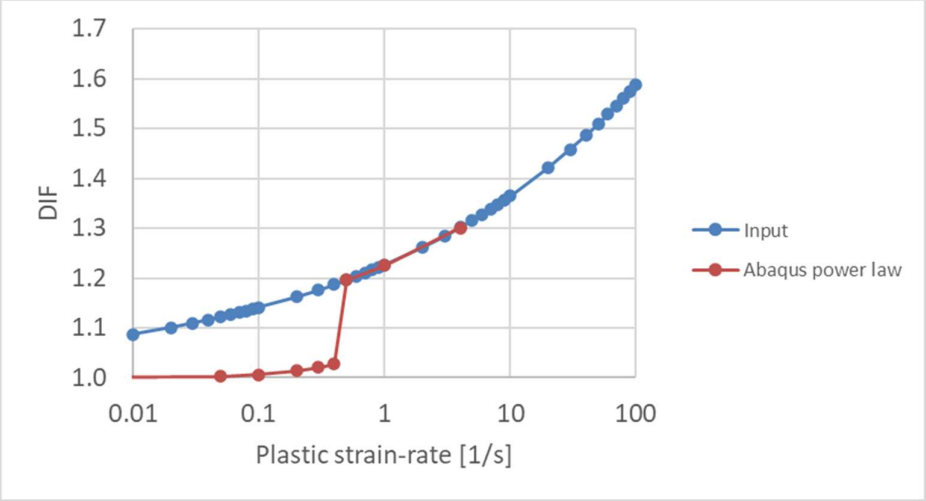

Figure 5.26 Relationship between Dynamic increase factor (DIF) and strain rate for a beam using the Cowper-Symonds power equation for D=1304 and q= 4.83.

5.6.3 Yield ratio method

The strain effect was also studied with the yield ratio method with the same values of D and q as when studying the Power law function, see Table 5.3. As when examining the Power law method, the resulting stresses and strains were extracted from Abaqus CAE and then compared with the graph based on the power law equation. This was done to see the response of the method and to see if the result is the same for both the methods. In Figure 5.27 to Figure 5.29 plots of the different results are shown which indicates the results of DIF values for different strain rates based on the calculation in Abaqus CAE and based on the Cowper-Symonds power equation.

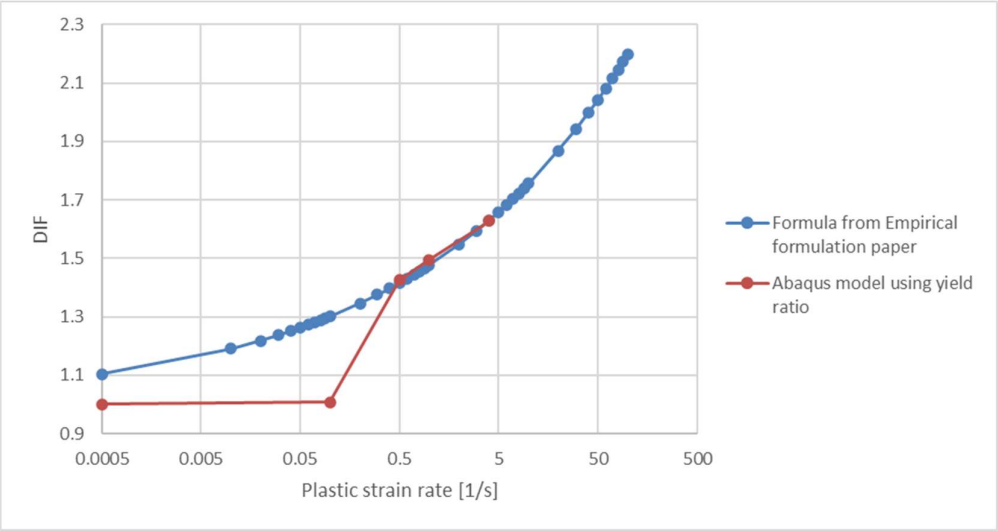

Figure 5.27 Relationship between Dynamic increase factor (DIF) and strain rate for a rod using the Yield ratio method with the parameters D=40.4 and q=5.

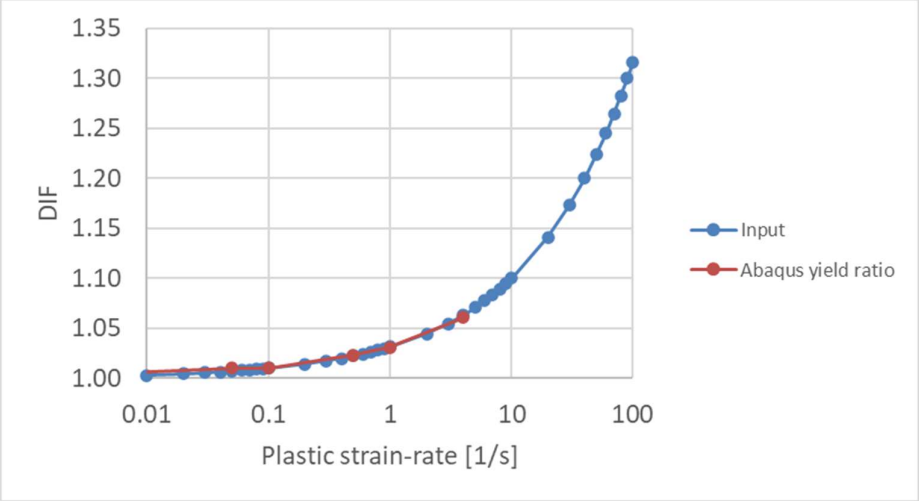

Figure 5.28 Relationship between Dynamic increase factor (DIF) and strain rate for a rod using the yield ratio method with the parameters D=1000 and q=2.

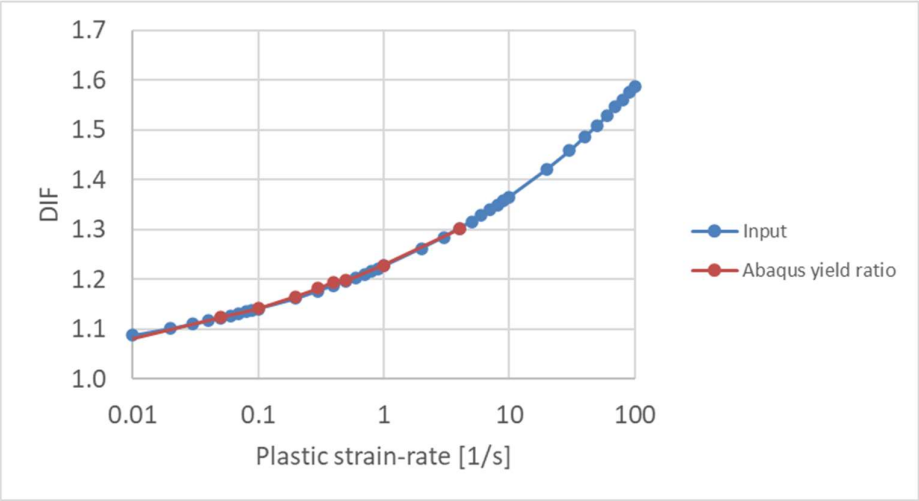

Figure 5.29 Relationship between Dynamic increase factor (DIF) and strain rate for a rod using the yield ratio method with the parameters D= 1304 and q=4.83.

Based on the graphs it is seen that the DIF values from the first two cases, where the parameters *D* and *q* are taken from the paper from Yang et al. (2018) and the Abaqus user manual (Dassault Systèmes Simulia Corporation, 2022), the achieved results are like the results where the Abaqus Power law function was used, presented in Subsection 5.6.2. If instead looking at the result where the parameters *D* and *q* are based on the material properties used in this study it is seen that when using yield ratio, the result for a strain rate of 0.05 or more is similar to the actual calculated value.

Based on the above curves, it is concluded that the parameter values from the research paper from Yang et al (2018) does not give the required results and it is not clear how the author interpreted the values. Additionally, it is not shown how the values were derived. Therefore, based on the strain rate study it was concluded that the actual formula is used in this study, where the parameters *D* and *q* are calculate using the material properties and the equations stated in Subsection 2.5.5.1.

5.7 Observations from strain rate study

As a next step in the analysis the same process was carried out on a single shell element to see if there is any influence when another type of element is used. In this case the load was applied as tension to the element and then studied to examine the strain rate effects on the element with both power law and yield ratio. A shell element is studied since this is the type of element used for the plain plate. The geometry and dimensions of the shell elements can be seen in Figure 5.30.

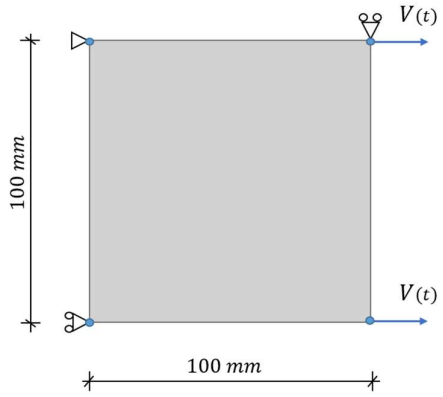

Figure 5.30 Geometry and dimensions of the single shell element used in Abaqus CAE.

The results obtained were very similar to the simple rod which indicates that there is no influence whether a beam element or a shell element is used. The shell element was then subjected to compression to see if there is any difference in response, but the results were the same as tension load, and therefore the shell element was not further studied. Additionally, different areas and lengths on the beam/rod were studied, which gave the same results which indicates that it does not influence the strain rate study. Therefor it was concluded that the plate geometry and areas do not affect the strain rate application.

5.8 Strain rate study on the plain plate element

Based on the strain rate study on a rod described in Section 5.6, the knowledge based on the result is used to apply strain rate on the plate element. The method which is used to apply the strain rate effect is the function yield ratio in Abaqus CAE and the strain rate effect which is based on the Cowper-Symonds power equation with the variables D=1304 and q=4.83, see equations in Subsection 2.5.5.1. The effect of adding yield ratio is studied for the velocities 1 mm/s, 10 mm/s, 20 mm/s, 50 mm/s and 100 mm/s. For each load case, the force vs. displacement relationship and the plastic strain in the plate are studied. The results are plotted in Figure 5.31, in which the element where the maximum applied load is located and where the plastic strain in the plate starts. The same element is used as shown in Figure 5.18 in Section 5.5.

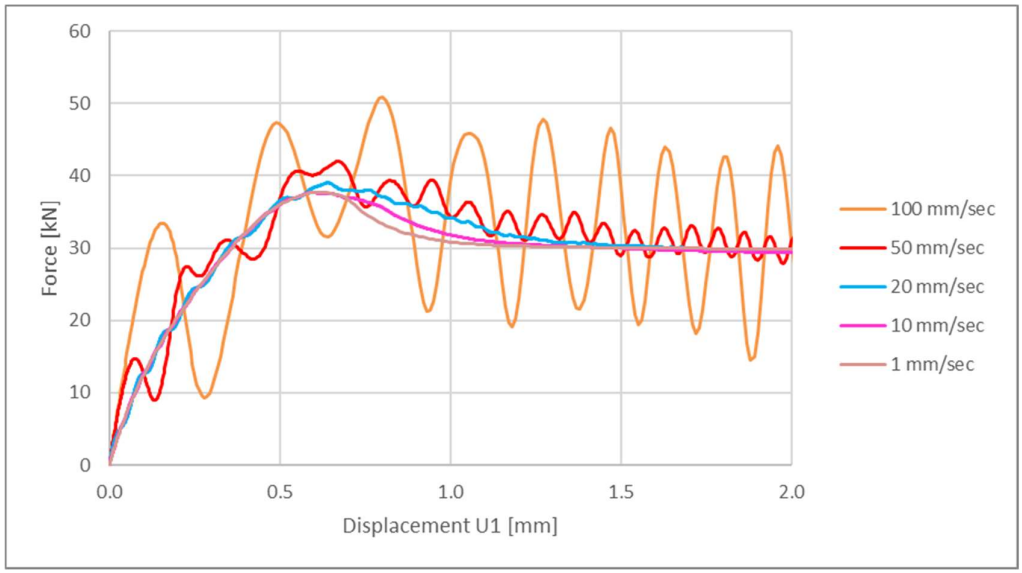

Figure 5.31 Force vs. in-plane displacement relationship for the plate when using different slower velocities with strain rate.

The location in the force vs. in-plane displacement curve where the maximum force appears and where plastic strain starts to appear are marked in Figure 5.32. In the graph, it is seen that for the velocities 1 mm/s, 100 mm/s and 400 mm/s, plastic strain appears in the plate before the ultimate force is reached. For 200 mm/s, the ultimate load is reached before the plastic strain starts to appear in the plate.

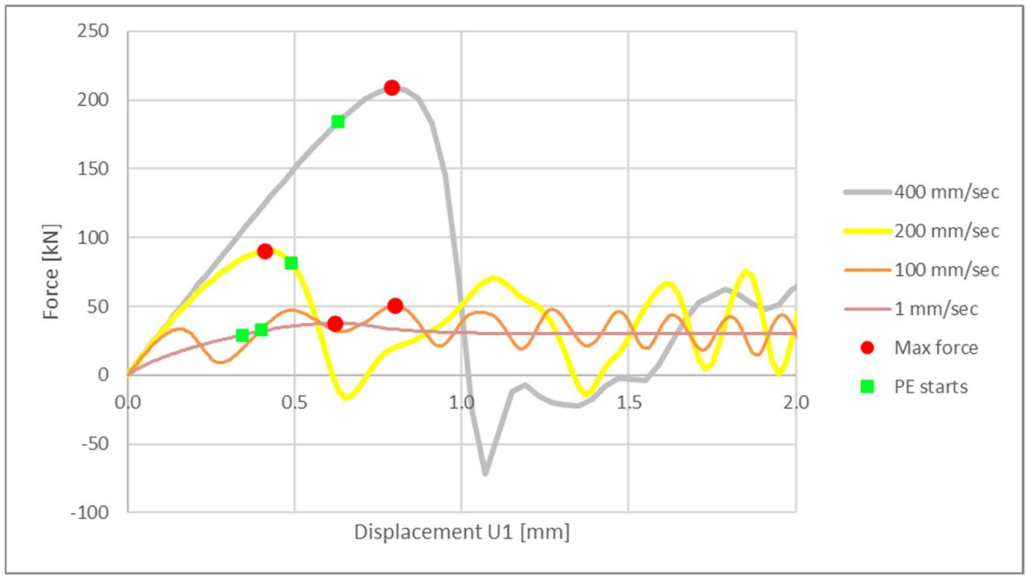

Figure 5.32 Locations where ultimate load and plastic strain starts to appear in the plate with strain rate.

Colour plots of the in-plane plastic strain distribution are created to see the location where plastic strain starts to appear in the plate and to see how the distribution is when maximum force is reached. An explanation of the plots is shown in Figure 5.33

and the plots for various velocities are shown without strain rate effect in Figure 5.34 and with strain rate effect in Figure 5.35.

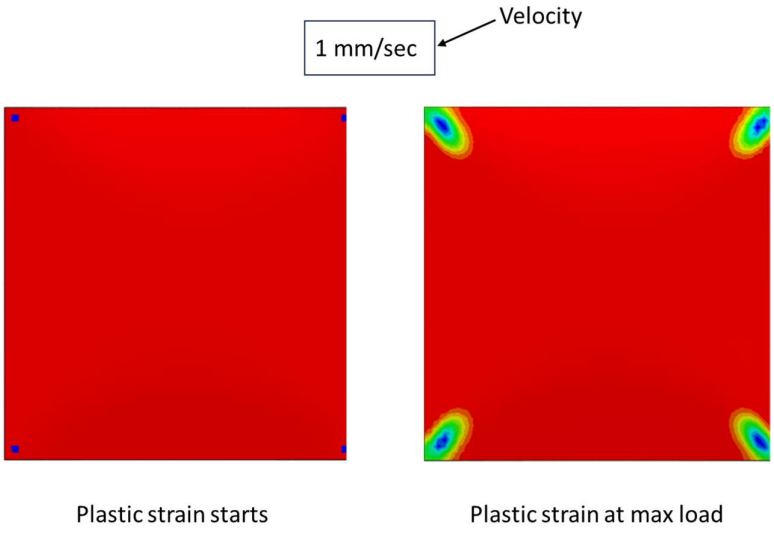

Figure 5.33 Sample plot of the Plastic strain distribution in the plate which shows for which velocity, and which force the plot is.

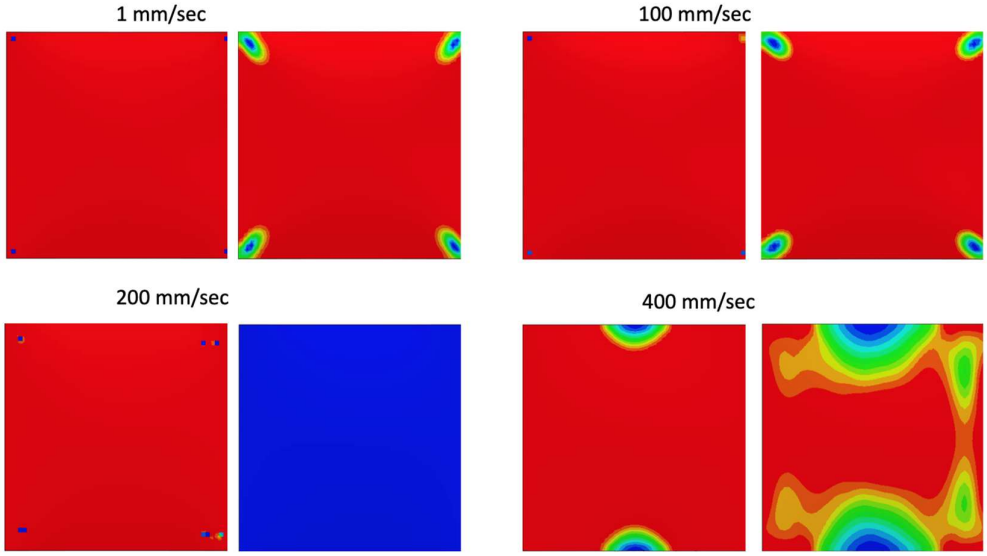

Figure 5.34 Plots for velocities that show when the Plastic strain starts to appear in the plate and how the plastic strain distribution is when the maximum force is reached, without strain rate effect in the model. See description in Figure 5.33.

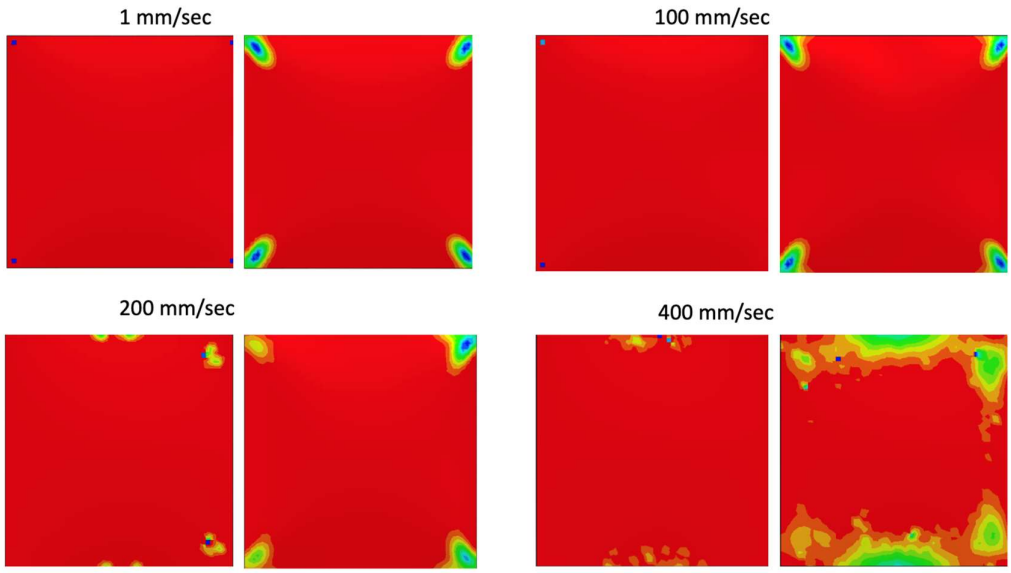

Figure 5.35 Plots for velocities that show when the Plastic strain starts to appear in the plate and how the plastic strain distribution is when the maximum force is reached, with strain rate effect in the model. See description in Figure 5.33.

Based on the graphs and the colour plots above it is seen that the location and shape of the first appearance of plastic strain is similar for the velocities 1 mm/s and 100 mm/s. Furthermore, it is seen that the distribution of the colour plots for these velocities are similar. Based on this, and the linear behaviour that can be seen in between the velocities in Figure 5.19, it is concluded that the behaviour for velocities in this range are behaving in a similar way.

If instead looking at the plots of 200 mm/s, it is seen that when strain rate is applied to the material, the same kind of behaviour as for the slower velocities can be seen. However, when studying the case where no strain rate is applied to the plate, the appearance of plastic strain is distributed in the same way as the slower velocities but in this case no plastic strain has appeared when the ultimate load is reached. This means that in this case, the ultimate load is not influenced by the plastic strain in the plate.

When looking at the plots when applying a velocity of 400 mm/s it is seen that for this case plastic strain is reached in the plate before maximum load is applied, both with and without strain rate. However, when studying the colour plot of the plastic strain it is seen that for this case, the plastic strain starts in the middle of the unloaded edges instead of in the corners where it starts in all other cases. The distribution of plastic strain when ultimate force is reached also has a different shape than the other velocities, both with and without strain rate.

For the same velocities, colour plots where the distribution of the von Mises stress, out-of-plane deflection and in-plane displacement are created. These plots are studied to see where yielding is reached in the plate and how the deformation in the plate looks like. An explanation of the plots is shown in Figure 5.36 and the plots for various velocities are shown with strain rate effect in Figure 5.37.

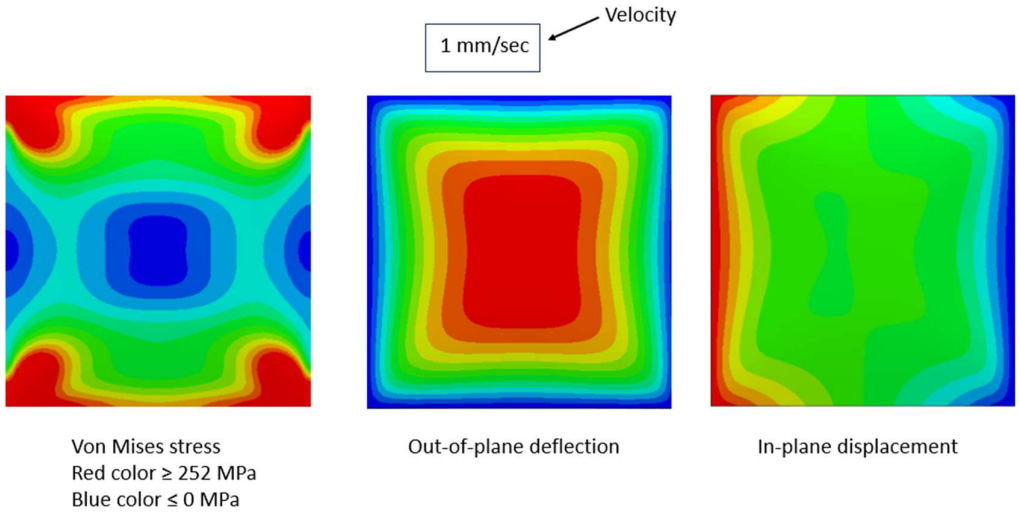

Figure 5.36 Sample plot of the colour plots which shows the von Mises stress, out-of-plane deflection, and in-plane displacement for the ultimate load of a specific velocity.

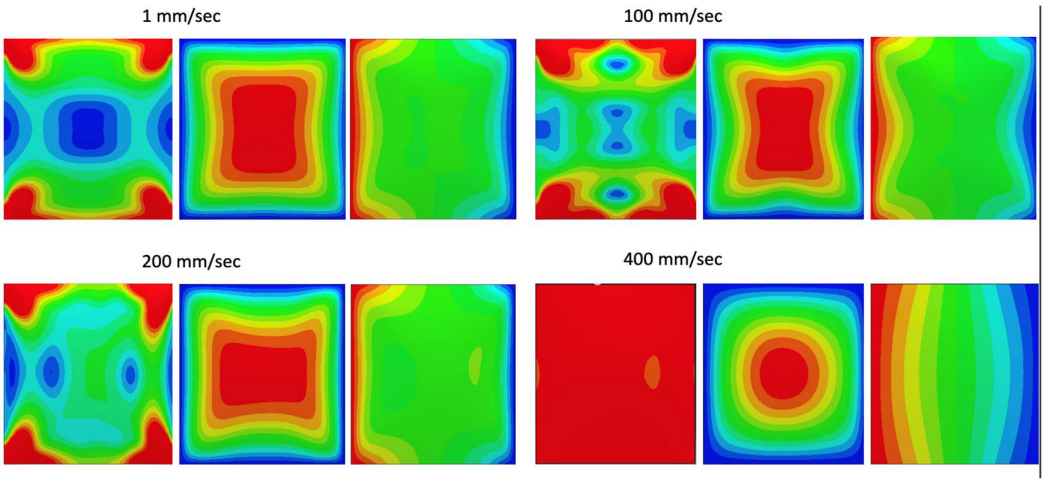

Figure 5.37 Plots for velocities that show the von Mises stress of the plate and out-of-plane, in-plane deformation with strain rate effect. See explanation in Figure 5.36.

The plot in Figure 5.37 shows that the behaviour of the plate is changing as the velocity increases from 1 mm/s to 400 mm/s. At 200 mm/s the von Mises stress response changes entirely and it does not follow a pattern anymore except that the region where it has reached yielding is in the corners. When looking at 400 mm/s it can be seen that yielding is reached in almost the entire plate. If instead looking at the out-of-plane deflection, the pattern is almost the same for the cases 1 mm/s up to 200 mm/s while for 400 mm/s the maximum values are still reached in the middle of the plate but here the pattern is more circular. When comparing the in-plane displacement, it is seen that for the velocity 400 mm/s, the colours have a gradually change over the entire plate while for the rest of the velocities the maximum and negative values are concentrated to the loaded edges.

Stress vs. strain curves are created for various velocities to see how the material strength is increased when strain rate is applied to the plate and to see when the strength appears, see Figure 5.38.

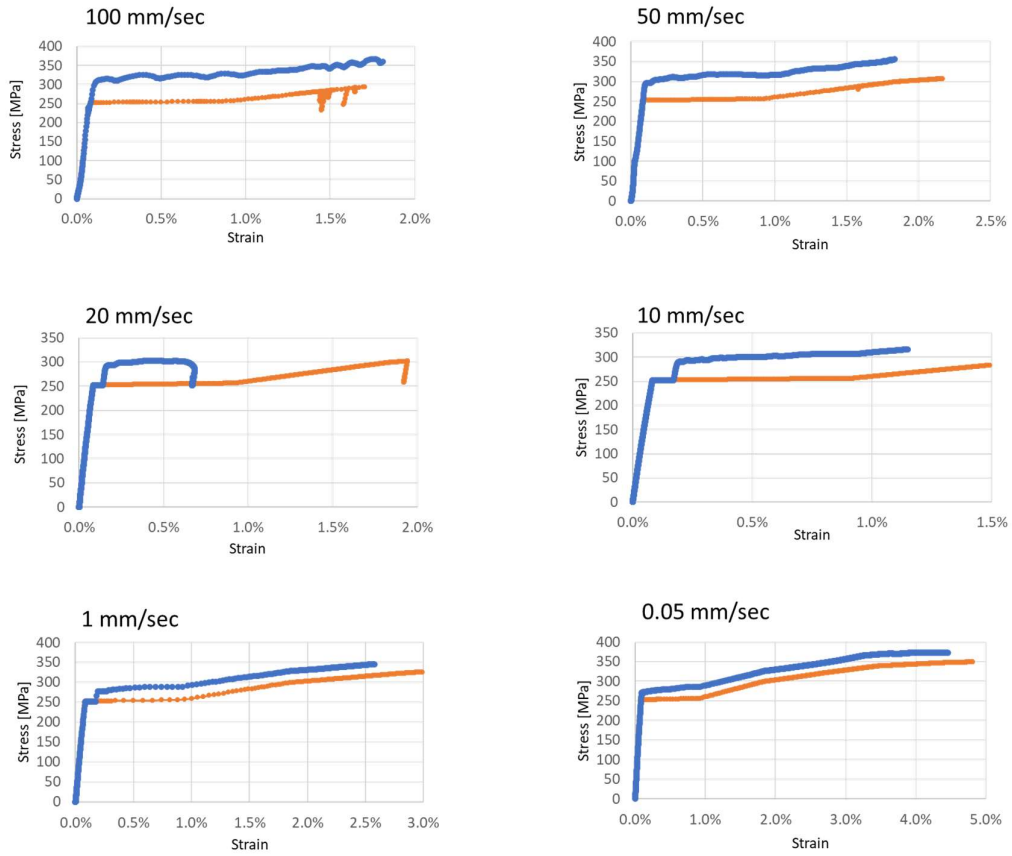

Figure 5.38 Stress vs. strain for different velocities with and without strain rate effect, where the orange curve shows without strain rate effect and the blue curve shows with strain rate effect.

When looking at the plots in Figure 5.38 it shows the stress vs strain behaviour of the plate for different velocities, and it shows that the yield capacity of the plate has increased with the strain rate effect in the model for all the cases. Based on the curves, it can be concluded that the increase in strength varies for the different velocities and the location where the increase starts changes. In some cases, the stress value increases at the start whereas for other cases it does not show any difference until a certain strain value is reached and then it increases from there. Generally, the higher the velocity, the earlier the change is while for slower velocities the curves remain the same for a part where the material has started to yield. Although when looking at the velocity 0.05 mm/s, the increase in strength can be seen from the initial part of the yielding.

6 Study of a thicker steel plate

6.1 Orientation

To examine the influence of the plate slenderness, an additional plate is studied where the thickness is 5 mm instead of 1.6 mm. In the study of this plate, the same geometry and material properties as mentioned in Section 3.4 are used.

A mesh convergence study is made to see if the same mesh size is valid as for the thin plate, see Figure 6.1.

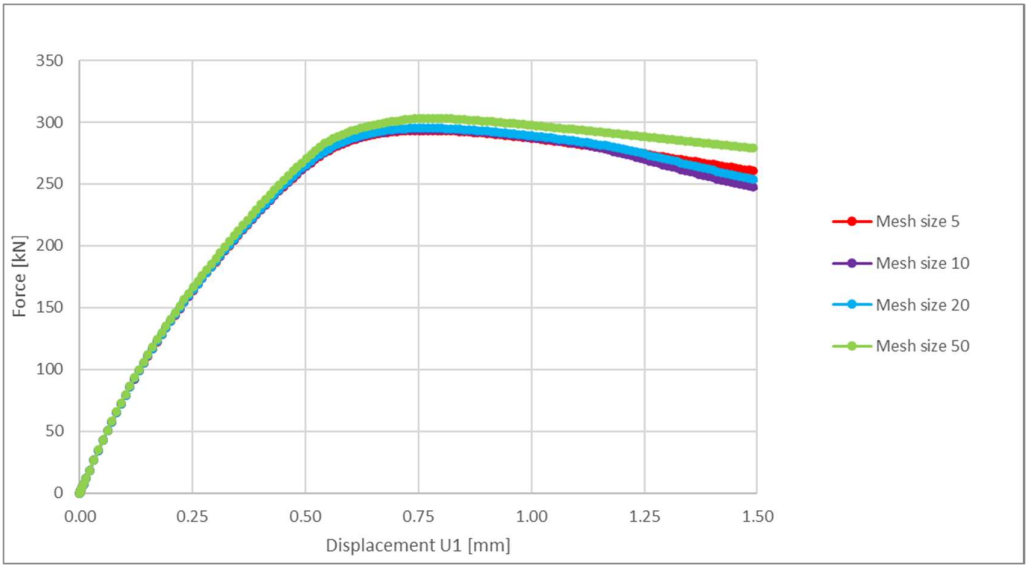

Figure 6.1 Mesh convergence study of the thick plate.

When studying the graph, it is seen that when using a mesh size of 20 mm or less the change in ultimate load of the plate is negligible and the result converges. Based on this, it is concluded that the same mesh size as for the thin plate can be used, that is a mesh size of 10 mm.

6.2 Static analysis

6.2.1 Initial imperfection

The effect of using different initial imperfection is studied for the thicker plate, see Figure 6.2.

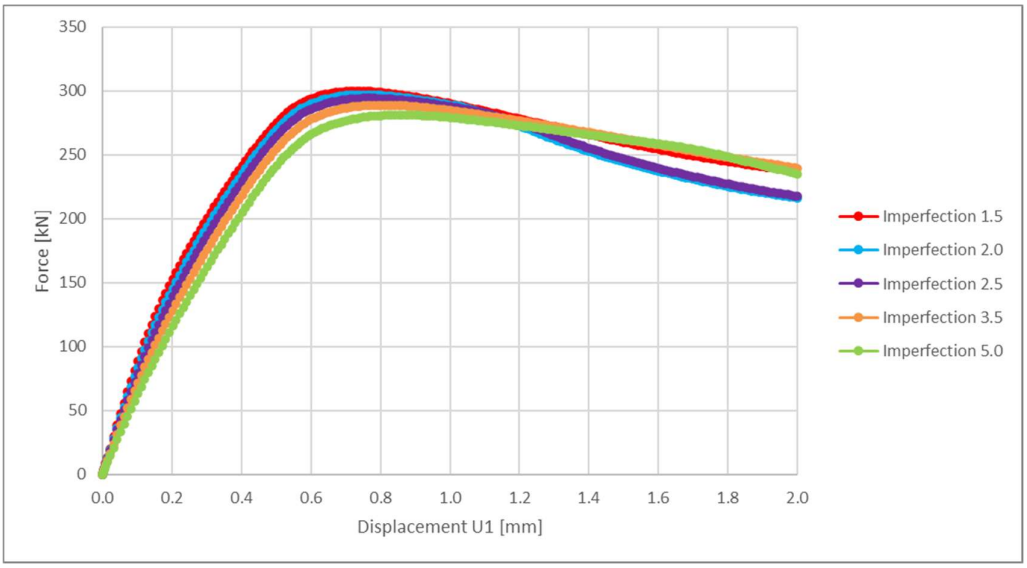

Figure 6.2 Static result of a thicker plate with different initial imperfections, given in mm.

When studying the plot, it is seen that the ultimate strength of the plate is decreased gradually when the initial imperfection is increased. It is also seen that after the ultimate strength is reached, the shape of the curve differs for various value of the initial imperfection.

By comparing the curves, it can be concluded that the initial stiffness of the plate, i.e. before the ultimate strength is reached, decreases with an increase in initial imperfection.

6.2.2 Material properties

The effect of using materials with different yield strength and ultimate strength is studied by examining the effect of the same materials as studied for the thin plate in Section 4.4, see Figure 6.3.

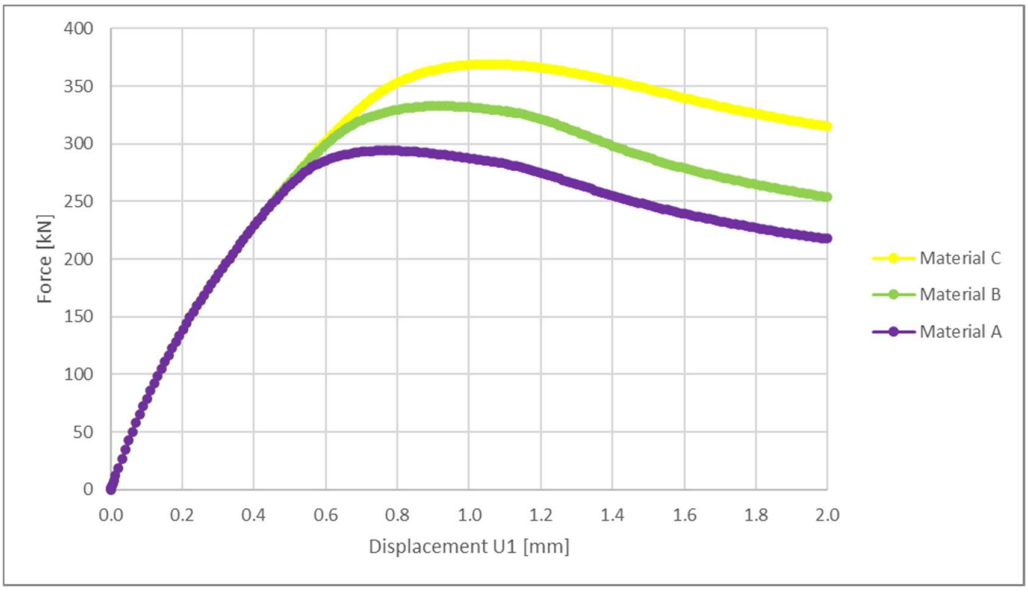

Figure 6.3 Force vs. in-plane displacement when using different steel materials, material settings shown in Table 3.6 and Table 3.7.

When studying the results, it is seen that the initial stiffness of the plate is the same, regardless of what yield- or ultimate strength. Comparing the curves, it can also be seen that the ultimate strength is increased when the yield strength is increased. The ultimate force for material A is 294 kN, for material B the ultimate force is increased with 13 % to 333 kN, and for material C the ultimate force is increased 25 % to 367 kN. The shape of the curve is almost the same for all three materials.

When studying the resulting curves of material B_2 and C_2, in which the yield strength is kept constant but the ultimate strength is increased, it can be noted that the same result as when using material A (original material) is obtained. Therefore, it is concluded that an ultimate strength > 252 MPa does not influence the force vs. in-plane displacement relationship for a thicker plate.

6.2.3 Boundary conditions

Two different boundary conditions are studied for the thick plate to see if the snap back behaviour appears like when studying the thin plate. The cases that are studied are case 1 and 3 described in Section 4.6, in which case 1 is seen as simply supported along all edges and case 3 is the boundary conditions given by Yang et al. (2018) which have more fixed degrees of freedom, both translation and rotation. The resulting force vs. deformation curves are shown in Figure 6.4 and Figure 6.5.

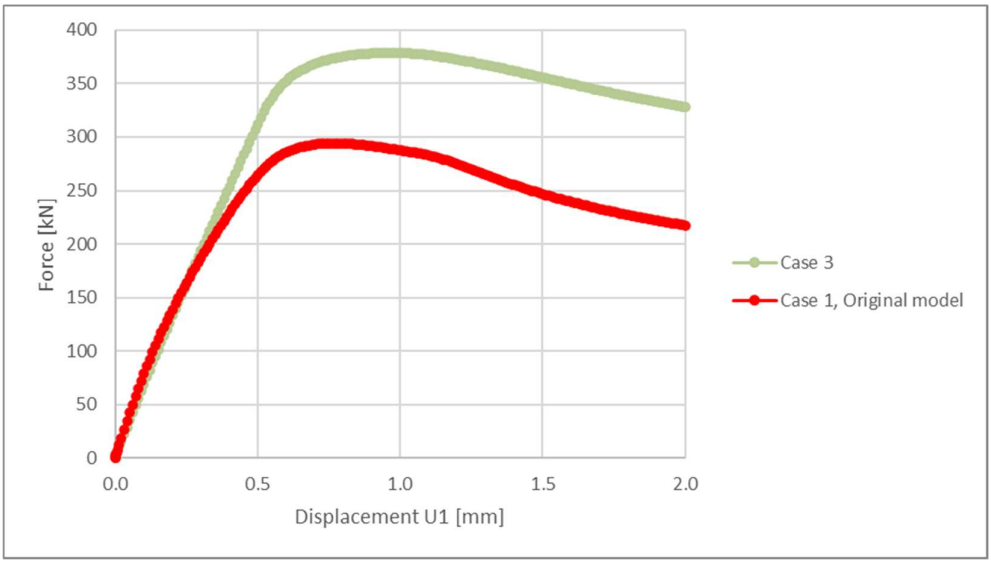

Figure 6.4 Force vs. in-plane displacement for a thicker plate with two different boundary conditions, settings described in Section Table 4.2.

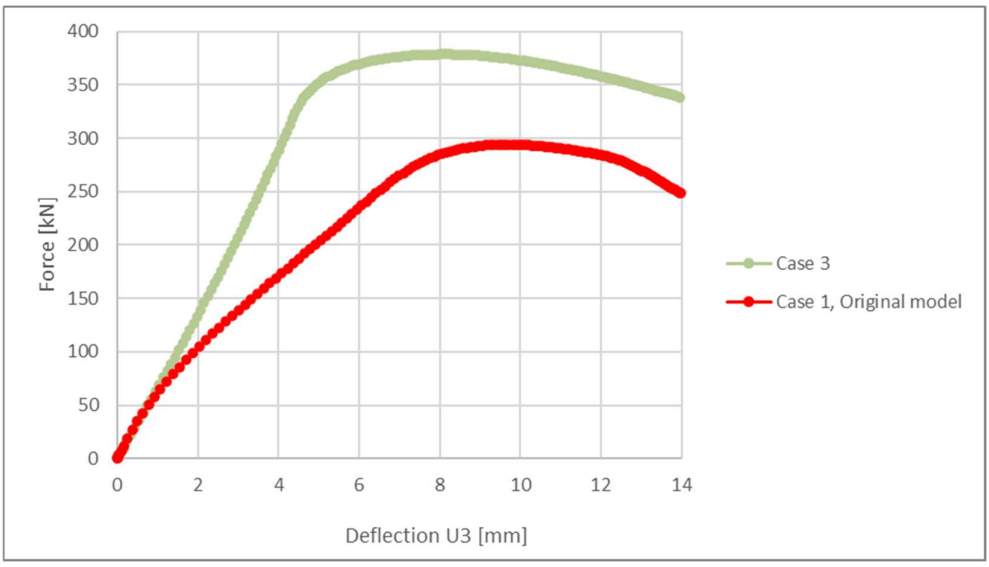

Figure 6.5 Force vs. out-of-plane deformation for a thicker plate with two different boundary conditions, settings described in Section Table 4.2.

For both cases studied, it can be noted that the boundary conditions do not influences the very initial stiffness of the plate. Additionally, in Figure 6.4 the same stiffness is seen for both cases after the ultimate strength is reached. When comparing the force vs. out-of-plane deflection, no clear relation can be observed, here the stiffness differs after the ultimate load is reached.

By comparing the ultimate strength of the two different cases, it is seen that case 3, where more degrees of freedom are fixed, has a higher ultimate strength than case 1 where the plate is simply supported.

No snap-back can be seen when studying how the deflections changes when the force is changed. By studying the buckling mode of the two different cases, it is seen that both cases result in one buckle, the same mode as for case 1 in Figure 4.8.

6.3 Dynamic analysis

6.3.1 Multi linear ramp-up

A dynamic study with multi linear ramp-up of the velocity is performed, in which different velocities are studied, see Figure 6.6. Since it was concluded in Section 5.4 that multi-linear ramp-up gives the most appropriate result, this is the type of load application which is used for the thick plate.

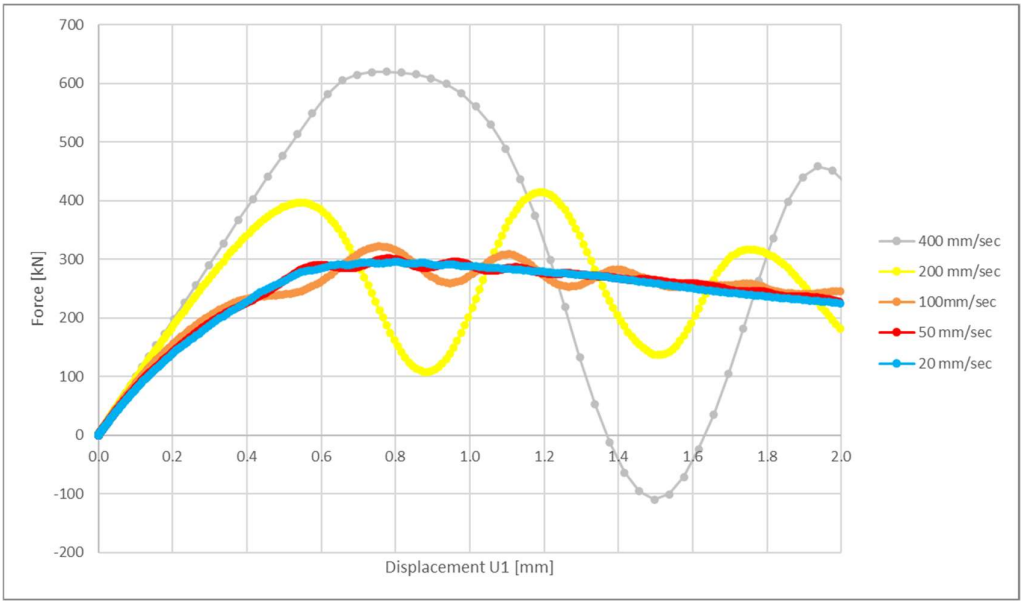

Figure 6.6 Dynamic study of the force vs. in-plane displacement for a thicker plate with various velocities.

When studying the curves, it is seen that the dynamic effect varies with varying velocities. For increased load velocity, increased dynamic effect is obtained. However, for velocities in between 0.05 mm/s and 20 mm/s the curves are smooth, and the difference is seen as negligible. Both for the velocity 400 mm/s and 200 mm/s an increase in the initial stiffness of the plate can be seen and for these two cases the ultimate strength is increased to a higher extent. Despite this, it is seen that the sinusoidal shape of the curves still follows the shape of the smooth curve obtained for lower load velocities. The curves for the velocities 100 mm/s and 50 mm/s have a sinusoidal shape of the curve with a small magnitude which also follows the shape of the smooth curve for 20 mm/s.

By comparing the curve for a load of 20 mm/s with the static result, it is concluded that the difference is negligible and therefor the velocity 20 mm/s can be regarded to give the same result as for static loading.

6.3.2 Strain rate study

The effect of applying strain rate effect to a thicker plate is studied by comparing the results from Subsection 6.3.1 with results from Abaqus CAE where strain rate effect is applied to the material by using yield ratio. The strain rate effect is based on Cowper-Symonds power equation, see (2.20), and the parameters D=1304 and q=4.83 are calculated based on the material properties and the equations (2.21) and (2.22). The resulting curves are shown in Figure 6.7 and Figure 6.8.

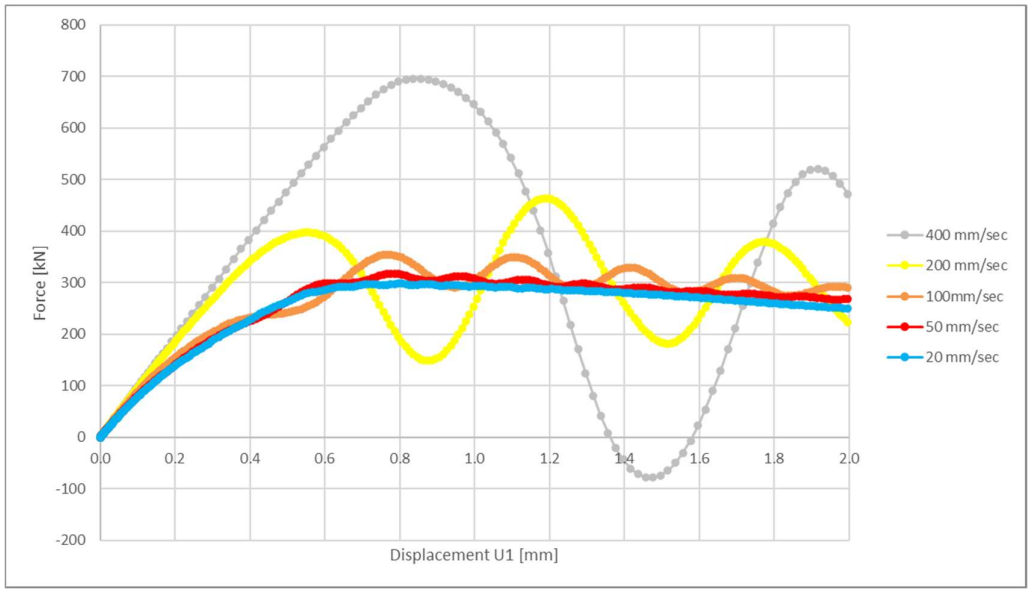

Figure 6.7 Dynamic study of the force vs. in-plane displacement for a thicker plate with strain rate effect, for various velocities.

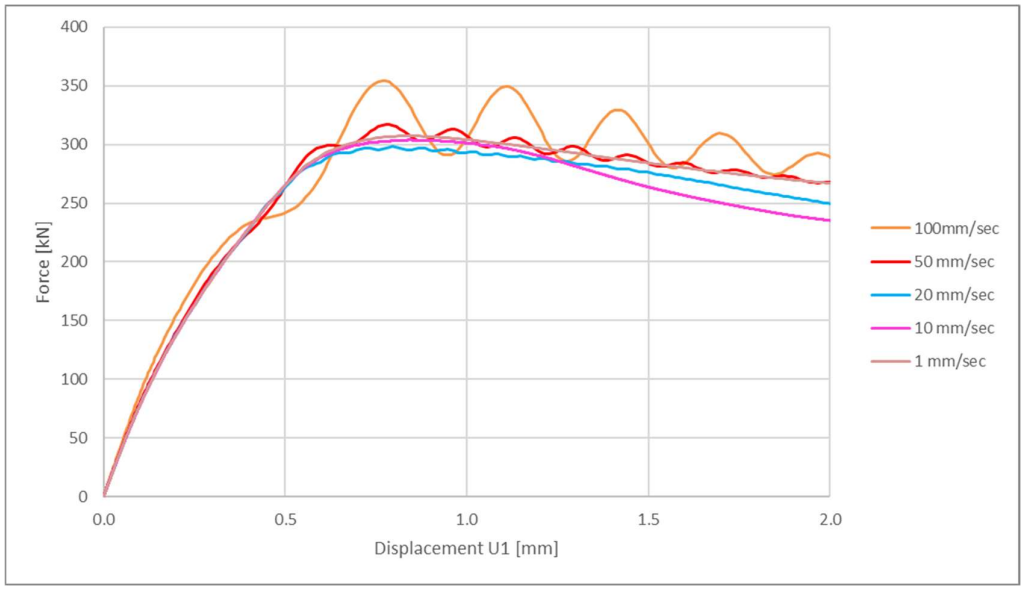

Figure 6.8 Zoomed graph of the force vs. in-plane displacement for a thicker plate with strain rate effect, for various velocities.

By comparing the curves to the curves where there is no strain rate, it is observed that there is an increase in load capacity due to strain rate and the magnitude of the increase differs between different velocities. The expected result would have been that the increase is linearly to the increase in velocity, the higher velocity the more increase in ultimate strength. However, this is not what is obtained. In the zoomed graph, it is seen that the increase for 1 mm/s is about 4 % while the increase for 20 mm/s is only about 1 %; these results are unexpected and the reason for the observed response is unknown.

To examine where the plastic strain first appears in the thicker plate, to see the distribution of plastic strain at maximum load and if the behaviour is the same for different velocities, several colour plots are made. The plots are made of the plastic strain distribution in the plate for the velocities 1 mm/s, 100 mm/s, 200 mm/s, and 400 mm/s with and without strain rate effect, see Figure 6.9 and Figure 6.10.

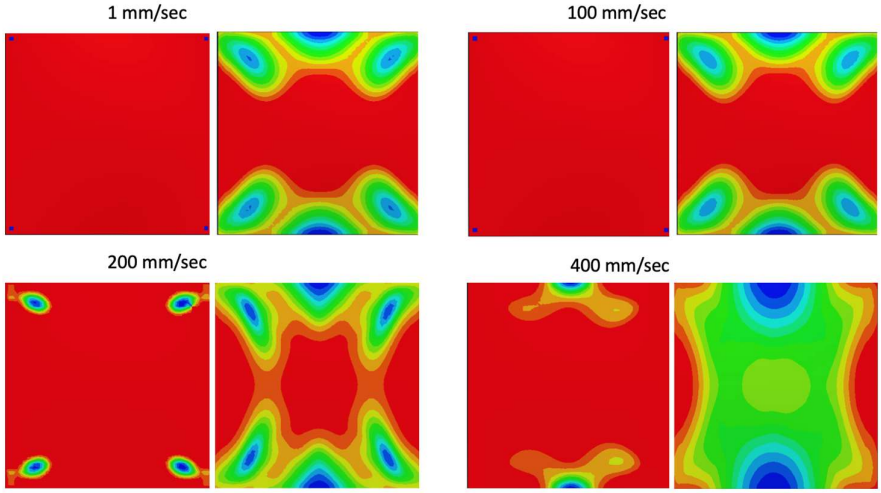

Figure 6.9 Distribution of the plastic strain in the thicker plate without strain rate effect, see explanation Figure 5.33.

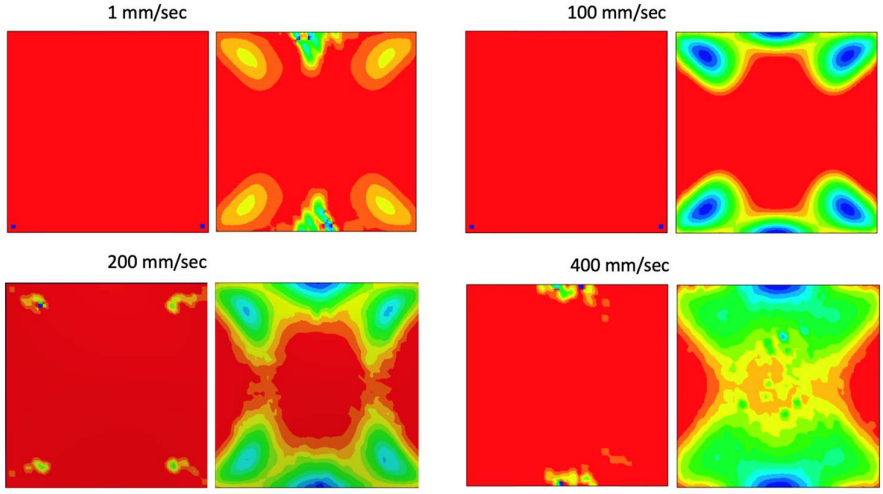

Figure 6.10 Distribution of the plastic strain in the thicker plate with strain rate effect, see explanation in Figure 5.33.

When comparing the colour plots, it is seen that the plastic strain distribution is very similar for velocities between 1 mm/s and 100 mm/s when no strain rate is applied to the material. When looking at 200 mm/s, a similar distribution can be seen when studying the plastic strain at ultimate force, but when looking at the point where the first plastic strain appears in the plate, a difference can be noted, even though the plastic strain first appears in the corners. For the velocity 400 mm/s the distribution differs for both the plots. When looking at the plots where strain rate effect is applied to the material similar distribution can be seen for the different velocities.

Additionally, colour plots are made of the distribution of the von Mises stress, the out-of-plane deflection, and the in-plane displacement at the ultimate load for the same velocities, see Figure 6.11.

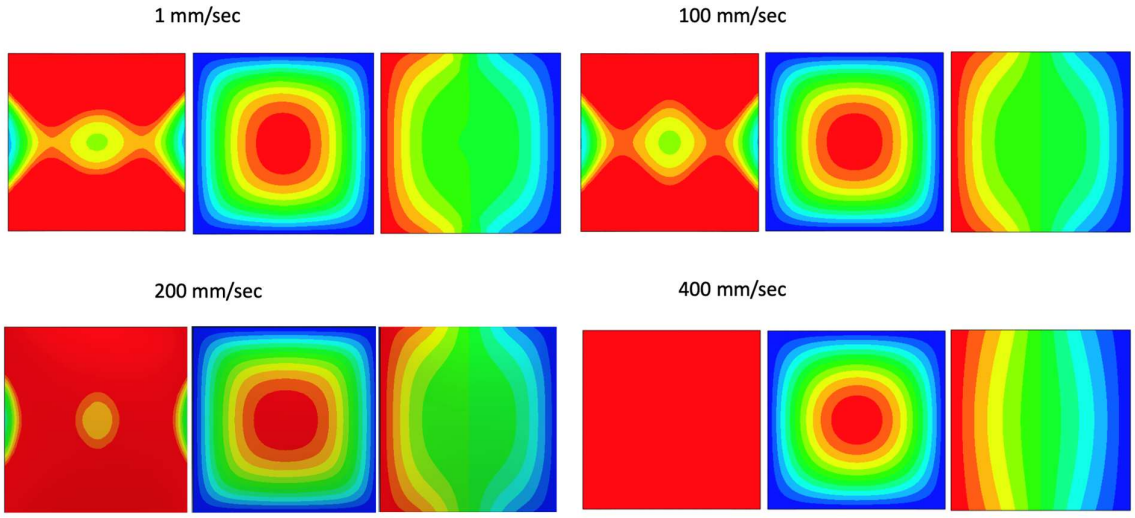

Figure 6.11 Colour plots of the distribution of the von Mises stress, out-of-plane deflection and in-plane displacement for the thicker plate with strain rate. See Figure 5.36 for description and explanation of the plots.

The plot depicts almost the same response for velocities between 1 mm/s and 100 mm/s. For velocities above 200 mm/s the von Mises response of the plate differs a bit and it can be seen that at 400 mm/s the stress has reached yielding in the whole plate.

Stress vs. strain curves is created for various velocities with and without strain rate to see the effect, see Figure 6.12.

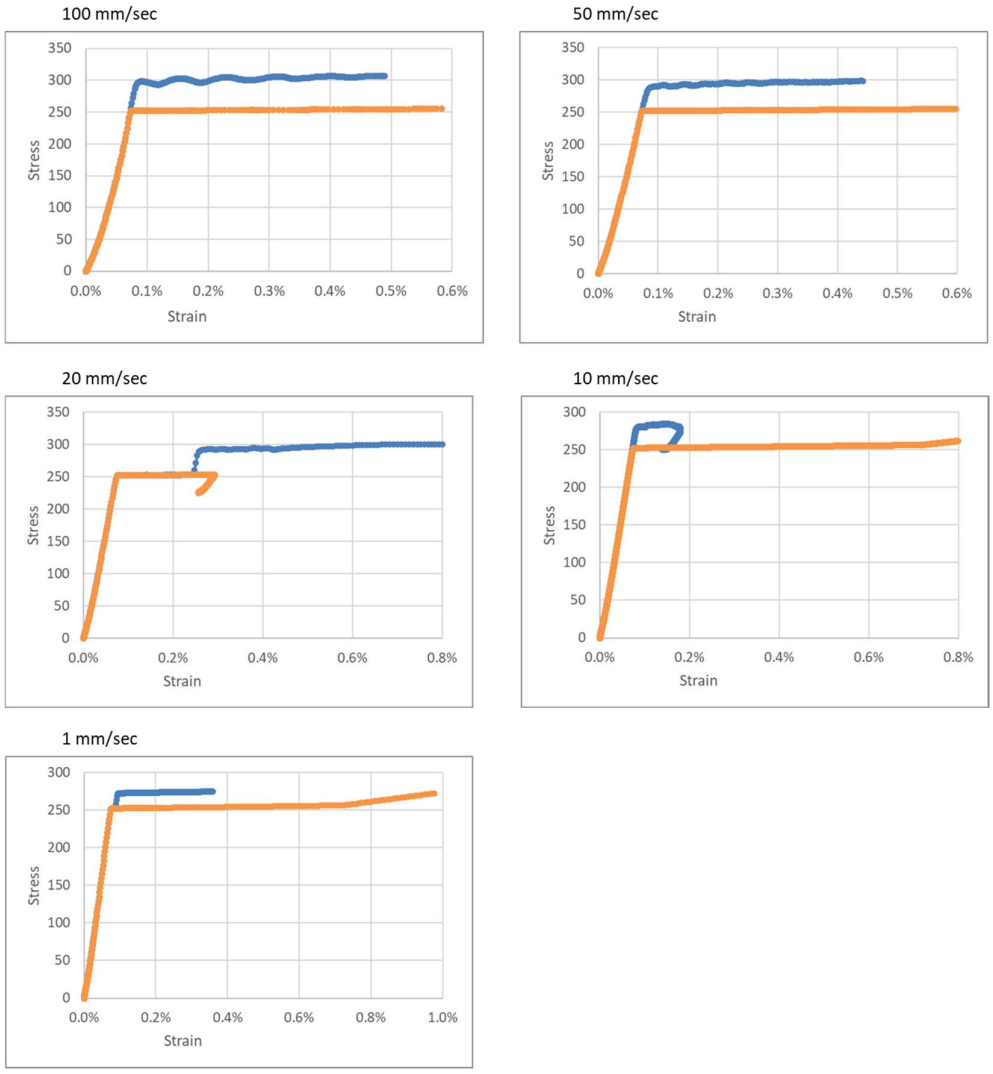

Figure 6.12 Stress vs. strain relationship for a thicker plate with and without strain rate effect.

In the above graphs there can be seen that there is an increase in capacity for all the different velocities as expected when including the strain rate effect in the analyses. For higher velocities the increase in stress capacity is visible from the beginning of the curve whereas for the lower velocities there is no difference in stress values until it reaches a certain plastic strain rate, a part of the yielding of the material. Although, 10 mm/s does not fall in this pattern, which it did for the thin plate. As shown in the graph, for this velocity the increase in capacity can be seen from the start of the yielding for the thicker plate.

7 Final remarks

7.1 Conclusions

A thin and a thick plate, subjected to axial compressive force, were analysed in Abaqus CAE for static and dynamic load cases of various load rates. For static loading, the influence of initial imperfection, yield and tensile strength, boundary conditions and presence of an edge beam along the two unloaded edges were examined. For dynamic loading, the influence of various load applications and strain rate effects were examined. The results and observations from this are concluded in this Section.

The magnitude of initial imperfections in the range studied had negligible effect on the resulting structural response (stiffness and strength) for a steel plate with high slenderness. When a plate with low slenderness is studied, however, it was found that the ultimate load of the plate is reduced gradually when the initial imperfection is increased; this indicates that for the studied case, the initial stiffness in the plate is affected by the initial imperfection. A decreased initial imperfection results in stiffer initial behaviour of the plate.

The yield strength of the steel material has a significant influence on the resulting load carrying capacity for both the plate with high and low slenderness. It is concluded that for the studied case the magnitude of the increase is higher for plates with lower slenderness; i.e. a thicker plate results in higher increase in ultimate load. On the other hand, the ultimate strength of the steel did not have any effect on the structural response for the plates studied. Therefore, it means that the mechanical properties beyond the yield strength did not have an impact on the results in the cases studied. The reason for this is that the stress in the plate only reached just above yielding due to the range of slenderness studied was such that buckling was governing.

The boundary conditions have high influence on the structural response of the plate. The boundary condition affects both the stiffness, the maximum load carrying capacity and which buckling mode is governing. Several different boundary conditions were studied, all of which resulted in the same initial buckling mode where one single buckle appeared in the plate. For the cases where the unloaded edges are fixed in y-direction a snap-back behaviour is found for the thin plate where the plate changes from one half-sinus wave to two or three half-sinus waves. For the thicker plate, this behaviour was not seen.

The effect of adding a stiffening edge beam to the supported (unloaded) edge of a thin plate has been studied by looking at three different heights of the beam. It is concluded that the presence of such a beam affects the plate's load carrying capacity. An increased beam height results in stiffer behaviour is and increased load carrying capacity. Though, it is seen that in-plane and out-of-plane deformation where the ultimate load is reached is not influenced by the presence of an edge beam.

Static response of tests that were obtained from the literature and on which the simulation is done was adequately described using FEM when comparing the in-plane displacement. For the out-of-plane deflection, though, the response obtained using FEM overestimated the out -of-plane deflection compared to that obtained in the test.

How the dynamic load is applied to the plate has a major influence on the result. The ramping of the amplitude curve gives a considerable difference in the resulting curves. Where it is found that constant loading and linear ramp-up have given large difference in the result than the multi-linear ramp-up of the amplitude. The result in the study shows that when rapid acceleration is applied to the plate, dynamic oscillation is introduced in the model which may cause problems in the result. The higher applied acceleration, the more oscillation. To be able to handle these problems in a better way, the load should be introduced to the plate with an acceleration which is not too high. By applying the load with a multi-linear ramp up, the resulting applied acceleration is linearly increasing and therefor the model handles the dynamic effects in a more suitable way.

Furthermore, it is concluded that the load velocity may have high influence on the structural response. When using a smooth load initiation, minor dynamic effects (oscillations around static response) could be seen for v = 20 mm/s while major effects were noticed at v = 100 mm/s. The dynamic response observed in tests for velocity loads v = 100-400 mm/s could not be adequately reproduced using FEM.

By comparing two plates with identical geometry but different thicknesses it is concluded that the slenderness of the plate plays an important role in determining the dynamic force vs. deformation curves. A thicker plate leads to higher stiffness and ultimate load. It is also concluded that the slenderness of the plate affects the dynamic response. For the thicker plate the dynamic response is less sensitive compared to the thin plate and it is seen that the curve follows the shape of the static curve.

Strain-rate effects, based on the Cowper-Symonds power equation, are examined in the study. Considering strain rate is of importance when the strain rate in the steel material is high enough. High strain rates should lead to increased material strength, but the results obtained show that the expected response is not always obtained. Examination of various strain-rate settings did not give satisfactory behaviour. In the FEM analysis, the strain rate effect gave minor or negligible influence for the studied cases. However, this conclusion can be affected by the fact that the results are not satisfactory.

7.2 Further studies

When using the Abaqus strain rate function Power law satisfactory results could not be obtained. Therefore, a detailed study of how and why the strain rate effect in Abaqus CAE is influencing the response would be of interest to further investigate.

Additionally, it would be of interest to study more combinations of plate geometry, material properties, initial imperfections, and load velocities to be able to compare more data and increase the knowledge of the subject.

8 References

Al-Emrani, M., & Åkesson, B. (2020). *Steel structures*. Report ACE 2020:13, Chalmers University of Technology, Sweden.

Carlsson, M., & Kristensson, R. (2012). *Structural response with regard to explosions - Mode Superposition, Damping and Curtailment*. Division of Structural Mechanics, Lund University, Master´s Dissertation, Sweden.

Dassault Systèmes Simulia Corporation. (2022). *Abaqus/CAE* (Version 2022.HF3) [Computer software.]. Dassault Systèmes Simulia Corporation. https://eu1.iam.3dexperience.3ds.com/

Degtyarev, V. V. (2020). Concentrated load distribution in corrugated steel decks: A parametric finite element study. *Engineering Structures*, 206. https://doi.org/10.1016/j.engstruct.2019.110158.

Dubina, D., Ungureanu, V., & Landolfo, R. (2012). *Design of Cold-formed Steel Structures*. ECCS - European Convention for Constructional Steelwork.

Izabel, D., Holz, R., & Fauth, C. (2016). *Test analysis following EN 1993-1-3 for corrugated sheets.* Guidelines and Recommendations for Integrating Specific Profiled steel sheets in the Eurocodes (GRIPSE).

Johansson, M., & Laine, L. (2012a). *Bebyggelsens motståndsförmåga mot extrem dynamisk belastning. Del 1 – Last av luftstötvåg*. MSB, Rapport MSB449, Sweden.

Johansson, M., & Laine, L. (2012b). *Bebyggelsens motståndsförmåga mot extrem dynamisk belastning. Del 3 – Kapacitet hos byggnader*. MSB, Rapport MSB142, Sweden.

Klorek, J., & Sandberg, A. (2013). *Structural Response of Reinforced Concrete Frames Subjected to Explosions*. Division of Structural Engineering, Chalmers University of Technology, Master´s Dissertation, Sweden.

Kubiak, T. (2013). Static and Dynamic Buckling of Thin-Walled Plate Structured. *Springer*. https://doi.org/10.1007/978-3-319-00654-3.

Kowal-Michalska, K., & Mania, R. (2008). *Some Aspects of Dynamic Buckling of Plates Under In-Plane Pulse Loading.* Division of Mechanics and Mechanical Engineering, Technical University of Lodz, Publication no. 02:12, Poland, 135-146.

Paik, J. K., & Thayamballi, A. K. (2003a). *Ultimate limit state design of steel-plated structures.* John Wiley & Sons Ltd.

Paik, J. K., & Thayamballi, A. K. (2003b). An experimental investigation on the dynamic ultimate compressive strength of ship plating. *International Journal of Impact Engineering*, 28(7), 803-811. https://doi.org/10.1016/S0734-743X(02)00154-9

Plos, M., Johansson, M., Zandi, K., & Shu, J. (2021). *Recommendations for Assessment of Reinforced Concrete Slabs*. Division of Structural Engineering, Chalmers University of Technology, Report ACE 2021:3, Sweden.

Rayleigh, Lord, (1877). *Theory of Sound (two volumes)*. Dover Publications, USA, reissued 1945, second edition.

Yang, B., Soares, G. C., & Wang, D. (2018). An empirical formulation for predicting the dynamic ultimate strength of rectangular plates under in-plane compressive loading. *International Journal of Mechanical Sciences*, 141, 213-222. https://doi.org/10.1016/j.ijmecsci.2018.04.015

Appendix A

Comparison of analytical result and static results in Abaqus CAE

Studied plate		
t_{plate} [mm]	w [mm]	L [mm]
1.6	500	500

Static analysis			
	Analytical	Abaqus	Difference (%)
σ	0.625	0.625	0.00

Where,

$$\sigma = \frac{F_{plate.edge}}{t_{plate}} = \frac{1}{1.6} = 0.625\ N/mm$$

Linear buckling					
Analytical		Abaqus			Difference (%)
	N_{cr}	Nref	Eigenvalue	$N_{crAbaqus}$	
[N]	11.79	318.401	0.018	11.75	0.29

Where,

$$k = \left(\frac{m \cdot w}{L} + \frac{L}{m \cdot w}\right)^2 = \left(\frac{1 \cdot 500}{500} + \frac{500}{1 \cdot 500}\right)^2 = 4$$

$$\sigma_{cr} = k \cdot \frac{\pi^2 \cdot E}{12 \cdot (1 - \upsilon^2) \cdot \left(\frac{w}{t_{plate}}\right)^2} = 4 \cdot \frac{\pi^2 \cdot 199\,000\ MPa}{12 \cdot (1 - 0.3^2) \cdot \left(\frac{500}{500}\right)^2} = 7.37\ MPa$$

$$N_{cr} = \sigma_{cr} * t_{plate} = 7.37\ MPa\ \cdot 1.6\ mm = 11.79\ N/mm$$

$$N_{cr.abaqus} = N_{ref} \cdot \lambda = 318.401\ N/mm \cdot 0.018 = 11.75\ N/mm$$

$$Ratio = \frac{N_{cr} - N_{cr.abaqus}}{N_{cr.abaqus}} = 0.29\ \%$$

DEPARTMENT OF ARCHITECTURE AND CIVIL ENGINEERING
CHALMERS UNIVERSITY OF TECHNOLOGY
Gothenburg, Sweden 2023
www.chalmers.se

CHALMERS
UNIVERSITY OF TECHNOLOGY